Water Research 188 (2021) 116543

Contents lists available at ScienceDirect

Water Research

journal homepage: www.elsevier.com/locate/watres

Review

Photocatalytic treatment of natural waters. Reality or hype? The case of cyanotoxins remediation

Albert Serrà [a,*], Laetitia Philippe [a], François Perreault [b], Sergi Garcia-Segura [b,*]

[a] Empa, Swiss Federal Laboratories for Materials Science and Technology, Laboratory for Mechanics of Materials and Nanostructures, Feuerwerkerstrasse 39, CH-3602 Thun, Switzerland

[b] Nanosystems Engineering Research Center for Nanotechnology-Enabled Water Treatment. School of Sustainable Engineering and the Built Environment, Arizona State University, Tempe, AZ, 85287-3005, USA

ARTICLE INFO

Article history:
Received 5 August 2020
Revised 18 October 2020
Accepted 19 October 2020
Available online 22 October 2020

Keywords:
Contaminants of emerging concern
Persistent organic pollutants
Advanced oxidation processes
Photo-assisted water treatment

ABSTRACT

This review compiles recent advances and challenges in the photocatalytic treatment of natural water by analyzing the remediation of cyanotoxins. The review frames the treatment need based on the occurrence, geographical distribution, and legislation of cyanotoxins in drinking water while highlighting the underestimated global risk of cyanotoxins. Next, the fundamental principles of photocatalytic treatment for remediating cyanotoxins and the complex degradation pathway for the most widespread cyanotoxins are presented. The state-of-the-art and recent advances on photocatalytic treatment processes are critically discussed, especially the modification strategies involving TiO_2 and the primary operational conditions that determine the scalability and integration of photocatalytic reactors. The relevance of light sources and light delivery strategies are shown, with emphasis on novel biomimicry materials design. Thereafter, the seldomly-addressed role of water-matrix components is thoroughly and critically explored by including natural organic matter and inorganic species to provide future directions in designing highly efficient strategies and scalable reactors.

1. Introduction

Blooms of algae in aquatic ecosystems can constitute a critical threat to the ecosystem. The environmental implications of excessive algal growth include a decrease in the dissolved oxygen concentration, a sequestration of nutrients by algae that reduces their availability to other species, and the absorption of sunlight by the blooming algal biomass, which reduces light penetration for other species (Sellner et al., 2003; WHO, 2013). From a health perspective, a major concern is the formation of harmful algal blooms (HAB), which are characterized by the presence of toxin-producing algae that can release toxic compounds in the water (Anderson, 2015; Sellner et al., 2003). Direct consumption of water contaminated by HAB has been associated with numerous events of death in pets and livestock animals. Although fatal exposure to cyanotoxins in human is much more rare, direct exposure through recreational activities have been associated with hospitalization due to pneumonia, liver damage, or hepatic failure (Bláha et al., 2009). There is an increasing amount of literature documenting potential chronic impacts, such as gastrointestinal illnesses and cancer in human populations (Kubickova et al., 2019). With the increasing frequency of HAB due to climate change and the intensification of agricultural activities (Anderson, 2015), there is an ever increasing need for efficient technologies able to treat cyanotoxins-contaminated water.

Cyanotoxins are produced by cyanobacteria, photosynthetic prokaryotes, as mostly cell-bound secondary metabolites that are released into the water after cell death (Paerl and Otten, 2013; Rastogi et al., 2014). Common species able to produce cyanotoxins include *Anabaena, Microcystis, Cylindrospermopsis, Nostoc, Synechococcus*, and several others (Anderson, 2015; Paerl and Otten, 2013). However, toxin production is not constant in most species and it is reported that between 25% and 75% of HAB worldwide are toxin producing (Bláhová et al., 2007; Chorus, 2001). Even within the same location and with blooms formed of the same species, the HAB may not always be toxin-producing (Dittmann et al., 2013). The exact cause why a bloom may or may not be producing toxin is unclear. Different strains of the same species may lack the gene cluster responsible for toxin production or possess them in an inactive state that prevent the synthesis of

* Corresponding authors.
E-mail addresses: albert.serraramos@empa.ch, a.serra@ub.edu (A. Serrà), Sergio.Garcia.Segura@asu.edu (S. Garcia-Segura).

https://doi.org/10.1016/j.watres.2020.116543

toxin (Dittmann et al., 2013). In strains able to produce toxins, the intracellular toxin content was found to be modulated by a variety of environmental or physiological factors such as temperature, light, nutrient availability, presence of heavy metals, hydrodynamic conditions, organic matter, cell density, and grazing by predators (Boopathi and Ki, 2014; Merel et al., 2013a). Given the complexity of interactions existing between these different environmental triggers, predicting toxic production in HAB is still a major challenge.

Cyanotoxins can be classified based on their chemical composition or toxicological interactions. In terms of composition, cyanotoxins are broadly divided into cyclic peptides (e.g. mycrocystin, nodularin), alkaloids (e.g. cylindrospermopsin, anatoxin, saxitoxin), and lipopolysaccharides (e.g. endotoxin) (Carmichael, 1992; Codd et al., 1999; Ferrão-Filho and Kozlowsky-Suzuki, 2011). However, cyanotoxins are produced by a wide variety of species, which result in a large diversity of structures even within one toxin type. For example, there are more than 85 variants of microcystins (MCs) alone (Rastogi et al., 2014). Likewise, different cyanotoxins can have different mechanism of action in mammals, which lead to a classification of cyanotoxins based on their toxic effects: hepatotoxins (e.g. mycrocystin, nodularin, cylindrospermopsin), neurotoxins (e.g. anatoxin, saxitoxin), or dermatotoxins (e.g. aplysiatoxin, lyngbyatoxin-A) (Carmichael and Boyer, 2016; Ferrão-Filho and Kozlowsky-Suzuki, 2011). Several of these cyanotoxins have also been shown to lead to carcinogenic impacts over time (Kubickova et al., 2019).

Because of these potential impacts on human health, reliable monitoring and treatment tools are critical to avoid deleterious effects of cyanotoxins in drinking water. Cyanotoxins monitoring can be based on a range of immunological, biological, or physicochemical approaches and will vary depending on the type of cyanotoxin considered (Kaushik and Balasubramanian, 2013; Melegari et al., 2012; Merel et al., 2013a; Perreault et al., 2011). The detection of cyanotoxins can be challenging because of the low detection limit of some analytical techniques for cyanotoxins, high analytical costs, and the co-occurrence of multiple cyanotoxins with multiple mechanisms of action which cannot be all detected within the same biological or immunochemical assay (Al-Sammak et al., 2014; Chia et al., 2019; Merel et al., 2013a). Similar challenges exist for the removal of cyanotoxins in water treatment systems, where a mixture of different compounds with dissimilar structure can coexists and can be potentially toxic at low concentrations. Treatment technologies for cyanotoxins therefore needs to be efficient, non-specific, and able to achieve high removal at low concentrations.

Conventional water treatments including flocculation, filtration, sedimentation, and chlorination generally remove cyanobacteria and low levels of (cyano) toxins. However, they are ineffective for completely degrading high levels of cyanotoxins produced during moderate and severe bloom events. The inability of these processes to completely degrade cyanotoxins has prompted the development and implementation of advanced oxidation processes (AOPs). In general, AOPs are based on the generation of highly active oxidizing species such as hydroxyl and other radicals via radiation, oxidation, catalysis, or a combination of these (Antoniou et al., 2016; Chatzitakis et al., 2008; Zhang et al., 2014a). During the last 20 years, studies on cyanotoxin removal have shown that AOPs can, in general, effectively remove cyanotoxins. However, further research may face important challenges related to economic, practical, and environmental improvements in order for AOPs to become a realistic technology for large-scale cyanotoxin-removal treatment (Schneider and Bláha, 2020).

Although many studies have not offered a holistic view considering economic and environmental aspects such as operational costs and the mineralization rate or toxic byproducts formed during cyanotoxin degradation, the degradation efficiency and energy consumption of UV/H_2O_2, UV/O_3, UV/PS, UV/PMS, and UV/chlorine are highly competitive. However, electrochemical oxidation, radiolysis, Fenton processes, and photocatalysis have also demonstrated strong potential for large-scale cyanotoxin removal (Schneider and Bláha, 2020). During the last two decades, photocatalysis has been established as a useful technology for degrading various cyanotoxins, including MCs and cylindrospermopsin (CYN) under UV, visible, and solar irradiation (Antoniou et al., 2008a; Liu et al., 2013; Pestana et al., 2015). The non-selective nature of the free radicals produced by AOPs makes them ideal for addressing the diversity of structures found in cyanotoxins. However, thus far, there have been few reports of photocatalytic technology adoption by water treatment utilities (Lawton et al., 2003; Lee et al., 2004; Mauter et al., 2018), which indicate that there are still technical and economic limitations to the use of photocatalysis for cyanotoxin remediation in water treatment. Even confronted with these challenges, the use of photocatalysis in large-scale environmental applications is expected to be widespread in the not-so-distant future as it gains the ability to emerge as an inexpensive, sustainable, and green technology.

In this review, we present the state of the art related to photocatalytic treatment processes for the removal of cyanotoxins from drinking water from the last 20 years. We discuss the current issues related to geographical distribution and legislation of cyanotoxins in drinking water and evaluate the potential of photocatalytic systems to achieve treatment goals for these contaminants. The role of the water matrix and the operational conditions are also presented to highlight the current research needs in photocatalytic treatment of cyanotoxins.

2. Geo-localization of cyanotoxin blooms and legislative actions taken

2.1. Geo-localization and geographical distribution of cyanotoxin blooms

Whereas the origins of cyanotoxins are certain, the conditions that provoke cyanobacteria to produce and release them remain poorly understood. In most cases, cyanotoxins emerge with the formation of cyanobacterial HABs (cyanoHABs), whose growth is sustained, if not enhanced, in water exceeding 25°C that exhibits high concentrations of nutrients, especially phosphorous and nitrogen (Gkelis and Zaoutsos, 2014; O'Neil et al., 2012; WHO, 2011). Because anthropological activities and eutrophication (e.g., water pollution and globally rising temperatures) promote such high temperatures and nutrient concentrations in water, they also sustain, if not promote, the production and release of cyanotoxins. At the same time, increased precipitation, changes in pH levels, extended periods of direct sunlight irradiation, stable stratification in bodies of water, and calm or stagnant water flows, among other environmental factors, can also increase the growth of cyanoHABs (Christophoridis et al., 2018; Environmental Protection Agency, 2014). Owing to those factors, cyanobacterial growth tends to occur more often in dams, lakes, ponds, reservoirs, and slow-moving rivers during the summer and autumn, especially in tropical and subtropical zones. Even so, cyanoHABs also grow in bodies of fresh water, including in Swiss alpine lakes, throughout colder regions of the world (Fig. 1) (Bernard et al., 2017; Du et al., 2019; Flores et al., 2018; Meriluoto et al., 2017).

Although cyanotoxins are often retained in the cytoplasm of cyanobacteria—that is, as *intracellular cyanotoxins*—in the presence of cyanoHABs, they can also be easily released when cyanobacteria die or when stress occurs. Other cyanotoxins, including CYN, are naturally released by healthy cyanobacteria during the occurrence of cyanoHABs—in that case, as *extracellular cyanotoxins*. Both intra-

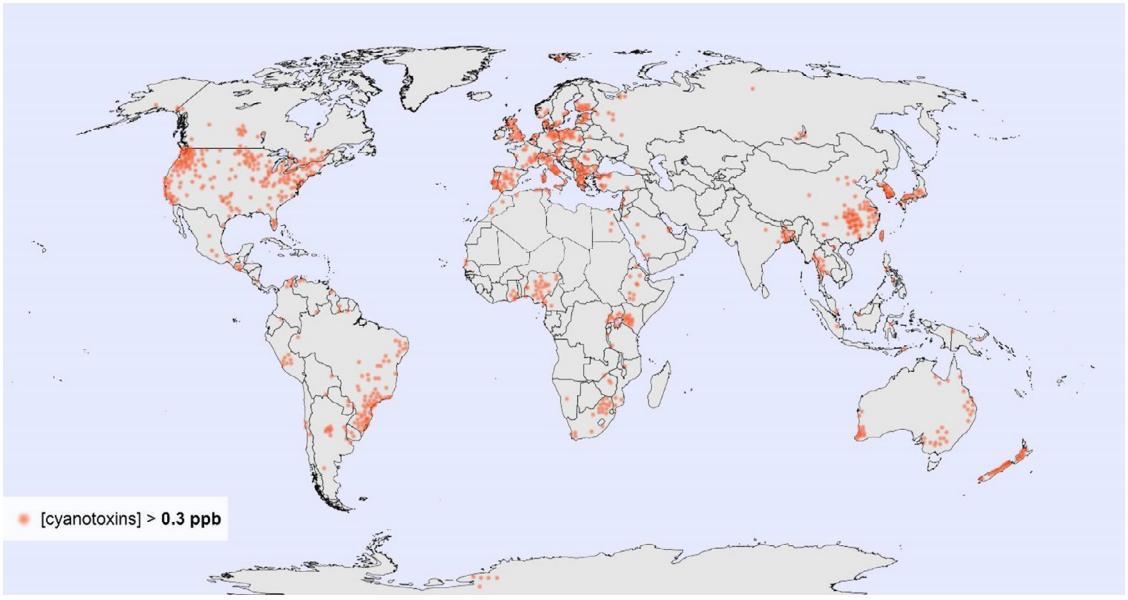

Fig. 1. Geographic worldwide distribution of cumulative number of the most commonly reported cyanotoxins. The map presents the regions in which toxins have been found in concentrations exceeding 0.3 ppb in at least five studies during the past 20 years.

cellular and extracellular cyanotoxins have to be considered in water treatment processes, because their ratio to each other when released during the growth of cyanoHABs is practically identical due to stress conditions and the death of cyanobacteria during that dynamic process (Buratti et al., 2017; Neilan et al., 2013; Wert et al., 2014). However, water treatment can also dramatically increase the release of intracellular cyanotoxins due to cyanobacterial cell lysis. In any case, the release of cyanotoxins, whether intracellular or extracellular, may depend more upon environmental conditions and the external manipulation of water bodies than the presence of species able to produce toxins (Pantelić et al., 2013; Pinho et al., 2015a).

Several circumstances—the incomplete understanding of bioactive substances produced by cyanobacteria, the increased occurrence of cyanoHABs, the complexity of cyanotoxins' release, and the limitations of analytical methods that preclude the rapid, simple, simultaneous identification of concentrations of cyanotoxins in water—explain the absence of a global study to systematically monitor geographical and temporal trends in the distribution of cyanotoxins (Du et al., 2019; Flores et al., 2018; Gkelis and Zaoutsos, 2014; O'Neil et al., 2012). Albeit estimated, the global distribution of the six most common cyanotoxins (i.e., microcystins, nodularins, CYNs, saxitoxins, anatoxins, and β-*N*-methylamino-L-alanine) appears in Fig. 1. Although governmental and nongovernmental reports about those cyanotoxins are more often released in Europe and North America than in Asia, South America, Oceania, Africa, and Antarctica, the map nevertheless shows that eradicating cyanotoxins is very much a global challenge (Du et al., 2019; Flores et al., 2018). A brief summary of the particularities of each region is presented here:

- *Europe:* Cyanotoxins are identified in western European regions (i.e., with an oceanic climate) characterized by cool summers, in far southern European regions (i.e., with a Mediterranean climate) characterized by hot summers, and in central–eastern European regions (i.e., with a continental climate) also characterized by relatively hot summers. In cold regions, including the Baltic Sea region and Serbia, the production of cyanotoxins intensifies during the summer due to increased water temperatures, especially on the water's surface. Although MCs are the most commonly found cyanotoxins in Europe, CYNs, saxitoxins, and anatoxins are significantly present as well. Cyanotoxins are detected predominately in lakes in more than 28 European countries; however, recent studies have also demonstrated their presence in slow-moving rivers (Cirés et al., 2014; Du et al., 2019; Dziga et al., 2019; Flores et al., 2018; Kurmayer et al., 2011; Lopes and Vasconcelos, 2011; Mantzouki et al., 2018; Meriluoto et al., 2017). According to the European Environment Agency, 88.2% of Europe's fresh water (i.e., for drinking, industry, agriculture, and recreation) comes from rivers and groundwater, whereas the rest comes from reservoirs and lakes. Although cyanotoxins are detected predominantly in lakes and lake water represents only approximately 1.5% of Europe's fresh water, the potential risks of cyanotoxins cannot be underestimated, because a truly global map of toxic cyanobacteria in Europe remains unavailable (Cirés et al., 2014; Du et al., 2019; Dziga et al., 2019; Flores et al., 2018; Kurmayer et al., 2011; Lopes and Vasconcelos, 2011; Mantzouki et al., 2018; Meriluoto et al., 2017).
- *Central and North America:* Cyanotoxins have been detected in North and Central America in inland freshwater lakes and coastal areas, especially in the United States and Canada. The climate of Central and North America, including rain-drenched mountains and drought-ridden deserts, ranges from tropical to polar. All six types of cyanotoxins are identified in Central and North America; however, MCs are clearly the predominant type in the regions, followed by a significant presence of anatoxins and a lesser but far from negligible presence of CYN and saxitoxins. In the Arctic region of North America, by contrast, MCs and nodularins are the predominant species, although cyanotoxins are clearly more intensely present in tropical and subtropical regions to the south. Importantly, significant amounts of MCs, CYNs, and saxitoxins have been detected in more than 30% of lakes and reservoirs in the United States. According to the U.S. Environmental Protection Agency, lakes and reservoirs are important sources of surface water for drinking, industrial purposes, and recreation; consequently, the widespread occurrence of cyanotoxins in the country's lakes and reservoirs can pose risks to public health (AWWA, 2016; Carmichael and Boyer, 2016; Du et al., 2019; Flores et al., 2018; Jacoby and Kann, 2007; Loftin et al., 2016; Wiltsie et al., 2018).

- *Asia:* All six types of cyanotoxins have frequently been detected in the lakes, ponds, and reservoirs in the temperate and tropical coastal areas of Asia. At the same time, a non-negligible concentration of cyanotoxins has been found in the inland lakes and rivers of various countries in southern Asia. As mentioned, however, a truly global map of the risk of cyanotoxins in Asia is impossible due to the limited number of reports and studies. The most prevalent climates in Asia—tropical rainforest, hot desert, warm humid continental, hot summer Mediterranean, humid subtropical, tropical savanna, and tropical monsoon climates—are ideal for the growth of cyanoHABs and, in turn, for the production of cyanotoxins. The most detected cyanotoxins in Asia are MCs, although significant concentrations of CYNs, anatoxins, nodularins, and saxitoxins have also been reported. Given the region's ideal conditions for the development of cyanoHABs, even partial data suggest that monitoring and removing cyanotoxins may be pivotal to managing Asia's water resources (Du et al., 2019; Flores et al., 2018; Greer et al., 2017; Liu et al., 2011; Wilhelm et al., 2011).
- *South America:* Up to five common types of cyanotoxins (i.e., MCs, nodularins, CYN, saxitoxins, and anatoxins) have been detected in several South American countries, whereas β-N-methylamino-l-alanine is only identified in Peru. Although cyanotoxins are predominantly found in South America's reservoirs, they have also been detected in its lakes and rivers. The continent's regions are dominated by a warm climate, which is most suitable for the growth of cyanoHABs, whether in tropical or temperate regions. Despite such excellent conditions for the growth of cyanoHABs and the high concentration of cyanotoxins detected in several sources of surface water (e.g., San Roque Lake, Cordoba, Argentina), South American countries have issued fewer reports than other countries, which makes monitoring the real distribution of cyanotoxins on the continent considerably difficult (Du et al., 2019; Flores et al., 2018; Hoff-Risseti et al., 2013; Ruiz et al., 2013; Vieira et al., 2005).
- *Oceania:* All six types of cyanotoxins have been detected frequently in the inland lakes, rivers, and ponds of eastern and southern Australia, as well as on surrounding islands such as New Zealand. As elsewhere in the world, the most commonly detected cyanotoxins in Oceania are MCs. Oceania has a number of different climates, ranging from desert to tropical rainforest, although the most prevalent are oceanic and tropical rainforest climates. The continent's hot, humid regions result in the growth of cyanoHABs (Du et al., 2019; Flores et al., 2018). However, in Australia, a mainly arid climate, major cyanoHABs occur under dry and hot conditions, thus affecting water-stressed areas.
- *Africa:* The six most common types of cyanotoxins have also been found in all countries in Africa, with the exception of Ethiopia, possibly due to the limitation in analytical methods. The most common are MCs, which have been detected in inland rivers, lakes, reservoirs, and ponds. Africa hosts many different climates, the most prevalent of which is tropical savanna. Because such environmental conditions, along with high pollution in some water sources, promote the growth of cyanoHABs, cyanotoxins are causing major problems in the lakes and water reservoirs of eastern and southern Africa (Du et al., 2019; Flores et al., 2018; Krienitz et al., 2013).
- *Antarctica:* Despite the cold temperatures of the region, MCs, nodularins, CYN, and saxitoxins have been detected in Antarctica, whereas anatoxins and β-N-methylamino-l-alanine have not. The detection of cyanotoxins in Antarctica especially demonstrates the strong adaptability of cyanobacteria and cyanotoxins, which can grow even in conditions unfavorable to the growth of cyanoHABs, which highlights the potential risk of cyanotoxins worldwide (Du et al., 2019; Flores et al., 2018).

Although fully depicting the geographical distribution of cyanotoxins around the world is impossible, their potential risk can be concluded from their detection on all seven continents. The bioactive substances pose a greater potential risk in tropical, subtropical, and warm areas; however, the global risk cannot be underestimated because not all cyanotoxins have been discovered and many have been detected in non-negligible concentrations even in regions with environmental conditions highly unfavorable to the growth of cyanoHABs.

2.2. Legislative actions taken to face a worldwide challenge

Cyanotoxin limits in drinking and recreational water bodies are increasingly being subjected to national and international advisories, guidelines, and regulations. Although the World Health Organization (WHO) has published a provisional guideline of 1 ppb of MC-LR for drinking water, no guidelines have been issued for other variants of MCs or other cyanotoxins (Edition and First, 2008; Farrer et al., 2015; Ibelings et al., 2014). Available toxicological data confirm the potential risks of various cyanotoxins for human health; however, they are insufficient to establish limits for their concentration in drinking water. Nevertheless, the data have justified health alerts, as well as advisories, guidelines, and regulations for drinking water, in countries such as Singapore, France, Spain, Uruguay, and Czech Republic. Other states such as Canada have set upper limits of 1.5 ppb for total MCs, whereas Australia has established guidelines of 1.3 ppb for total MCs and published health advisories of 1 ppb and 3 ppb for CYNs and saxitoxins, respectively (Farrer et al., 2015; Funari et al., 2017; Hudnell, 2010; Ibelings et al., 2014; Vogiazi et al., 2019). In the European Union, European Directives 1998/83/EC and 2013/397EU govern the drinking water legislation of the various member states, with the aim "to protect human health from the adverse effects of any contamination of water intended for human consumption by ensuring that it is wholesome and clean." Despite the wide distribution of cyanotoxins in European bodies of water (Fig. 1), the most recent EU Decision (2018/840) to update the substances of environmental concern for European Union does not specifically address cyanotoxins. In the United States, there are no established regulations for cyanotoxins, although MCs, CYN, saxitoxins, and anatoxin-a are included in the Candidate Contaminant List 4 of the U.S. Environmental Protection Agency (EPA). In 2015, the EPA published a 10-day health advisory for CYN of 0.7 ppb in drinking water for bottle-fed infants and preschool children and of 3 ppb for school-age children and adults. For total microcystins, the advisories state a limit of 0.3 ppb in drinking water for bottle-fed infants and preschool children and of 1.6 ppb for school-age children and adults. In addition, several states have established internal health advisories or actions applicable for their domains (Edition and First, 2008; Farrer et al., 2015; Hudnell, 2010; Ibelings et al., 2014).

In the context of recreational water, the WHO considers current guidelines for cyanotoxins to be inappropriate. The WHO has recommended guidelines and regulations based upon cyanobacterial cell density, bio-volume, and pigment levels, all of which directly relate to the concentration of cyanobacteria and cyanotoxins. Based on those criteria, in most cases, countries apply two- or three-tier alert levels indicating the potential risk for human health (Hudnell, 2010; WHO, 2006). However, to further advance how the cyanotoxins is regulated, the development of more precise, rapid monitoring and analytical methods is urgently required, as is the improvement of available toxicological data that can guide the establishment of more informed regulatory limits for cyanotoxins in drinking water.

3. Fundamental principles of photocatalytic treatment for cyanotoxins remediation

Photocatalytic behavior of semiconductor materials was firstly reported by Fujishima and Honda in 1972 (Akira Fujishima and Kenichi Honda, 1972). The fundamental principle of photocatalysis relies in the photo-excitation of an electron (e_{CB}^-) from the filled valence band (VB) to the empty conduction band (CB). The electron transition to the excited state is induced by the material absorption of photons with energy equal or superior to the band gap energy (E_g) (Etacheri et al., 2015; Hoffmann et al., 1995). The photo-excited e_{CB}^- leaves a positively charged hole or vacancy at the valence band (h_{VB}^+) according to reaction (1). Photogenerated species e_{CB}^-/ h_{VB}^+ are referred as charge carriers.

$$\text{Semiconductor} + h\nu \rightarrow e_{CB}^- + h_{VB}^+ \quad (1)$$

Both charge carriers can be involved in different charge transfer processes. Indeed, h_{VB}^+ are strong oxidants that can oxidize organic compounds up to their complete mineralization. In aqueous media h_{VB}^+ can react with water yielding hydroxyl radical ($^\bullet$OH) following reaction (2), the second strongest oxidant known after fluorine (Etacheri et al., 2015; Hoffmann et al., 1995). On the other hand, photogenerated e_{CB}^- is a reducing species. Reaction of e_{CB}^- with dissolved oxygen can produce the weak oxidant superoxide radical ($O_2^{\bullet -}$) according to reaction (3). Note that other e_{CB}^- scavengers such as H_2O_2 can enable additional oxidants production from reaction (4). These oxidant species produced on the catalyst surface remain adsorbed or close to the catalyst surface. The degradation of pollutants is then dependent of their adsorption and/or limited by their mass transfer towards/from the photocatalyst surface (Chong et al., 2010; Etacheri et al., 2015; Hoffmann et al., 1995).

$$H_2O + h_{VB}^+ \rightarrow {}^\bullet OH + H^+ \quad (2)$$

$$O_2 + e_{CB}^- \rightarrow O_2^\bullet \quad (3)$$

$$H_2O_2 + e_{CB}^- \rightarrow {}^\bullet OH + OH^- \quad (4)$$

Photocatalysis is a light-driven process that produces oxidant species *in situ*. The kinetics of oxidant generation is causally related to the number of photons delivered to the catalyst surface per second as can be deduced from reaction (1). In this context, it is extremely relevant to provide information of the photon fluence or irradiance of any experimental set-up. Failure to report these values will result in technical reports that cannot be benchmarked or compared to other works in literature (Duta et al., 2018; Ovhal and Thakur, 2010).

Process efficiency is defined by the usage of delivered photons for the reaction of interest or quantum yield. Light transport to the surface catalyst is one of the relevant elements that can affect overall process efficiency. Turbidity and competing species in solution may diminish the absorption of photons on the catalyst surface. One of the major drivers of photocatalytic efficiency is related to the stability of charge carriers. Species in excited state (i.e., e_{CB}^-) are unstable and tend to return to the ground state of lower energy. Recombination reaction (5) is the main drawback for photocatalytic degradation of organic pollutants such as cyanotoxins (Gaya and Abdullah, 2008; Hoffmann et al., 1995; Kisch, 2010).

$$e_{CB}^- + h_{VB}^+ \rightarrow \text{heat} \quad (5)$$

Titanium dioxide (TiO_2) has been widely reported as photocatalyst material for cyanotoxins abatement. Nanosized TiO_2 is an *n*-type semiconductor with a characteristic E_g of ~3.0 eV reported for its main crystalline structures: anatase, rutile, and brookite. Photocatalysis of pure TiO_2 is therefore conducted with UV light with wavelengths (λ) < 400 nm that corresponds to energies of >3.1 eV. Anatase is the most photo-active due to the higher spatial separation between charge carriers induced by the crystalline structure, which results in a prolonged lifetime of e_{CB}^- /h_{VB}^+. However, heterojunctions formed between these different TiO_2 crystalline structures have shown also increased photocatalytic performance (Dávila-Jiménez et al., 2018; El-Sheikh et al., 2017; Han et al., 2011; Pelaez et al., 2012).

The spectrum of solar radiation has a small component of UV-light (<4.0 %). Low UV irradiance from natural sunlight limits the likelihood of high efficiency and performance of pure TiO_2 photocatalysis. To enable visible light photocatalysis, TiO_2 doping has been the most explored strategy. Even though the E_g of TiO_2 remains almost identical, dopants introduce energy levels within TiO_2 bandgap. Existence of these intraband levels allows photoexcitation to occur in two transition steps that require two photons of lower energy (within visible light spectra). Use of these visible active materials do not affect dramatically fundamental mechanisms of TiO_2 photocatalysis (El-Sheikh et al., 2017; Han et al., 2011; Pelaez et al., 2012).

4. Large molecules: complex degradation pathways

Description and understanding of mechanisms of oxidation and degradation pathways enlighten the development of treatment strategies to ensure complete inactivation of these recalcitrant cyanotoxins. The complexity of the molecular structure of cyanotoxins (i.e. MCs) is deemed as the major challenge for the definition of degradation pathways. Photocatalytic treatment of organics involves the *in situ* generation of strong oxidants (Orha et al., 2017; Spasiano et al., 2015; Villaluz et al., 2019). Many research articles have identified the photogenerated h_{vb}^+ and $^\bullet$OH as the main species involved in oxidation processes (Dávila-Jiménez et al., 2018; Ohtani, 2011; Spasiano et al., 2015). These oxidant species can completely mineralize organic pollutants through three main kind of reactions: (i) hydroxylation, (ii) dehydrogenation, and (iii) charge transfer processes (Oturan and Aaron, 2014). These reactions have been also identified in the degradation pathway of different types of cyanotoxins as described herein (Hu et al., 2017; Yang et al., 2011). It is well known that $^\bullet$OH is a non-selective oxidant, which leads to a myriad of possible pathways. However, identification of intermediates by LC-MS has been key to identify pieces of this complex puzzle and to elucidate preferential degradation mechanisms of the two major cyanotoxins studied in literature: MCs and CYN.

4.1. Insights into microcystin macrocycles cleavage

MCs are cyclic heptapeptides with a similar basic structure that is solely differentiated by the variation of two aminoacids found in the position Y and Z described in Fig. 2. This variability leads to at least 85 different MCs that can be naturally found in water sources (Christoffersen and Kaas, 2000; Lawton et al., 2003). The different MCs are named by the single letter abbreviation of these two variable aminoacids. For example, the most common MC-LR is named after the aminoacids leucine (L) and arginine (R). In this section the degradation pathways will be described for MC-LR as the most representative MC, but similar degradation pathways can be associated to other MCs (Antoniou et al., 2008a; Chen et al., 2012).

Fig. 2 summarizes the scission of the Adda side chain of MC as initial step for MC mineralization. The initial step is defined by the hydroxylation of the double bounds of Adda either at the chain position C4-C5 or C6-C7 yielding product **2** and **3**, respectively (Antoniou et al., 2008b; Fan et al., 2020). Further oxidation of **2** by $^\bullet$OH leads to the breakage of the C-C bond forming aromatic

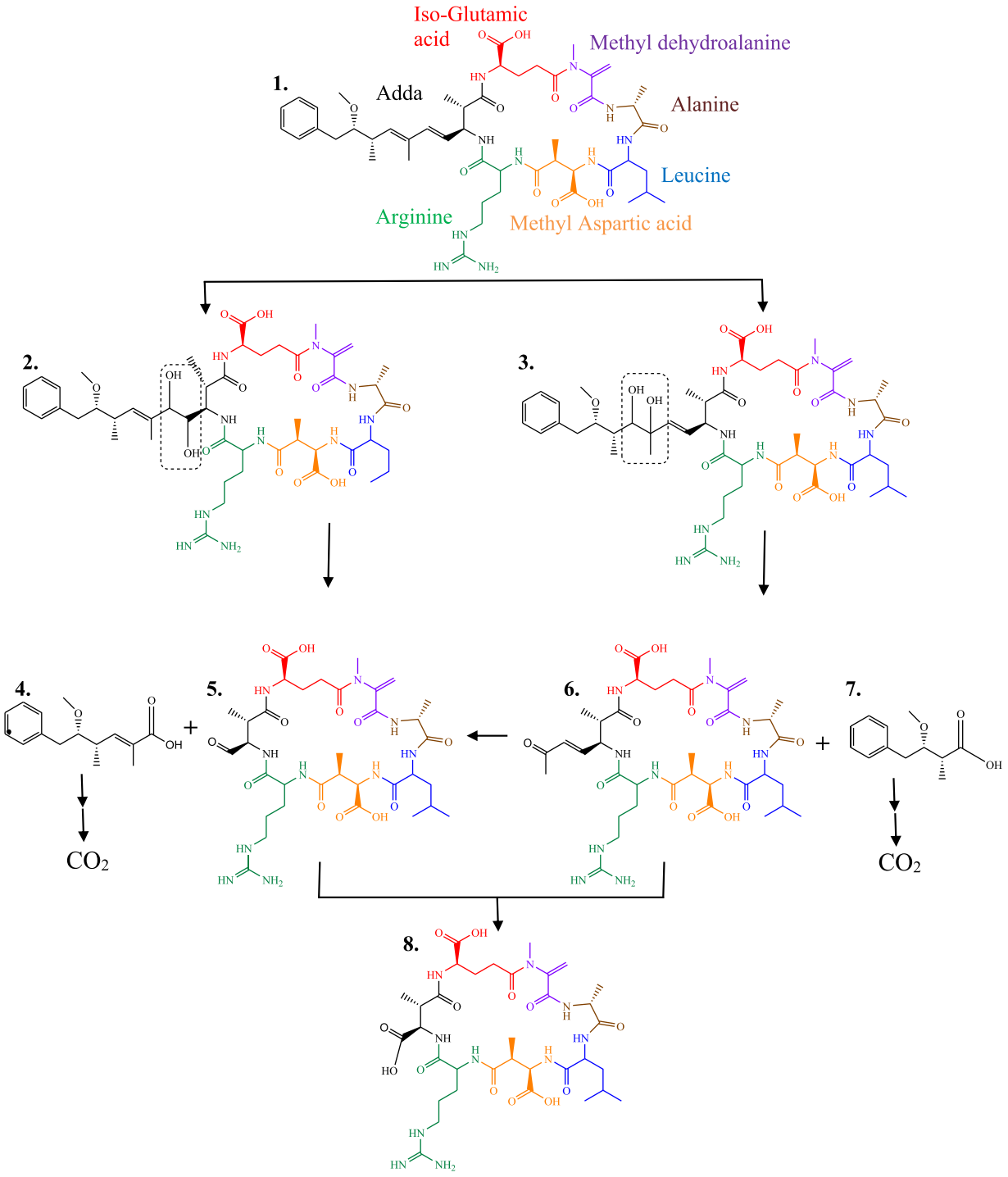

Fig. 2. Degradation pathway of MC-LR mediated by oxidants generated during photocatalytic treatment (Antoniou et al., 2008b; Fan et al., 2020; Hu et al., 2017; Yang et al., 2011).

acid **4** and peptide macrocycle **5** with an aldehyde group at the former C4 position. Whereas, the cleavage at C6-C7 forms ketone **6** and shorter aromatic acid **7**. It is important that intermediate **6** can be further oxidized at the carbonyl position of the ketone to form **5**. Oxidation of this terminal position generates **8**, which has been identified as the previous stage to cleavage of peptide bonds of the macrocycle (Yang et al., 2011). Note that hydroxylation of the aromatic ring can occur simultaneously (Hu et al., 2017).

Fig. 3 illustrates the opening of the macrocycle by the cleavage of the peptide bonds. Hydrolysis of the peptide bond is activated by $^{\bullet}$OH addition on the carbonyl group, which may occur in different positions. Chen's group identified preferential cleavage in four positions yielding intermediates **9-12**. Further scission of peptide bonds results in the accumulation of different oligopeptides such as **13-20**. Complete mineralization of aminoacids forms inorganic ions from N-heteroatoms that are released as ammonia, nitrate, or N-volatiles promoted by $^{\bullet}$OH oxidation (Triantis et al., 2012).

The main mechanistic steps described are hydroxylation reactions via substitution, addition to double bonds, and oxidative bond cleavage. These steps are clearly associated to $^{\bullet}$OH me-

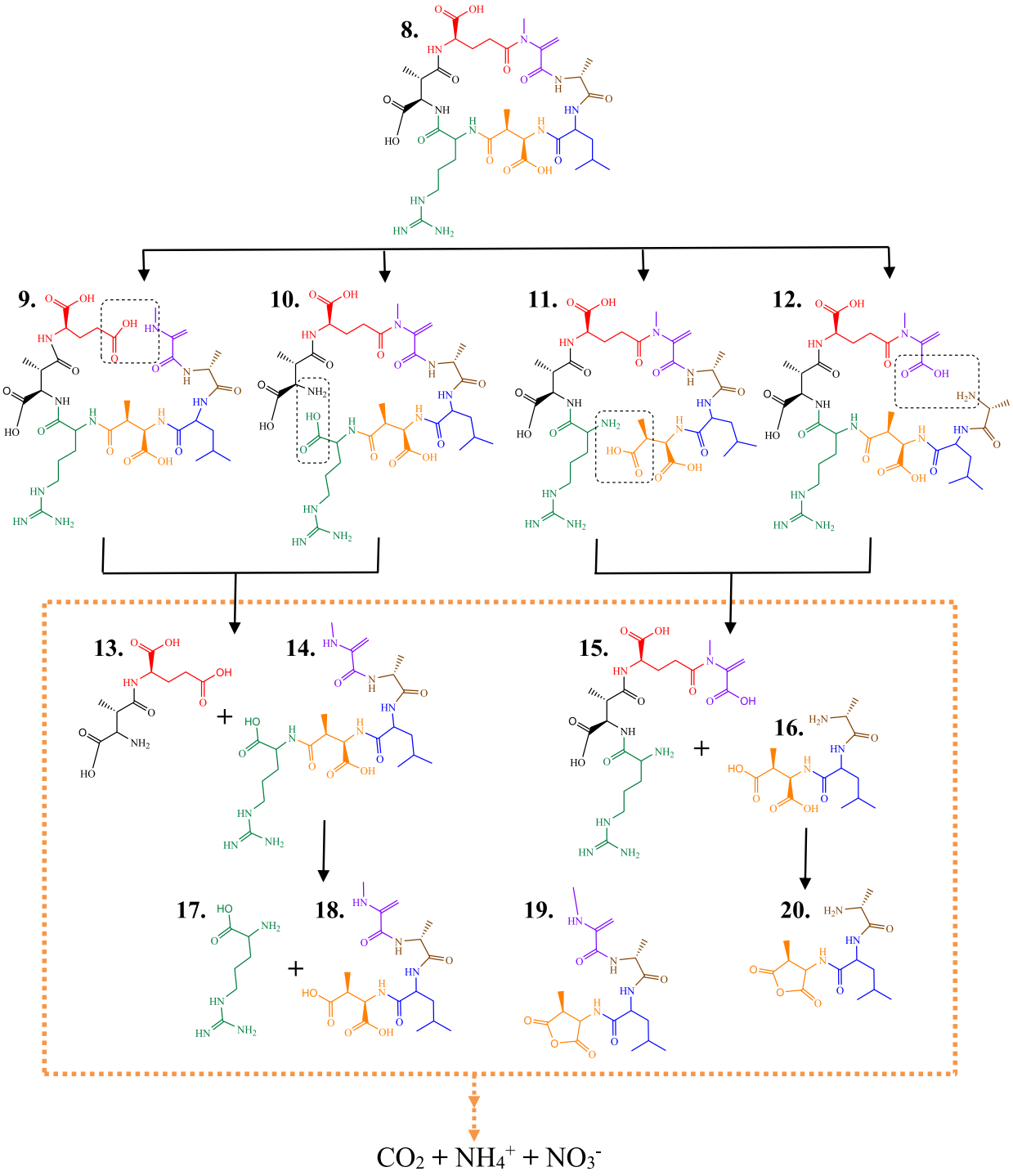

Fig. 3. Degradation pathway of MC-LR mediated by oxidants generated during photocatalytic treatment (continuation) (Antoniou et al., 2008b; Fan et al., 2020; Hu et al., 2017; Triantis et al., 2012; Yang et al., 2011)..

diation, in agreement with scavenging experiments that identified this species as main oxidant of MCs (Antoniou et al., 2009; Cornish et al., 2000). These reactions can lead to different pathways beyond the simplified mechanisms described herein. Indeed, identification of additional by-products suggest that cleavage of the peptide macrocycle can occur prior to Adda scission. Coexistence of both pathways must be considered. Indeed, breakage of the peptide macrocycle can be associated to the quick detoxification of MCs via photocatalysis, which can be assumed that takes place prior complete mineralization.

4.2. Insights into Cylindrospermopsin breakage

CYN degradation can be initiated by hydroxylation of the uracil ring yielding product **2**, which is under tautomeric equilibria with **3**. Both tautomers undergo further hydroxylation at the uracil ring yielding **4** and **5** (Chen et al., 2015). A redox equilibrium exists between **4** and **5**, that can be interconverted by charge transfer processes at the catalyst surface. Alternatively, the first CYN degradative step can involve the oxidation of the hydroxylated carbon between the uracil and tricyclic guanidine cycles yielding **6** followed

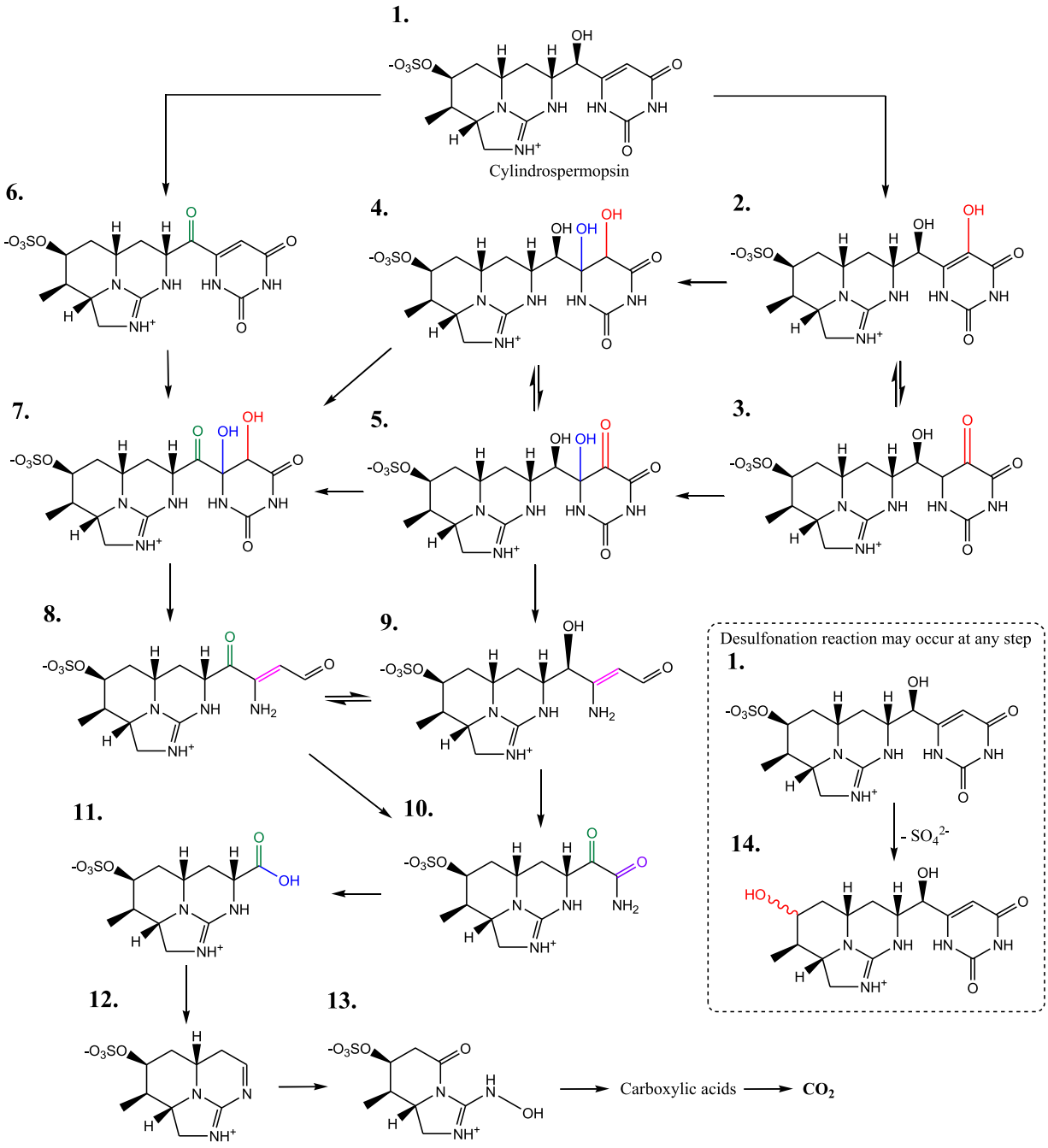

Fig. 4. Photocatalytic degradation pathway of CYN (Chen et al., 2015; Fotiou et al., 2015).

by further hydroxylation to give **7**. Whereas, hydrogen abstraction by •OH requires electron rich substrates and it is relatively slow compared to •OH addition (Fotiou et al., 2015). Subsequent oxidation steps induce the uracil cleavage yielding N-species into solution such as ammonia, nitrate, or N-organics (i.e. formamide) and tricyclic guanidine derivatives **8** and **9**. Oxidation of the side chain leads to formation of intermediates **10** - **12**. Cleavage of tricyclic guanidine cycle mediated by •OH and other oxidants forms **13**, which degradation is followed by the release of low molecular weight carboxylic acids and eventually complete mineralization into CO_2 and inorganic ions sulfate, ammonia, and nitrate (Fotiou et al., 2015). Note that desulfonation reaction mediated by •OH addition can take place at any step (exemplified in the inset panel of Fig. 4).

Toxicity steadily decreases during treatment time, but there is residual activity until advanced degrees of samples mineralization (Chen et al., 2015). These results allow inferring that the by-products formed during the photocatalytic treatment may have analogous biological activity to the parent compound CYN. In contrast to MC, complete cleavage of uracil and tricyclic guanidine cycles of CYN must be attained to diminish toxicity.

5. Photocatalytic degradation of cyanotoxins

5.1. Photocatalytic performance

Complete abatement of cyanotoxins has been attained with photocatalytic treatment with reported kinetic constants ranging

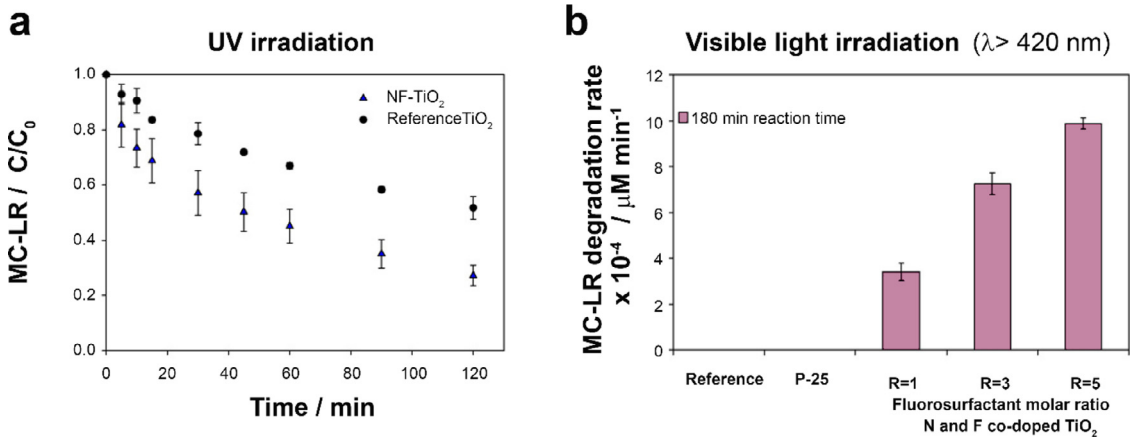

Fig. 5. (a) Photocatalytic degradation of MC-LR at pH 3.0 under UV irradiation with NF-TiO_2 and reference TiO_2 films under 4.6×10^{-5} W cm^{-2} irradiance. (b) MC-LR degradation rate at pH 3.0 with reference TiO_2, commercial P-25 TiO_2, and NF-TiO_2 photocatalysts films after 180 min of visible light irradiation ($\lambda > 420$ nm) under 7.8×10^{-5} W cm^{-2} irradiance.
Reproduced with permission from reference (Pelaez et al., 2010).

from 10^{-3} min^{-1} to 10^{-1} min^{-1} as summarized in Tables 1–3. However, experimental data is hard to compare due to the wide differences in experimental conditions that influence removal performance (*i.e.*, pH, catalyst dose, irradiance, lamp source, etc.) that explain such wide variability of orders of magnitude on kinetic constants.

Titania (TiO_2) has been the most extensively investigated photocatalyst among photoactive semiconductor materials for cyanotoxins abatement (Andersen et al., 2014; Pestana et al., 2015; Robertson et al., 2012; Sharma et al., 2012; Zhang et al., 2014b). The wide bandgap of TiO_2 (3.2 eV for anatase, 3.0 eV for rutile, and ~3.2 eV for brookite) limits its application to UV light sources (El-Sheikh et al., 2017; Han et al., 2011; Pelaez et al., 2012). Thus, extensive research efforts have been devoted to pure TiO_2 modification to enable visible light/natural sunlight photoactivity. Doping of pure semiconductors can decrease their bandgaps and activate a photocatalytic response within the visible light spectra. The semiconductor lattice and the relative atomic size of the dopant define two different classes of doping: (i) interstitial, and (ii) substitutional. Interstitial doping is generally observed in TiO_2 lattices (i.e., rutile and anatase) when doping with non-metal elements such as carbon, nitrogen, fluoride, or sulfur (Asahi et al., 2001; Chen and Mao, 2007; Serpone, 2006; Umebayashi et al., 2002; Yu et al., 2002). For example, Pelaez et al. have reported that TiO_2 photocatalysts co-doped with nitrogen and fluorine (NF-TiO_2) exhibited less bandgap energy than commercial P-25 TiO_2 (2.85 *vs.* 3.20 eV) (Pelaez et al., 2010). As shown in Fig. 5, after 180 min of visible-light irradiation, no MC-LR degradation could observed using reference TiO_2 and P-25 TiO_2, whereas non-negligible degradation was observable under UV irradiation. Conversely, the NF-TiO_2 photocatalyst achieved excellent photocatalytic degradation of MC-LR during the irradiation period. Meanwhile, metal dopants of larger atomic radius may replace Ti atoms in the lattice, such as observed with bismuth or rhodium (Lv et al., 2009; Wei et al., 2009; Wu et al., 2009).

Conversely, a different alternative for visible light photoactive catalysts has been the nano-engineering of semiconductor/semiconductor or metal/semiconductor interfaces. The use of nanocomposites demonstrates synergistic effects between the different crystalline phases in terms of catalysts photoresponse and stabilization of charge carriers (Serrà and Philippe, 2020; Wang et al., 2014, 2013; Xiong et al., 2018). In other investigations, visible light-sensitive photocatalysts such as $ZnFe_2O_4$-, ZnO-, and Ag_2CrO_4-based ones have demonstrated success in photocatalysis by allowing the use of artificial visible light for the complete photodegradation of cyanotoxins, even when the UV light was filtered. Nevertheless, those strategies have often complicated synthesis that may hinder effective translation (Chen et al., 2012; Fan et al., 2020; Serrà et al., 2020b; Zhang et al., 2009). Nano-decoration of semiconductor with metals and other materials such as graphene oxide (GO) or graphitic carbon nitride (g-C_3N_4) are also widely explored (Lv et al., 2019; Oliveros et al., 2021; Sampaio et al., 2015b; Tugaoen et al., 2017). The individual components of the composite usually remain separate and distinct within the finished photocatalytic material. The formation of an interface can modify the space-charge region near due to the higher electron affinity of the conductive material (i.e., metal, GO, g-C_3N_4), which makes these materials behave as electron sinks. The Schottky barrier potential formed at the interface delays the recombination of charge carriers and extends the time of life of e_{cb}^- and h_{VB}^+. Apart from the electron trapping mechanism enabled when considering photocatalyst nano-decoration with a conductive material, the formation of such interface can in some cases contribute to achieving a *pseudo*-lower band gap that allows for lower excitation energies (Kochuveedu et al., 2013).

The high competitiveness of photocatalysis as a remediation technology for cyanotoxin polluted water sources is clearly supported with experimental evidences. Unfortunately, these experiments are hardly benchmarked using comparative conditions nor considering engineering figures of merit. Future research efforts must consider a baseline of comparison to truly evaluate photocatalyst performance beyond the casuistic abatement of target cyanotoxins, in which techno-economic evaluation can assist researchers to define the road map for successful technology translation.

5.2. Role of pH on the photocatalytic performance and removal kinetics

The pH of water bodies plays a vital role in the photocatalytic degradation of cyanotoxins due to several physicochemical phenomena governed by pH. Herein it is discussed the effect of pH on catalyst surface characteristics and its interaction with target pollutants.

In aqueous environments, the surface charge of a semiconductor is attributed to two mechanisms: (i) the amphoteric dissociation of surface MOH groups; and (ii) the adsorption of primary hydroxo complexes and other functional groups. Both mechanisms

Table 1
Operational conditions for and catalytic performance of the photodegradation of MCs.

Concentration / ppm	pH	Photocatalyst	Dose / g L^{-1}	Volume / mL	Light source	Irradiance	Removal / %	Time of treatment / min	k_1 / min^{-1}	k / min^{-1} g^{-1}	Ref
UV- driven photocatalysts											
1.0	3.0	TiO_2 films	5.0	10	2 15 W	35×10^{-6} W cm^{-2}	100	30	1.5×10^{-1}	~3.0	(Antoniou et al., 2008a)
10	3.0	$BiWO_3$-Ph1.0	0.2	5	100 W LP Hg	n.a.	100	30	1.3×10^{-1}	~130	(Chen et al., 2012)
0.2	4.0	TiO_2 P-25	10	n.a.	Xe 280 W 330-450 nm	n.a.	100	8	$\sim 6.8 \times 10^{-1}$	*n.a.*	(Cornish et al., 2000)
0.2	4.0	TiO_2 P-25	10	10	Xe 480 W 330-450 nm	2.48×10^5 Einstein min^{-1}	97	10	*n.a.*	*n.a.*	(Lawton et al., 2003)
							100	30	*n.a.*	*n.a.*	
0.2	4.0	TiO_2 P-25	10	10	Xe 480 W 330-450 nm	2.48×10^5 Einstein min^{-1}	53	10	*n.a.*	*n.a.*	(Lawton et al., 2003)
							83	30	*n.a.*	*n.a.*	
0.2	4.0	TiO_2 P-25	10	10	Xe 480 W 330-450 nm	2.48×10^5 Einstein min^{-1}	100	10	*n.a.*	*n.a.*	(Lawton et al., 2003)
0.2	4.0	TiO_2 P-25	10	10	Xe 480 W 330-450 nm	2.48×10^5 Einstein min^{-1}	100	10	*n.a.*	*n.a.*	(Lawton et al., 2003)
10	4.0	C/N/S-TiO_2	0.4	40	UV-A (max = 365 nm)	2×10^{-3} W cm^{-2}	100	15	0.26	~16	(Light and Using, n.d.)
80	4.0	TiO_2 P-25	10	n.a.	Xe 280 W 330-450 nm	n.a.	100	50	8.8×10^{-2}	*n.a.*	(Robertson et al., 1998)
5	5.6	TiO_2-P-25 PMS-4mg/L	0.01	10	Xe UVA	9.88 10^{-3} W	100	5	*n.a.*	*n.a.*	(Antoniou et al., 2018)
0.56	6.4	TiO_2 P-25	1	20	HP Hg 100 W	55×10^{-3} W cm^{-2}	100	40	4.4×10^{-2}	~2.2	(Feitz et al., 1999)
1	6.5	TiO_2 P-25	0.05	40	4 UV-LED 1.6 W 365 nm	28.6×10^{-3} W cm^{-2}	99.9	15	0.261	~130	(Yang et al., 2020)
2.0	6.8	TiO_2 films	0.14	10	2 15 W	35×10^{-6} W cm^{-2}	~37.5	240	$\sim 2.1 \times 10^{-3}$	~1.4	(Antoniou et al., 2009)
	3.0						~92	240	$\sim 8.8 \times 10^{-3}$	~5.0	
0.01	n.a.	TiO_2 P25	1	*n.a.*	Xe 480 W 250-600 nm	11×10^{-3} W cm^{-2}	100	45	n.a.	n.a.	(Liu et al., 2009)
Visible light- driven photocatalysts											
0.5	3.0	NF-TiO_2 films	n.a.	n.a.	15 W fluorescent (UV filter)	7.81×10^{-5} W cm^{-2}	75	120	$\sim 1.3 \times 10^{-2}$	n.a.	(Pelaez et al., 2010)
0.5	3.0	TiO_2 P-25 film	n.a.	n.a.	15 W fluorescent (UV filter)	7.81×10^{-5} W cm^{-2}	47	120	$\sim 6.1 \times 10^{-3}$	n.a.	(Pelaez et al., 2010)
0.5	3.0	S-TiO_2 films	n.a.	n.a.	15 W fluorescent (UV filter)	9.05×10^{-5} W cm^{-2}	60	720	n.a.	n.a.	(Han et al., 2011)
0.5	3.0	NF-TiO_2	n.a.	n.a.	15 W fluorescent (UV filter)	7.81×10^{-5} W cm^{-2}	100	240	$\sim 6.3 \times 10^{-2}$	n.a.	(Pelaez et al., 2011)
0.5	3.0	NF-TiO_2	n.a.	n.a.	2 × 15W Fluorescent	7.81×10^{-5} W cm^{-2}	50	300	n.a.	n.a.	(Likodimos et al., 2013)
		S-TiO_2	n.a.	n.a.			70	300	n.a.	n.a.	
0.5	3.0	CN-TiO_2	n.a.	20	2 × 15W Fluorescent	9.05×10^{-5} W cm^{-2}	75	300	n.a.	n.a.	(Liu et al., 2013)
0.6	3.0	N-TiO_2	1	n.a.	2 × 15W Fluorescent	7.5×10^{-5} W cm^{-2}	100	300	$\sim 2.8 \times 10^{-3}$	n.a.	(Livraghi et al., 2013)
2	3.0	Bi-TiO_2	0.25	n.a.	500 W halogen	n.a.	80	120	$\sim 1.3 \times 10^{-2}$	n.a.	(Yang et al., 2011)
							100	720	n.a.	n.a.	
2	3.0	TiO_2-P-25	0.25	n.a.	500 W halogen	n.a.	50	720	n.a.	n.a.	(Yang et al., 2011)
10	4.0	C/N/S-TiO_2	0.4	40	LED (max = 420 nm)	1×10^{-3} W cm^{-2}	100	180	0.04	~2.5	(Light and Using, n.d.)
100	4.0	TiO_2 P-25	10	5	500 W halogen	393 μM^{-1}	40	60	n.a.	n.a.	(Graham et al., 2010)
100	4.0	TiO_2-Rh(III)	10	5	500 W halogen	393 μM^{-1}	100	60	n.a.	n.a.	(Graham et al., 2010)
100	4.0	TiO_2-C	10	5	500 W halogen	393 μM^{-1}	80	60	n.a.	n.a.	(Graham et al., 2010)
100	4.0	TiO_2-Pt	10	5	500 W halogen	393 μM^{-1}	90	60	n.a.	n.a.	(Graham et al., 2010)
0.3	5.0	Ag_2CO_3-GO	250	20	Xe	n.a.	100	60	n.a.	n.a.	(Fan et al., 2020)
0.3	5.0	Ag_2CrO_4-GO	250	20	Xe	n.a.	100	150	n.a.	n.a.	(Fan et al., 2020)
0.5	5.0	$BiVO_4/TiO_2$	0.5	10	15 W LED	n.a.	98	90	n.a.	n.a.	(Jafari et al., 2020)

(*continued on next page*)

Table 1 (*continued*)

Concentration / ppm	pH	Photocatalyst	Dose / g L^{-1}	Volume / mL	Light source	Irradiance	Removal / %	Time of treatment / min	k_1 / min^{-1}	k / min^{-1} g^{-1}	Ref
2	5.0	TiO_2	0.5	20	300 W Xe	0.150 W cm^{-2}	10	120	0.0009	~0.09	(Khadgi and Upreti, 2019)
2	5.0	$ZnFe_2O_4$	0.5	20	300 W Xe (UV filter)	0.150 W cm^{-2}	20	120	0.0021	~0.21	(Khadgi and Upreti, 2019)
2	5.0	$ZnFe_2O_4$-Ag	0.5	20	300 W Xe (UV filter)	0.150 W cm^{-2}	40	120	0.0046	~0.46	(Khadgi and Upreti, 2019)
2	5.0	$ZnFe_2O_4$-/rGO	0.5	20	300 W Xe (UV filter)	0.150 W cm^{-2}	55	120	0.007	~0.7	(Khadgi and Upreti, 2019)
2	5.0	$ZnFe_2O_4$-Ag/rGO	0.5	20	300 W Xe (UV filter)	0.150 W cm^{-2}	100	90	0.0515	~5.15	(Khadgi and Upreti, 2019)
0.45	5.7	TiO_2-G-$NiFe_2O_4$	1	*n.a.*	2 × 15W Fluorescent	7.81×10^{-5} W cm^{-2}	100	300	7.8×10^{-3}	*n.a.*	(Pelaez et al., 2013)
0.5	5.7	SNC-TiO_2	0.5	10	2 × 15W Fluorescent	1.33×10^{-3} W cm^{-2}	80	300	$\sim 2.5 \times 10^{-3}$	~0.5	(Zhang et al., 2014a)
0.2	5.7	Nanodiamond-TiO_2	0.5	10	Xe 300 W	47.1×10^{-3} W cm^{-2}	100	20	4.4×10^{-1}	~88	(Sampaio et al., 2015a)
0.2	5.7	TiO_2	0.5	10	Xe 300 W	47.1×10^{-3} W cm^{-2}	100	120	2.8×10^{-2}	~5.6	(Sampaio et al., 2015a)
10	5.7	N-TiO_2	0.2	*n.a.*	4 F15W/T8 black tubes	71.7×10^{-3} W cm^{-2}	96	20	$\sim 1.8 \times 10^{-1}$	*n.a.*	(Triantis et al., 2012)
10	5.7	TiO_2 P-25	0.2	*n.a.*	4 F15W/T8 black tubes	71.7×10^{-3} W cm^{-2}	100	12	$\sim 4.6 \times 10^{-2}$	*n.a.*	(Triantis et al., 2012)
0.5	5.8	S-TiO_2	*n.a.*	*n.a.*	2 × 15W Fluorescent	9.05×10^{-5} W cm^{-2}	75	300	$\sim 2.3 \times 10^{-3}$	*n.a*	(Han et al., 2014)
0.5	5.8	SNC-TiO_2	0.5	10	2 × 15W Fluorescent	1.33×10^{-3} W cm^{-2}	100	300	9.5×10^{-3}	~2	(El-Sheikh et al., 2014)
0.5	5.8	α-Fe_2O_3/γ-Fe_2O_3 nanopowders	0.5	10	2 Cole-Parmer 15-W fluorescent	3.99×10^{-4} W cm^{-2}	60	300	$\sim 1.4 \times 10^{-3}$	~0.28	(Han et al., 2017)
10	5.8	TiO_2 P-25	0.2	5	4 F15W/T8 black tubes	71.7×10^{-6} W cm^{-2}	100	10	$\sim 4 \times 10^{-1}$	~40.2	(Fotiou et al., 2016)
3.1	5.9	$Bi_3Nb_{0.6}Ta_{0.4}O_7$	1.5	100	200W Dy LAMO	n.a.	92	240	*n.a.*	*n.a.*	(Zhang et al., 2009)
0.1	7.0	TiO_2-P-25/ H_2O_2	films	2400	1700 W air-cooled Xe arc	500 W m^{-2}	100	100	*n.a.*	*n.a.*	(Pinho et al., 2015b)
Sunlight											
10	4.0	C/N/S-TiO_2	0.4	40	SOL1200	20×10^{-3} W cm^{-2}	100	60	0.11	~6.9	(Light and Using, n.d.)
0.1	6.0	TiO_2	0.2	*n.a.*	Sun	500 lux	100	360	n.a.	*n.a.*	(Pinho et al., 2015a)
50	*n.a.*	AgBr/Ag_3PO_4/TiO_2	0.1	30	Simulated solar lamp	4 W m^{-2}	96	60	0.64	*n.a.*	(Wang et al., 2015)
0.5	6.0	TiO_2–Graphene@Fe_3O_4	0.5	20	Sun	*n.a.*	93	50	*n.a.*	*n.a.*	(Liang et al., 2014)

Table 2
Operational conditions for and catalytic performance of the photodegradation of CYNs.

Concentration / ppm	pH	Photocatalyst	Dose / g L^{-1}	Volume / mL	Light source	Irradiance	Removal / %	Time of treatment / min	k_1 / min^{-1}	k / min^{-1} g^{-1}	Ref
UV- driven photocatalysts											
0.1	4.0	TiO_2 P-25	0.1	*n.a.*	UV	17.5×10^{-6} W cm^{-2}	100	5	9.4×10^{-1}	*n.a.*	(Senogles et al., 2001)
0.1	4.0	TiO_2 Hombikat	0.1	*n.a.*	UV	17.5×10^{-6} W cm^{-2}	95	15	2.1×10^{-1}	*n.a.*	(Senogles et al., 2001)
4	4.0	TiO_2 P-25	0.1	30	Hg (blazed at 350 nm)	1.12×10^{6} photons s^{-1} cm^{-3}	100	10	8.7×10^{-1}	~290	(Chen et al., 2015)
Visible light- driven photocatalysts											
10	5.7	TiO_2 P-25	0.2	5	4 F15 W/ T8 black tubes	71.7×10^{-6} W cm^{-2}	100	15	*n.a.*	*n.a.*	(Fotiou et al., 2015)
10	5.7	TiO_2 P-25	0.2	5	Oriel AM1.5 G	85×10^{-3} W cm^{-2}	100	30	*n.a.*	*n.a.*	(Fotiou et al., 2015)
10	5.7	TiO_2 P-25	0.2	5	Photomax (435 nm cut-off filter)	107×10^{-3} W cm^{-2}	10h	5	*n.a.*	*n.a.*	(Fotiou et al., 2015)
10	5.7	Kronos vlp-7000	0.2	5	4 F15 W/ T8 black tubes	71.7×10^{-6} W cm^{-2}	100	40	*n.a.*	*n.a.*	(Fotiou et al., 2015)
10	5.7	TiO_2 P-25	0.2	5	Oriel AM1.5 G	85×10^{-3} W cm^{-2}	100	120	*n.a.*	*n.a.*	(Fotiou et al., 2015)
10	5.7	TiO_2 P-25	0.2	5	Photomax (435 nm cut-off filter)	107×10^{-3} W cm^{-2}	25	600	*n.a.*	*n.a.*	(Fotiou et al., 2015)
10	5.8	TiO_2 P-25	0.2	5	4 F15 W/ T8 black tubes	71.7×10^{-6} W cm^{-2}	100	10	2.1×10^{-1}	~360	(Fotiou et al., 2015)
0.07	7.0	TiO_2 P-25 H_2O_2 (25 mg/L)	films	2400	1700 W Xe arc	500×10^{-3} W cm^{-2}	100	*n.a.*	*n.a.*	*n.a.*	(Pinho et al., 2015b)
0.4	7.0	TiO_2	0.25	*n.a.*	2 Fluorescent (310–720 nm)	2.37×10^{-3} W cm^{-2}	100	15	$\sim 1.8 \times 10^{-1}$	*n.a.*	(El-Sheikh et al., 2017)
0.4	7.5	TiO_2	0.5	10	2×15W Fluorescent	2.4×10^{-6} W cm^{-2}	100	10	$\sim 1.8 \times 10^{-1}$	~36	(Zhang et al., 2014a)
Sunlight											
0.07	7.0	TiO_2	0.1	*n.a.*	Solar irradiation	50×10^{-3} W cm^{-2}	50	360	*n.a.*	*n.a.*	(Pinho et al., 2015a)

Table 3
Operational conditions for and catalytic performance of the photodegradation of various cyanotoxins.

Cyanotoxin	Concentration / ppm	pH	Photocatalyst	Dose / g L^{-1}	Volume / mL	Light source	Irradiance	Removal / %	Time of treatment / min	k_1 / min^{-1}	k / min^{-1} g^{-1}	Ref
Nodularin	1000	*n.a.*	TiO_2 P-25	0.01	10	Xe UV- 480 W (330-450 nm)	1.91×10^{-5} Einstein s^{-1}	100	20	*n.a.*	*n.a.*	(Liu et al., 2005)
6-hydroxymethyl uracil	5	7.0	NF-TiO_2	0.05	150	350 nm Lamp	*n.a.*	100	120	3.5×10^{-2}	~4.7	(Zhao et al., 2014)
6-hydroxymethyl uracil	5	7.0	PF-TiO_2	0.05	150	350 nm Lamp	*n.a.*	100	240	1.7×10^{-2}	~2.3	(Zhao et al., 2014)
6-hydroxymethyl uracil	5	7.0	S-TiO_2	0.05	150	350 nm Lamp	*n.a.*	80	240	7.3×10^{-3}	~0.97	(Zhao et al., 2014)
Anatoxin-a	5	7.0	Ni@ZnO@ZnS-Spirulina	0.6	5	Xe lamp	680 lux	97.4	120	7.2×10^{-2}	24.2	(Serrà et al., 2020b)

are governed by the solution's pH (Henderson, 2011; Thiel and Madey, 1987). The pH at which the net surface charge of photocatalysts becomes neutral is called the isoelectric point (IEP) or point of zero charge (pH_{pzc}). The pH_{pzc} depends on the intrinsic nature of the semiconductor material being used and its composition (Gaya and Abdullah, 2008; Haque and Muneer, 2007; Lee et al., 2016; Mrowetz and Selli, 2006). For example, TiO_2- based photocatalysts present pH_{pzc} of ~6.2. Whereas, ZnO-based materials have a higher pH_{pzc} close to ~ 9.0. For metal-oxides (MOH) with predominantly oxygen terminated groups, the net surface charge of photocatalysts is positive in solutions with pH below pH_{pzc} since terminal groups are protonated and positively charged as deduced from Eq. (6). Conversely, surface is negatively charged in solution with pH higher than the pH_{pzc} since terminal groups are deprotonated according to reaction (7) (Gaya and Abdullah, 2008; Haque and Muneer, 2007; Lee et al., 2016; Mrowetz and Selli, 2006).

$$MOH + H^+ \leftrightharpoons MOH_2^+ \quad pH < pH_{pzc} \tag{6}$$

$$MOH \leftrightharpoons MO^- + H^+ \quad pH > pH_{pzc} \tag{7}$$

Surface charge of photocatalyst nanoparticles generates electrostatic repulsion between them which enhances their stability in slurries. At pH close to the pH_{pzc} value in which surface is not-charged, nanoparticles may tend to agglomerate. It is observed that suspended particles become larger in diameter due to formation of flocs, which minimizes available surface area and photocatalytic efficiency for a given mass of catalyst (Gaya and Abdullah, 2008; Haque and Muneer, 2007; Lee et al., 2016; Mrowetz and Selli, 2006).

Solution pH has a direct influence on the speciation of cyanotoxins. The ratio of the different charged and non-charged species is determined by the respective pK_a values of each cyanotoxin. Significant differences on pK_a can be seen in Table 4 between the main cyanotoxins: (i) MCs, (ii) CYN, and (iii) anotoxin-a (Antoniou et al., 2008a; De Maagd et al., 1999; Pinho et al., 2015b).

The interplay between target cyanotoxin speciation and surface charge are instrumental in photocatalysis. Heterogeneous processes occur at the interface of the catalyst and are governed by the mass transfer of species from/towards the catalyst surface. As discussed previously, the adsorption of cyanotoxins (or at least close interaction with the surface) is essential to ensure effective degradation. Fig. 6 illustrates the critical impact of pH on the photocatalytic degradation kinetics of MC-LR under identical conditions (Pinho et al., 2015b). It can be observed that complete abatement is attained in short treatment times at acidic pH (i.e., pH = 3.0) but drastically decreases at higher pH conditions. Under acidic conditions, TiO_2 surface remains positively charged, which enable electrostatic attraction of zwitterionic and negatively charged MC-LR species. Noteworthy is the transition zone between acidic pH-pH_{pzc} in which MC-LR degradation is still competitive and occurs within natural pH range. When increasing pH above TiO_2 pH_{pzc} of ~6.2, a complete transition towards negatively charged surface occur, whereas MC-LR speciation remains negatively charged (Antoniou et al., 2009; Feitz et al., 1999; Yang et al., 2020). Under such conditions, electrostatic repulsion hinders adsorption and decreases photocatalytic degradation performance. These noticeable differences on MC-LR degradation in function of pH impelled researches to focus their studies on MCs degradation at acidic pH. Application of these conditions to treat natural waters (pH 5.0-8.0) would require acid addition prior treatment, followed by base neutralization prior release of treated effluent. However, compromise solutions to treat large volumes of natural water may be required when translating technology towards true environmental remediation.

Table 4
Dominant species of cyanotoxins at different pH.

Cyanotoxin	Dissociation constants	pH	Dominant species	Net charge of cyanotoxin
MC-LR	$pK_{a1} = 2.09$	pH < 2.09	$(COOH)_2(NH_2^+)$	positive
	$pK_{a2} = 2.19$	2.09 < pH < 2.19	$(COO^-)(COOH)(NH_2^+)$	neutral
	$pK_{a3} = 12.48$	2.19 < pH < 12.48	$(COO^-)_2(NH_2^+)$	negative
		pH>12.48	$(COO^-)_2(NH_2)$	negative
CYN	$pK_a = 8.8$	pH < 8.8	(OSO_3^-) $(CH_5N_3^+)$	neutral
		pH > 8.8	(OSO_3^-) (CH_5N_3)	negative
Anatoxin-a	$pK_a = 9.36$	pH < 9.36	(NH_2^+)	positive
		pH > 9.36	(NH_2)	neutral

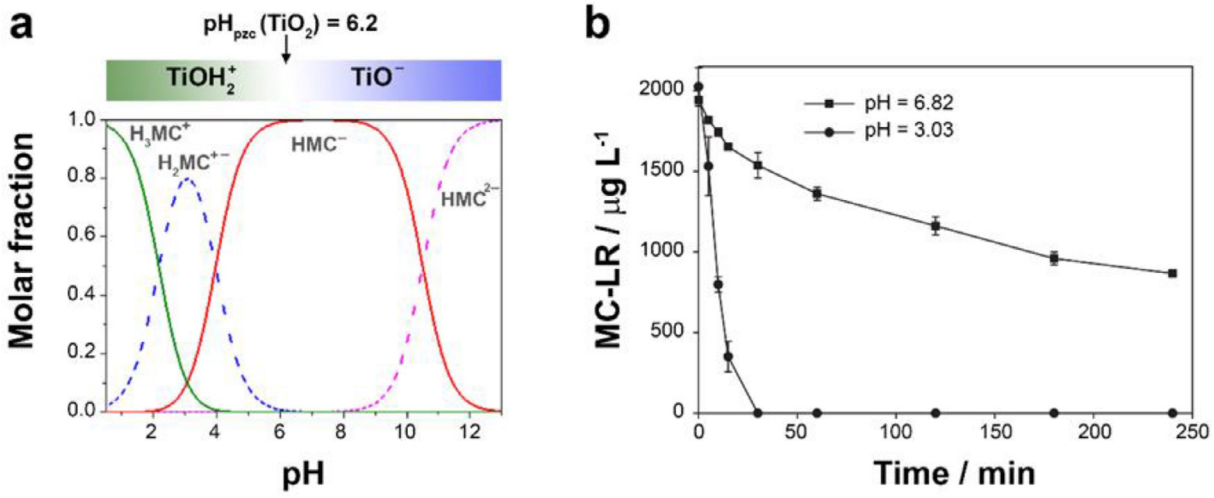

Fig. 6. (a) Speciation of MC-LR as a function of pH. Reproduced with permission from reference (Pinho et al., 2015b). (b) Effect of pH on the photocatalytic degradation of MC-LR using TiO_2 films under UV irradiation at 35 μW cm^{-2}.
Reproduced with permission from reference (Antoniou et al., 2008a).

In the case of CYN, the rate of photocatalytic degradation does not usually strongly depend on pH. Based on the pK_a of CYN, the zwitterionic toxin is the primary specie at pH values lower than 8.8. In this range of pH, the electrostatic interaction with $TiOH_2^+$ (pH < 6.2) and TiO^- (pH > 6.2) does not govern the photocatalytic performance (Chen et al., 2015; El-Sheikh et al., 2017; Pinho et al., 2015b; Zhang et al., 2014a). For TiO_2 or TiO_2-based photocatalysts, the optimum conditions are expected to be slightly basic or slightly acid to prevent the photocatalyst agglomeration. Values of pH higher than 8.8 may be detrimental, as both photocatalyst surface and cyanotoxin are negatively charged. Nevertheless, it should also be noted that research on the topic to date has overwhelmingly focused on the degradation of CYN only in relatively acidic conditions. It is important to remark that photocatalytic degradation of CYN performance is insensitive to pH variations within the range of natural waters pH (5.0 -8.0). CYN photocatalytic treatment can be conducted without requiring pH adjustments for operation. Meanwhile in the case of anatoxin-a, the optimum conditions are expected to be neutral and slightly basic—pH values ranging from 6.2 to 9.4 —due to the stronger adsorption of positively charged cyanotoxins on the negatively charged photo-catalyst's surface, hence faster degradation.

5.3. Photocatalyst dosage impacts performance and technology translation

Photocatalyst dose for optimal operation is a parameter that is thoroughly evaluated in research articles. It is obvious that this parameter is directly related to capital expenses in terms of the cost of semiconductor materials ($ kg^{-1}) required for water purification. Indeed, photocatalyst dose impacts competitiveness beyond cost of material (Gaya and Abdullah, 2008; Lee et al., 2016). The performance of heterogeneous processes depends on the availability of catalytic sites and on the total surface area (i.e., higher mass loading). However, such a simplistic view disregards effects associated to effective light transport. Excessive catalyst doses can cause undesired effects. First, high loading of catalysts can increase solution opacity and significantly decrease light penetration depth. This effect may induce dead zones where catalyst loading will not be photo-activated due light hindering. Second, high mass of catalyst in suspension may induce particle aggregation, which diminishes significantly active surface area (Chatzitakis et al., 2008; Hayat et al., 2011; Kositzi et al., 2007; Mrowetz and Selli, 2006).

Experimental observations suggest optimum doses of photocatalysts up to 1.0 g L^{-1} as summarized in Table 1–3. Slight differences may be observed in function of cyanotoxins initial concentration and the nature of photocatalyst material tested. It is important to remark that such tests are conducted in small volumes of water of few milliliters (ca. 5-20 mL) as summarized in Table 1–3. Photocatalytic treatment of cyanotoxins would be intended in principle for environmental remediation of lakes and large volumes of water. For example, the Lake Leman in Switzerland has an estimated volume of 89 km^3. While the and the Lake Michigan in the United States has an even larger volume of 4,918 km^3. As a rule of thumb assuming that dosage metrics are independent of the volume of water to be treated and considering a continuous treatment to decontaminate lake water, it is clear the huge amount of catalyst that may be required and/or the long times required for

high treatment volumes. These are obviously insane numbers that would raise questions regarding catalyst recovery from lakes after use. However, providing a big picture on such dimensions allows illustrating the need of designing optimized reactors that reuse semiconductor photocatalysts to solve a problem with a realistic approach.

5.4. Light source selection and photocatalyst activity

One of the fundamental elements in photocatalytic processes is the delivery of photons of energy required for charge carriers generation following reaction (1). Even though often overlooked, selection of light source impacts photodegradation kinetics and energy requirement. Pure photocatalysts of TiO_2 ($E_g = 3.20$ eV) and ZnO ($E_g = 3.37$ eV) present band-gaps photosensitive only in the UV domain (Ong et al., 2018; Pelaez et al., 2010; Pirhashemi et al., 2018). Hence, UV-emitting lamps within the range of 270-400 nm such as Xe and Hg lamps are the most common choice as irradiation source. Table 5 collects detailed information regarding characteristics of different UV-emitting lamps. To analyze the viability of the light source related to photocatalytic activity, the critical parameters to consider are energy consumption and irradiance.

On the one hand, energy consumption can be translated into the cost associated with photocatalytic treatment. Energy consumption is tightly related to the wattage of the lamp, which readily highlights Hg and Xe lamps in Table 5 as high-energy intensive sources. Engineering figures of merit such as electrical energy per order (EE/O) can provide a comparative magnitude between different lamps, although these are rarely reported for photocatalytic treatment of cyanotoxins. The EE/O magnifies the electric energy requirement to diminish target pollutant concentration (i.e., cyanotoxins) one order of magnitude in a unit of volume as calculated from Eq. (8) for batch or (9) for flow-through operation, respectively (Bolton et al., 2001; Cater et al., 2000):

$$\mathrm{EE/O}\left(\mathrm{kWhm^{-3}order^{-1}}\right) = \frac{Pt1000}{V \ \lg\left(c_i/c_f\right)} \rightarrow \text{batch} \tag{8}$$

$$\mathrm{EE/O}\left(\mathrm{kWhm^{-3}order^{-1}}\right) = \frac{P}{Q \ \lg\left(c_i/c_f\right)} \rightarrow \text{flow} - \text{through} \tag{9}$$

Where P is the rated power of the lamp in kW, t is the time of treatment in h, V is the volume in L, 1000 is a conversion factor (1000 L m^{-3}), Q is the flow rate in m^3 h^{-1}, and $\lg(c_i/c_f)$ is the decadic logarithm of the concentration decay in one order of magnitude. Note that the prior equations can be simplified when assuming pseudo first-order decay kinetics as it is defined by $\lg(c_i/c_f) = 0.4343 k_1 t$.

On the other hand, irradiance (W m^{-2}) indicates the power of the radiation incident per unit of surface area. Irradiance also directly relates to photon flux (photons m^{-2} s^{-1}), which influences the kinetics of degradation because photocatalysis is determined by the number of photons absorbed on the photocatalyst's surface. Another important parameter in selecting the light source is spectral irradiance ($Wm^{-2}\mu m^{-1}$), which corresponds to the irradiance of a surface per unit per wavelength (or frequency) (Duran et al., 2010; Marks and Doudrick, 2019; Valadés-Pelayo et al., 2015).

As shown in Tables 1–3, most studies are centered on the use of conventional light sources such as Hg and Xe lamps to irradiate commercial TiO_2 Degussa P-25. However, the use of high-pressure Hg and Xe lamps is energetically unsustainable since most of the

Table 5
Characteristics of the principal light sources.

Lamp	Spectral distribution / nm	Spectral range	Characteristic spectral lines / nm	Wattage / W	Luminous efficiency / Lumen W^{-1}	Energy consumption / kWh (1000 h)
High-pressure mercury	200 to 700	UV to Visible	313, 365, 366, 405, 407, 436, 546, 577 and 579	50-2000	40-96	90-2156
Low-pressure mercury	<280	UV-C predominant	185 and 254	18-240	30-60	22-290
UV-A lamps	300 to 360	UV-A (predominant) and UV-B	340	100	-	-
UV-B lamps	<280–340	UV-B (predominant) and UV-C and UV-A	313	80	-	-
Xenon	185 to 2600	UV to IR	Continuous spectrum from UV to visible	240-1800	36-55	258-1920
Fluorescent	160 to 2000	UV to Visible	Continuous	9-70	50-95	22-81
Halogen	185 to 2000	UV to Visible	Continuous	10-2000	10-22	13-1996
UV-LED	365	UV-A	365	1.6	60	0.26
White-LED	420 to 750	UV to Visible	Continuous	0.5-15	60-130	0.36-3.2
Natural sunlight	> 250	UV to IR	Smooth continuous spectrum from UV to visible	-	-	-

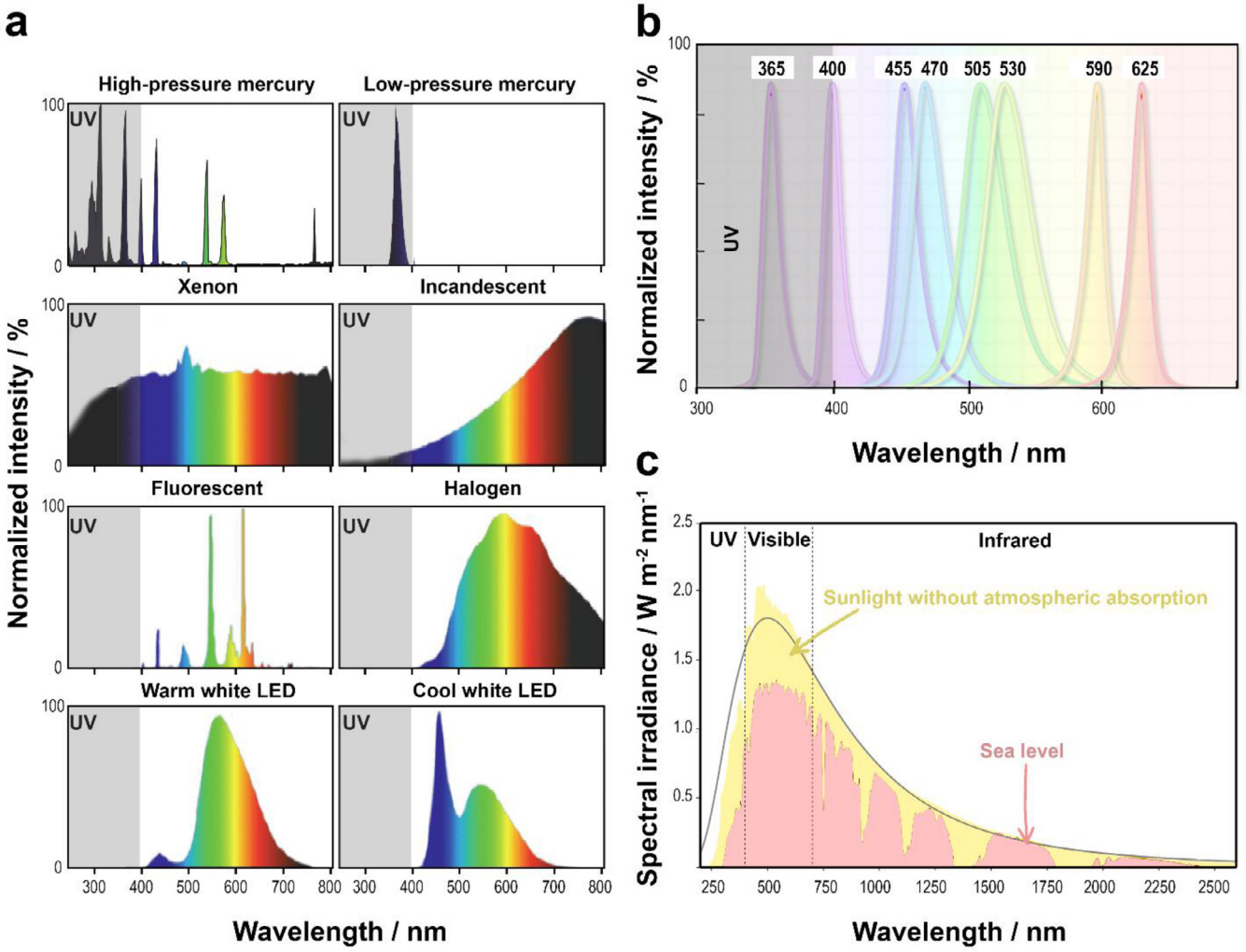

Fig. 7. (a) Typical normalized spectral of irradiance emitted by high-pressure mercury, low-pressure mercury, xenon, incandescent, fluorescent, halogen, warm white LED, and cool white LED lights.
Adapted with permission from reference (Kim et al., 2019). (b) Normalized spectral of irradiance of the currently available monochromatic LEDs. Adapted with permission from reference (Gustafsson et al., 2013). (c) Spectral of irradiance of sunlight above atmosphere on surface of Earth. Adapted with permission from reference (Nitoda et al., 2008).

photons delivered do not have enough energy for photoexcitation (Fig. 7**a**). Unfortunately, the spectral irradiance of other conventional light sources such as incandescent, fluorescent or halogen lamps, which can reduce the energy consumption, centers on the visible domain. In terms of energy consumption, the use of UV-driven photocatalysts is neither energy-efficient nor economically viable. The recent addition of LEDs to the water treatment toolbox brought alternative non-energy intensive light sources into play (Chen et al., 2017). Notably, LEDs are mercury-free systems, providing a safer and more environmentally friendly source of light. Conventional UV and UV-visible lamps typically contain 5 to 210 mg of Hg per lamp. Excellent performance has been reported on the use of LEDs in the photocatalytic treatment of cyanotoxins. For example, based on data reported in Table 1, using commercial TiO_2 Degussa P-25, EE/O of 23.5 kW h m^{-3} $order^{-1}$ and 4361 kW h m^{-3} $order^{-1}$ was needed when four 1.6-W UV-LEDs and a 100-W HP Hg lamp were used, respectively. In similar experimental conditions, the EE/O when UV-LEDs were used was approximately 186 times lower. These results highlight how LEDs become more competitive than conventional light sources. However, challenges remain on how to fully exploit LEDs while enhancing homogeneous light distribution in larger scale reactors. The development of light transport frameworks such as radial-emitting optical fibers show promising perspectives for LEDs/photocatalytic treatments (Lanzarini-Lopes et al., 2019; Tugaoen et al., 2017). More research on the photocatalytic degradation of cyanotoxins using LED technology is required prior to integrating photocatalyst synthesis and photoreactor design.

Prior to the appearance of technologies such as LEDs, photocatalytic research roadmap aimed the use of natural sunlight to reduce operational costs. Solar irradiation is a free and renewable source of photons. Nevertheless, Fig. 7**c** illustrates the low intensity of UV light in the solar spectra (<4.0%). The low irradiance of UV cannot substantially activate photocatalytic response in pure semiconductor materials (i.e., TiO_2, ZnO). To exploit that untapped resource, research efforts focused on the development of visible light-driven photocatalysis which harness solar energy as environmentally benign strategy to promote photocatalysis application. Tables 1–3 reports visible light active photocatalysts that can efficiently remove various cyanotoxins, including MC-LR and CYN, by using artificial visible light or even direct sunlight. Despite of this promising research steps, the complexity of using solar light and designing efficient solar photocatalytic reactors cannot be ignored.

5.5. Biomimicry based designs of photocatalysts for improved light trapping

The biomimetism and bioinspiration approach is one of the most promising challenges in materials design and fabrication for the coming years. Nature is a true school when it comes to developing basic or highly sophisticated materials and systems with improved properties. Natural structures are already optimized for defined functionalities and can inspire smart design of more effective materials. Biomimetic materials are artificial human-made materials that mimic the characteristics of natural materials. Beyond bioinspired design, biomimetic research also incorporates the principles of circular and green chemistry to enable a more sustainable and cleaner production of artificial materials (Sanchez et al., 2005; Serrà et al., 2019a; Wang et al., 2015; Zan and Wu, 2016).

In the context of photocatalysis, biomimetism could play an important role in the coming years for the development of architectures and systems for improved light trapping. Photocatalyst synthesis and design should be implemented with the intelligence of the sophisticated architectures and strategies of plants, algae, and photosynthetic bacteria. Photosynthetic organisms (*i.e.*, plants, algae, and certain types of bacteria) and photocatalysts use light as an energy source. However, photosynthetic organisms have developed, throughout centuries, cooperative light-harvesting mechanisms for the efficient photon capture of solar radiation (Qian et al., 2019a; Serrà et al., 2020a, 2020c, 2019b; Zhou et al., 2009).

In the context of fixed photocatalysts, fractal and flexible architectures have been proved as smart strategies in photocatalyst design. As shown in Fig. 8**a**, the phototropism mechanism (i.e., self-orientation towards the sun throughout the day) of the sunflower inspired the design of sunflower-like biomimetic omnidirectional trackers. This strategy found that the omnidirectional trackers were able to achieve up to 400% solar energy-harvesting improvement compared with non-phototropism materials at oblique illumination angles (Qian et al., 2019b). Natural hierarchical architectures such as plants and leaves exhibit excellent multilevel light scattering, high electron-diffusion length, open and accessible porosity, high surface-to-volume ratios, and high light absorption independent from the incident light angle. Therefore, mimicking their architecture and surface properties may result in improved light trapping. As shown in Fig. 8**b-c**, the porous morphology of artificial N-doped ZnO photocatalysts, inspired in the macro, micro, and nanoscale architecture of green leaves, increases light absorption by 84–131% (Zhou et al., 2009). As shown in Fig. 8**d**, fractal and dendritical architectures of ZnO-based photocatalysts mimicking fern leaves can drastically improve light harvesting, even at very high angles of incidence (Serrà et al., 2019b, 2019a).

In the context of non-fixed photocatalysts, algae and photosynthetic bacteria can also play an important role in the development of micro- and nano-architectured photocatalysts with improved self-propulsion mechanisms. As shown in Fig. 8**e**, the *Spirulina platensis* microalga was used as a biotemplate for the synthesis of magnetic biohybrid based on ZnO for the efficient integration of solar photocatalytic water decontamination and bioethanol production. The microalgae was selected due to its shape, which has been demonstrated effective for harvesting light as well as minimizing sedimentation and agglomeration (Serrà et al., 2020a, 2020b). Similarly, various shapes and architectures based on aquatic biota can inspire the design of new photocatalysts.

6. Decrypting water matrix effects on photocatalytic treatment of cyanotoxins

Cyanotoxins removal in ultrapure water has been a key stepstone to advance the understanding of photocatalytic technologies. However, the focus on such unrealistic water matrices may result in an overestimation of photocatalysis capabilities based on academic hype (Loeb et al., 2019). Evaluation of challenging conditions, even when showing unfavorable assessment in comparison to ideal conditions, will not preclude technology transfer opportunities. Conversely, realistic water matrix studies contribute to identify honest challenges and barriers to overcome. Thus, becoming essential elements to ensure successful translation to higher technology readiness levels and actual application.

Water sources contaminated with cyanotoxins (e.g. lakes, reservoirs, slow-moving rivers etc.) are heterogeneous mixtures of solutes and solids in suspension. Higher concentration of other organics may compete with cyanotoxins for photogenerated oxidants. Most natural waters contain natural buffers that limit versatility of easy pH modulation to unrealistic optimum pH conditions reported in Tables 1–3, such as high acidic pH 3.0. Modification of natural conditions may arise as a major hindrance when considering environmental remediation of lakes. This section discusses how photocatalytic degradation of cyanotoxins is critically influenced by characteristics of the water matrix, including: the presence of natural organic matter (NOM), alkalinity, and inorganic ions.

6.1. Critical influence of natural organic matter

Natural organic matter (NOM) not only derives from the natural breakdown of terrestrial plants (allochthonous plants) and as byproduct of aquatic biota (autochthonous plants) but may also result from human activities. NOM is an extremely complex mixture of organic compounds—humic substances, polysaccharides, amino sugars, proteins, peptides, lipids, protein, carbohydrates, carboxylic acid, amino acid, and hydrocarbons—with varying polarity, acidity, molecular mass, charge density, and biodegradability (Sillanpää et al., 2015; Yamamura et al., 2014; Zhang et al., 2009). Due to its complexity, NOM is usually categorized according to its polar (i.e., hydrophobic and hydrophilic) and acidic (i.e., acidic, neutral, or alkaline) properties. Of all organic compounds, hydrophobic acids, frequently described as humic substances, are the chief constituents of NOM in bodies of water. Humic substances consist of humic acids (HA), which are soluble in alkaline and insoluble in acid; fulvic acids, which are soluble in alkaline and acidic conditions; and humins, which are insoluble in both of those conditions (Bhatnagar and Sillanpää, 2017; Sillanpää et al., 2015).

Although ubiquitous, NOM occurs to varying degrees depending upon the climate, geology, biodiversity, and topography of each of Earth's zones, as well as varies spatially and temporally in concentration and composition. NOM appears in great quantities in bodies of water worldwide. Concentrations of NOM typically range from 2 to 10 mg L^{-1} in drinking water; however, its concentration is impossible to generalize in natural bodies of water due to the hydrological and biogeochemical processes that determine its formation (Matilainen et al., 2011, 2010; Metsämuuronen et al., 2014). For example, in Canada's rivers and lakes, concentrations ranging from 3 to 16 ppm are typical, whereas concentrations of dissolved NOM up to 59 mg L^{-1} have been detected in northern China's Lake Hulun, located in the sparsely populated Hulun Buir steppe, where minimal direct anthropic effects can be expected (Chen et al., 2012). In the photocatalytic decontamination of cyanotoxins, NOM has to be considered, for it can appear in high concentrations in water sources contaminated with cyanotoxins.

Humic substances can act as photosensitizers by the absorption of sunlight (290 nm – visible light). It has been reported that under irradiation humic acids may generate small amounts of reactive oxygen species (i.e. $^{\bullet}OH$, H_2O_2, etc.). This photoactivation event happens about 600 times per hour per humic molecule in mid-European natural waters during the summer (Hoigné et al., 1989). These natural photolytic effects are very slow and have negligible

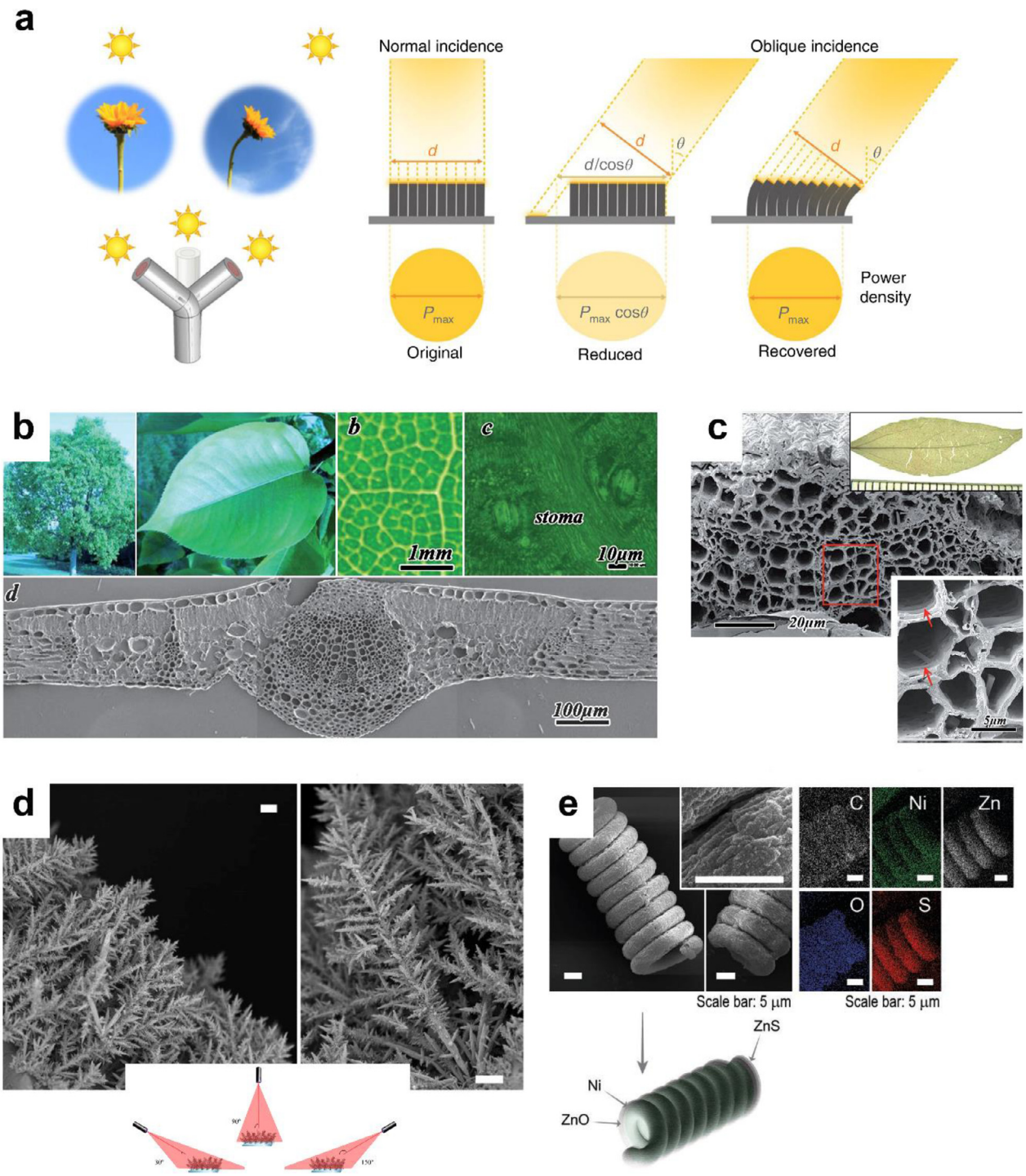

Fig. 8. (a) Schematic illustration of the of sunflower-like biomimetic omnidirectional trackers (Qian et al., 2019b). Copyright 2019, Nature publishing group. (b) *Cinnamomum camphora* leaf from macroscale to nanoscale (Zhou et al., 2009). Copyright 2009, Royal Society of Chemistry. FE-SEM micrographs of (c) the artificial N-doped ZnO photocatalyst system inspired from *Cinnamomum camphora* leaf (Zhou et al., 2009). Copyright 2009, Royal Society of Chemistry; (d) fern-like bioinspired microleaves of ZnO (scale bar: 5 μm (left) and 1 μm (right)). Reproduced with permission from reference (Serrà et al., 2019b); and (e) helical hybrid ZnO@ZnS photocatalytic systems inspired from the *Spirulina platensis* microalga (Serrà et al., 2020a). Copyright 2020, Wiley-VCH.

effects on cyanotoxins removal (half lifetime of about 10 h experimentally estimated for MC-RR) (Welker and Steinberg, 1999). Photocatalysis, in this regard, is not comparable to photocatalytic treatment that can degrade MCs in few minutes (see Table 1). Indeed, no photolytic degradation was observed by Pelaez et al. under visible light irradiation in presence of humic and fulvic substances but in absence of catalyst (Pelaez et al., 2011).

Yang et al. recently reported an excellent study on the effect of NOM during photocatalytic treatment of MC-LR by UV/TiO_2. Percentage of removal of MC-LR after 15 min decreased from 99.9 % in ultrapure water to 89.0% and 74.3 % for increasing NOM concentrations of 5 and 10 mg L^{-1}, respectively. Similar trend is observed when comparing the NOM effect on the kinetic rate decrease from 0.261 min^{-1} at 0.0 mg L^{-1} of NOM, 0.144 min^{-1} at 5.0 mg L^{-1}

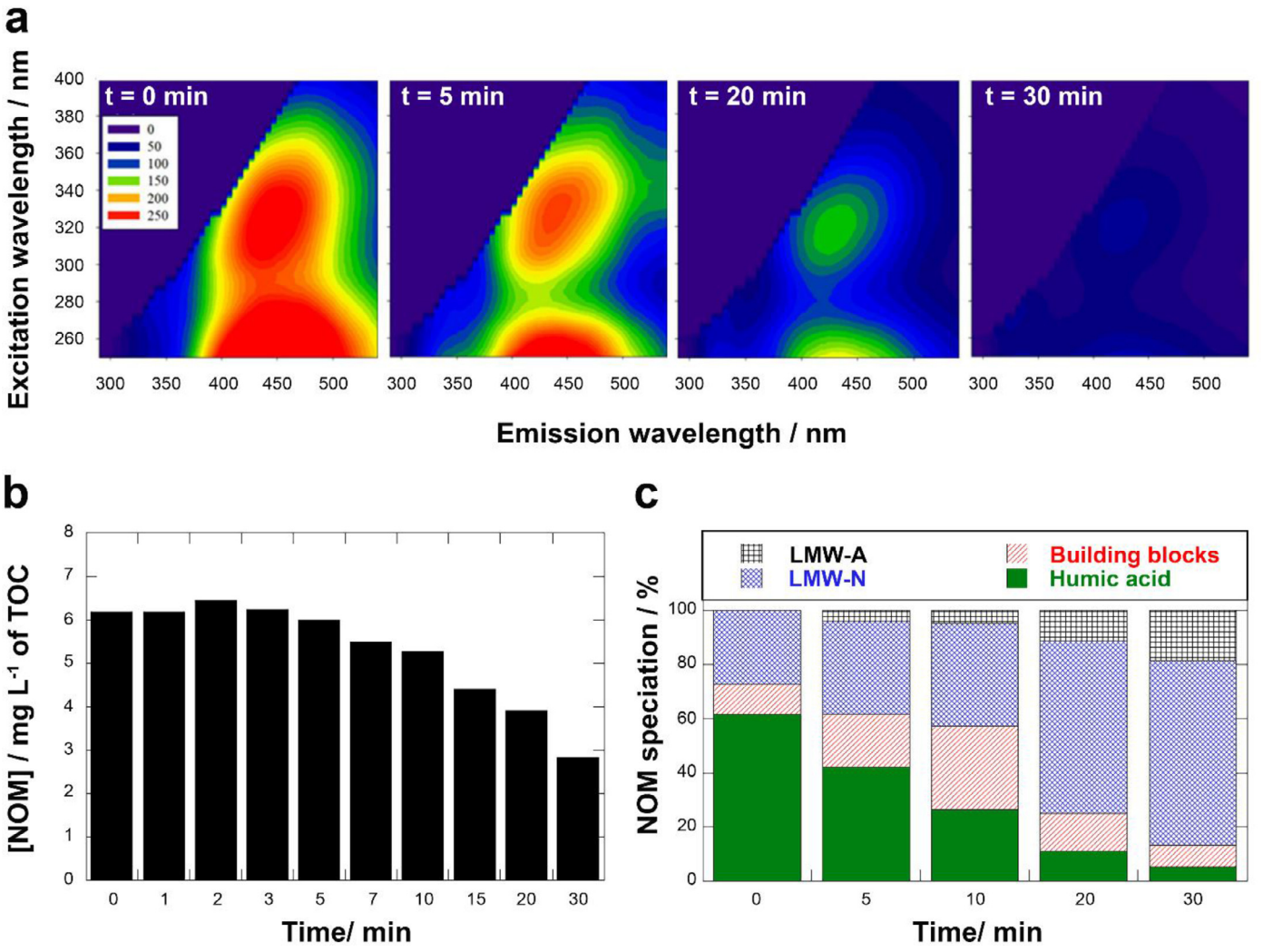

Fig. 9. Photocatalytic treatment of solutions containing 5.0 mg L^{-1} of NOM at pH. 6.5 by UV-LED/TiO_2 photocatalysis with 0.05 g L^{-1} of TiO_2 under 28.6 mW cm^{-2}: (a) Excitation emission fluorescence matrix (EEFM) spectroscopy contours during treatment, (b) NOM mineralization during treatment, and (c) relative speciation of NOM remaining TOC in solution at given treatment time. NOM species are classified as low molecular weight acids (LMW-A), low molecular weight neutral species (LMW-N), building blocks, and humic acids.
Adapted with permission from reference (Yang et al., 2020).

of NOM, and 0.113 min^{-1} at 10.0 mg L^{-1} of NOM. These results prove the inhibitory effect of NOM that can be associated to different factors such as (i) oxidants scavenging, (ii) nanoparticles aggregation induced by surface charge neutralization, and (iii) hindering of light transport (Feitz et al., 1999; Zhang et al., 2014a). However, the scavenging effect is considered to be the governing factor of the decrease of photocatalytic performance.

NOM can act as scavenger of photogenerated $^{\bullet}OH$, which decreases effective degradation of cyanotoxins in solution during photocatalytic treatment. Fig. 9**a** shows the excitation emission fluorescence matrix (EEFM) spectroscopy changes during photocatalytic treatment of samples containing 1 mg L^{-1} of MC-LR and 5 mg L^{-1} of NOM. EEFM is a sensitive and selective technique that process data on NOM fractions based on the differences between chromophores of dissolved organic matter. The EEFM contour plots show a shift on the fluorescence peak ($\lambda_{ex}/\lambda_{em} = 325/449$ nm) to shorter wavelengths ($\lambda_{ex}/\lambda_{em} = 325/431$ nm) till complete signal disappearance after 30 min of treatment. Fig. 9**b** shows the TOC decrease of NOM during photocatalytic treatment, attaining 53.6 % mineralization of initial 5 mg L^{-1} NOM. The decrease in fluorescence index observed during EEFM analysis reflected a decrease in aromaticity during photocatalytic treatment related to the cleavage of aromatic moieties. These results suggest that high molecular fraction of NOM is degraded to low molecular weight compounds as verified by organic carbon detection chromatography (LC-OCD) speciation of organics in solution illustrated in Fig. 9**c**. It can be observed that the most representative NOM were humic acids with close to a 60 % in content, that is drastically reduced to less than 5.0 % in remaining NOM. Whereas, the content of low molecular weight neutral and acid species increase in relative content. All these results demonstrate the scavenging role of NOM and identify humic acids as major competitor in the consumption of photogenerated oxidants (i.e., h_{vb}^{+}, $^{\bullet}OH$) (Yang et al., 2020).

NOM are complex since scavenging effect is also related to the relative content of humic and fulvic acids, as well as the solution pH. Experimental results of Pelaez demonstrate that photocatalytic inhibition is higher with fulvic acid than with humic acid at all pH conditions (see Table 6) (Pelaez et al., 2011). This trend can be explained by the higher adsorption of fulvic acids on TiO_2, which results in the direct competition with cyanotoxins for active sites and surface-generated oxidants. For instance, TiO_2 adsorption in dark conditions showed that 5.0 mg L^{-1} of Suwannee river humic acids achieve 30.1 % removal at pH 3.0, 22.5 % removal at pH 5.0, and 16.7 % removal at pH 7.0 after 5 h. Meanwhile higher re-

Table 6
Initial degradation rates of MC-LR after 120 min of visible light photocatalytic treatment with NF-TiO_2. Results show effect of Suwannee river humic acid (SRHA) and fulvic acids (SRFA) on degradation kinetics at different initial pH (Pelaez et al., 2011).

	[NOM] / mg L^{-1}	MC-LR initial reaction rate x 10^{-3} (μM min^{-1})		
		pH 3.0	pH 5.0	pH 7.0
	0	3.50 ± 0.02	2.29 ± 0.07	0.54 ± 0.02
SRHA	5.0	3.49 ± 0.02	2.31 ± 0.07	0.29 ± 0.03
	10.0	3.48 ± 0.05	2.27 ± 0.07	0.26 ± 0.06
SRFA	5.0	3.20 ± 0.06	2.12 ± 0.11	0.46 ± 0.03
	10.0	3.08 ± 0.06	2.01 ± 0.07	0.31 ± 0.06

movals were attained for 5.0 mg L^{-1} of Suwannee river fulvic acids corresponding to 55.1 % removal at pH 3.0, 32.3 % removal at pH 5.0, and 24.1 % removal at pH 7.0 after 5 h. Interestingly, lower kinetic removal of cyanotoxins is reported at higher pH despite of the lower adsorption of NOM (i.e., humic and fulvic acids). Pelaez et al. suggested that the coordination complex NOM-TiO_2 can mediate the electron transfer from the conduction band of TiO_2 to an appropriate electron acceptor, thus enhancing the stability of oxidants (Pelaez et al., 2011). This effect would compensate up to some extent the competitive consumption of oxidants by NOM, explaining the lower decrease observed on cyanotoxins removal rate at acidic pH. Whereas the scavenging effect becomes dominant at alkaline pH due to the lower adsorption of NOM (lower e_{cb}^- scavenging effect). These mechanisms require further research to fully understand the synergistic effect of NOM as electron scavenger.

Solution pH modifies electrostatic surface charge of the solid surface of metal oxides as well NOM speciation. As discussed above, surface of photocatalysts can be neutral, positively or negatively charged (Batista et al., 2017; Tugaoen et al., 2017). The transition between the different conditions is defined by the isoelectric point or point of zero charge (pH_{pzc}). In the case of TiO_2, the pH_{pzc} is ~ 6.2. Photocatalyst particles suspended in solutions of pH < pH_{pzc} are positively charged, meanwhile in solutions of pH > pH_{pzc} are negatively charged according to reactions (10) and (11), respectively. It has been reported that adsorbed NOM can neutralize surface charge of photocatalysts, which induce nanoparticles aggregation (Yang et al., 2020; Zhang et al., 2014a). Photocatalyst aggregation decreases available catalytic sites and irradiated photocatalyst surface, therefore decreasing photocatalytic degradation performance (Jefferson et al., 2016).

$$TiOH + H^+ \leftrightharpoons TiOH_2^+ \quad pH < pH_{pzc} \tag{10}$$

$$TiOH \leftrightharpoons TiO^- + H^+ \quad pH > pH_{pzc} \tag{11}$$

The third detrimental effect of NOM load in water is associated to decrease on photon delivery to the photocatalyst surface due to hindering of light transport from emission source (i.e. solar light, lamp, LED). Indeed, the photocurrent response of semiconductors is directly associated to the number of photons efficiently delivered per second (Garcia-Segura et al., 2018). Fig. 10 shows the absorption spectra of Suwannee river humic acids and fulvic acids (Pelaez et al., 2010). It can be seen that both typical NOM components have high absorption at the UV-visible wavelength range (200 nm – 400 nm) which will result in the absorption of delivered photons. Absorption of light by solutes diminish the depth of light penetration reducing photocatalyst activation. Therefore, increase in NOM concentration can undermine efficient photoexcitation and diminish generation rate of oxidants. It has been observed that highly active UV radiation activity may be limited to near surface layer in eutrophied lakes, especially during algal blooms and lyses (De Lange, 2000).

6.2. Scavenging effects and synergies of inorganic species

The content of inorganic species in bodies of water derives primarily from the weathering and leaching of rocks and soils. However, anthropological activities, especially industrial ones, are responsible for the discharge of a large number of inorganic species, including heavy metals, nitrate, phosphate, perchlorate, and fluorides. Those species are currently considered to be critical pollutants when in excess of permissible limits in bodies of water due to their potential devastating effects upon aquatic biota and human health. The content of inorganic species is significantly greater in lakes, reservoirs, ponds, and slow-moving rivers than in rivers and streams due to the accumulation of suspended sediments caused by the low velocity of the flow of water. In natural water, Na^+, K^+, Mg^{2+}, Cu^{2+}, Fe^{3+}, and Ca^{2+} cations and Cl^-, NO_3^-, SO_4^{2-}, HCO_3^-, CO_3^{2-}, and HPO_4^{2-} anions are the most often found (Nakatani et al., 2011; Nikanorov et al., n.d.).

The presence of inorganic cations generally exerts few relevant effects upon the photo-oxidation of organic pollutants. Common cations (e.g., Na^+, K^+, Ca^{2+}, and Mg^{2+}) in bodies of water cannot capture electrons or holes in solutions, because they are all in their highest and most stable states of oxidation. However, insoluble species of divalent cations associated to water hardness may precipitate on catalyst surface producing scaling (i.e., undesirable crystallization of inert salts on catalyst surface) (Chong et al., 2015; Sontakke et al., 2011). Inorganic scaling can inhibit reactivity due to blocking of catalytic sites. Precipitation of inorganic species can be promoted on catalyst surfaces due to localized pH changes due to heterogeneous photocatalytic reactions (Bhatkhande et al., 2002; Kudlek et al., 2016). However, these aspects are seldomly addressed in research works that focus on the evaluation of catalysts in single use. Other cationic species of anthropogenic origin may be found in water samples such as heavy metals. The presence of Cr(VI) and Cu(II) can result in the photoreduction of these species on the catalyst surface. Depending on the conditions, that phenomenon can synergistically enhance or inhibit the photo-oxidation of organic pollutants. Deposition of metals on catalysts surfaces can generate metal/semiconductor interfaces that act as electron sinks, which minimizes recombination reaction (5) and stabilizes oxidants generation (Beydoun et al., 2002; Zhao et al., 2015). However, excess of these species can inhibit photocatalytic activity due to poisoning of catalytic sites or even act as recombination center. More attention should be given to these uncontrolled effects that are not usually considered in the study of synthetic water matrices. In the case of cyanotoxins, the presence of cations slightly affects the kinetics of degradation, primarily by reducing the adsorption of MC-LR on the photocatalyst's surface due to their interaction with negatively charged MC-LR molecules (Antoniou et al., 2010; Pinho, 2014; Zhao et al., 2015).

The most common inorganic anions in bodies of water (i.e., Cl^- and HCO_3^-/CO_3^{2}) have demonstrated to chemically active species in presence of photocatalysts. Herein it is further described the different roles and effects that each individual species may play on the photocatalytic degradation of cyanotoxins.

Chloride is a ubiquitous anion found in the environment in a wide range of concentrations ranging between fresh (< 0.05%), brackish (0.05-3%) and saline seawater (3-5 %). Chloride ions can be oxidized by hydroxyl radicals as proven by different AOPs yielding different active chlorine species (Lu et al., 2005; Mostafa et al., 2018). Fundamentals of reaction mechanisms of chloride with $^{\bullet}OH$ were described in the 70s from pulse radiolysis studies, which involves several equilibria described in reactions (12-14) (Hasegawa and Neta, 1978; Jayson et al., 1973).

$$^{\bullet}OH + Cl^- \leftrightharpoons HOCl^{\bullet -} \qquad k = 4.3 \times 10^9 M^{-1} s^{-1} \tag{12}$$

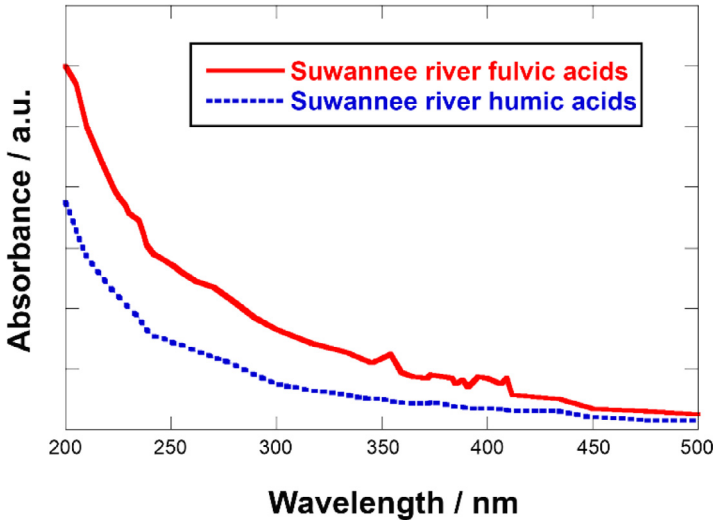

Fig. 10. UV-vis absorbance spectra of fulvic acid and humic acid as representative natural organic matter components. Adapted with permission from reference (Pelaez et al., 2011).

$$HOCl^{\bullet -} + H^+ \leftrightharpoons H_2O + Cl^{\bullet} \qquad k = 2.1 \times 0^{10} M^{-1}s^{-1} \tag{13}$$

$$Cl^{\bullet} + Cl^- \leftrightharpoons Cl_2^{-\bullet} \qquad k = 2.1 \times 10^{10} M^{-1}s^{-1} \tag{14}$$

Non-radical chlorine species can be formed from the dimerization of $Cl^{\bullet}$ radical according reaction (15) or through redox reaction (16) of $Cl_2^{-\bullet}$ radical. In the case of photocatalysis, chloride can be directly oxidized by direct charge transfer processes on the catalyst surface following reaction (17). Then, chlorine disproportionate yielding hypochlorite by reaction (18), which is in acid-base equilibria (19) with hypochlorous acid. It is important to remark that chlorine radical can be generated through UV/chlorine process when using UV irradiation through reaction (20) and (21) with reported quantum yields above 1.0. The quantum yields of HClO and ClO^- at 254 nm ranged from 1.4 to 1.7 and from 1.1 to 1.4 mol Es^{-1}, respectively. Conversely, at 200–350 nm, they ranged from 3.3 to 4.1 mol Es^{-1} for HClO and from 1.4 to 2.1 mol Es^{-1} for ClO^- (Watts et al., 2007; Watts and Linden, 2007). Thus, these reactions are expected to have significant relevance when photocatalytic operational conditions rely on the use of UV lamp sources.

$$2Cl^{\bullet} \rightarrow Cl_2 \tag{15}$$

$$Cl_2^{-\bullet} \rightarrow^{\rightarrow} Cl_2 + e^- \tag{16}$$

$$2Cl^- \rightarrow Cl_2 + 2e^- \tag{17}$$

$$Cl_2 + 2OH^- \rightarrow ClO^- + Cl^- + H_2O \tag{18}$$

$$HClO \leftrightharpoons ClO^- + H^+ \rightarrow pK_a = 7.5 \tag{19}$$

$$HOCl + h\nu \rightarrow Cl^{\bullet} + {}^{\bullet}OH \tag{20}$$

$$OCl^- + h\nu \rightarrow Cl^{\bullet} + O^{\bullet -} \tag{21}$$

The reactions described above can consume photogenerated $^{\bullet}OH$ and h_{VB}^+, but the contribution of active chlorine species on cyanotoxins abatement cannot be neglected. Despite their lower oxidation capabilities when compared to $^{\bullet}OH$ radical ($E^{\circ} = 2.80$ V vs SHE), active chlorine species are still strong oxidants that quickly react with organics (Lei et al., 2019). The standard reduction potential of the different active chlorine species involved in above mechanisms can be classified in decreasing order of oxidative power as follows: $Cl^{\bullet}$ ($E^{\circ} = 2.55$ V vs SHE) > $Cl_2^{-\bullet}$ ($E^{\circ} = 2.13$ V vs SHE) >>> HClO ($E^{\circ} = 1.49$ V vs SHE) > Cl_2 ($E^{\circ} = 1.36$ V vs SHE) >> ClO^- ($E^{\circ} = 0.89$ V vs SHE). The competitive aspect of those oxidants is that they are not limited by mass transfer due to their homogeneous character. Yang's group demonstrated that the formation of reactive chloride species contributes to attain significant removal of MC-LR in a UV–chlorine system (Chuang et al., 2017; Zhang et al., 2019a). Zhang et al. concluded that the reactive chlorine species attack the conjugated dienes in MC-LR by reacting selectively with electron donors (Sun et al., 2018; Zhang et al., 2019b). The participation of reactive chlorine species in the degradation of MC-LR during photoelectrocatalytic degradation using TiO_2-based photocatalysts was also demonstrated (Fraga et al., 2009; Shi et al., 2005). Nevertheless, thorough studies on the effect of chloride ion during cyanotoxins photocatalytic degradation have yet to be conducted. Special attention should be given to possible yield of chlorinated organics and disinfection by-products.

Also common in bodies of water are bicarbonate and carbonate. The speciation of carbonates in natural waters is defined by their in acid-base equilibria according reactions (22) and (23). Bicarbonate, carbonate and hydroxide ions are the main species responsible for alkalinity in water. Water alkalinity is a crucial water quality parameter that indicates the buffering capacity of water (i.e., the capacity to resist changes in the pH). Alkalinity is usually measured in parts per million of the equivalent carbonate ions (Jefferson et al., 2016; Olivo-Alanis et al., 2019). Bicarbonate and carbonate anions react with hydroxyl ions to form carbonate radicals following reactions (24) and (25), respectively. Carbonate radicals pose a significantly lower redox potential ($E^{\circ} = 1.78$ V vs SHE) than hydroxyl radicals ($E^{\circ} = 2.80$ V vs SHE) (Liu et al., 2016). Thus, these weaker oxidants decrease the overall efficiency of the photocatalytic degradation of cyanotoxins. Carbonates inhibit the photodegradation of cyanotoxins and other organic compounds due to their strong scavenging activity for hydroxyl radicals. Figure 11 shows that the initial reaction rate of the degradation of MC-LR under a visible light-activated TiO_2 is dramatically affected by the presence of carbonates (Pelaez et al., 2011). First, it can be inferred that speciation depending on pH is one of the key aspects of alkalinity inhibition. It can be observed that at given

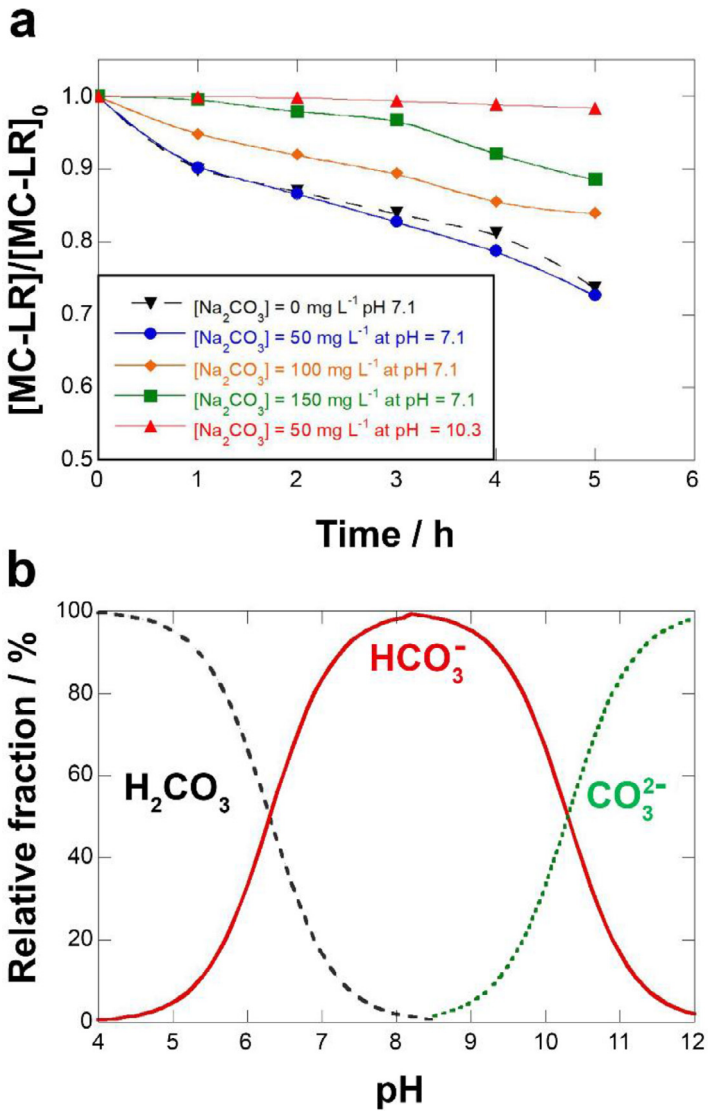

Fig. 11. (a) Effect of alkalinity at different Na_2CO_3 concentrations on the photocatalytic degradation of 500 μg L^{-1} of MC-LR in ultrapure water using visible light irradiation (irradiance 7.8×10^{-5} W cm^{-2}) on doped NF-TiO_2. Influence of pH conditions is also depicted showing differences between pH 7.1 of buffered solutions and pH 10.3. (b) Speciation diagram of carbonate species in function of the pH.
Adapted with permission from reference (Pelaez et al., 2011).

concentration of 50 mg L^{-1} of Na_2CO_3 at pH 7.1, the photocatalytic degradation of MC-LR was not statistically different from the blank experiments conducted in absence of Na_2CO_3. Conversely, identical concentration of 50 mg L^{-1} of Na_2CO_3 at pH 10.3 resulted in complete inhibition of photocatalytic removal of MC-LR. This trend is explained by the stronger scavenger activity of carbonate that reacts with $^{\bullet}OH$ according (25) with a kinetic constant ($k = 8.5 \times 10^6$ M^{-1} s^{-1}) two order of magnitude higher than bicarbonate ($k = 8.5 \times 10^6$ M^{-1} s^{-1}). Second, the increasing concentration of carbonate/bicarbonate ions has a detrimental effect on MC-LR degradation kinetics. Despite the negligible effect observed at pH 7.1 for 50 mg L^{-1} of Na_2CO_3 with a degradation rate of MC-LR of 0.54×10^{-3} μM min^{-1}, inhibition due to $^{\bullet}OH$ scavenging was observed at higher Na_2CO_3 concentrations. Thus, doubling content of Na_2CO_3 to 100 mg L^{-1} of Na_2CO_3 decelerates degradation rate by ca. 35% down to 0.34×10^{-3} μM min^{-1}. Further addition of alkalinity reaching 150 mg L^{-1} of Na_2CO_3 slows down degradation rate by 80% to 0.09×10^{-3} μM min^{-1}. These results agree with the trends observed for other specific scavengers of $^{\bullet}OH$ and identify water alkalinity as one of the major hindrances for photocatalytic application in natural waters (Pelaez et al., 2011).

$$H_2CO_3 \leftrightharpoons HCO_3^- + H^+ \qquad pK_a = 6.4 \tag{22}$$

$$HCO_3^- \leftrightharpoons CO_3^{2-} + H^+ \qquad pK_a = 10.2 \tag{23}$$

$$^{\bullet}OH + HCO_3^- \rightarrow CO_3^{\bullet -} + H_2O \quad k = 8.5 \times 10^6 M^{-1}s^{-1} \tag{24}$$

$$^{\bullet}OH + CO_3^{2-} \rightarrow CO_3^{\bullet -} + OH^- \quad k = 3.9 \times 10^9 M^{-1}s^{-1} \tag{25}$$

Studies have demonstrated that not only ionic strength, but also natural organic matter and pH are some of the primary factors governing the surface charge of photocatalysts (Borgnino, 2013; Brown et al., 1997; Hu et al., 2010; Zareei et al., 2019). The stability and aggregation kinetics of photocatalysts have important effects on the adsorption of cyanotoxins and their photocatalytic degradation. The DLVO (Derjaguin, Landau, Verwey, and Overbeek) theory is normally used to explain the stability and aggregation

behavior of particles in aqueous environments. Based on this theory, the total interaction energy (W_T) is the sum of Lifshitz/Van der Waals forces (W_{LW}) and the electrical double layer interactions (W_{EL}) between particles. However, other non-DLVO forces, such as hydration, steric effects, and hydrophobic forces, can also dramatically affect the interaction between particles. Variations in the ionic strength govern the range of the double-layer interaction and contribute to the modification of the particles' effective charge (Schwegmann et al., 2013; Zareei et al., 2019). The Debye-Hückel thickness can be decreased by increasing the ionic strength. Consequently, the electrostatic repulsion weakens. Increased ionic strength translates to decreased columbic contribution, which induces particles aggregation. The aggregation of suspended photocatalysts is detrimental for photocatalytic performance since substantially decreases the active surface area available as interface for the photocatalytic reaction with cyanotoxins. Moreover, larger particulates obstruct light transport diminishing the extent photoexcitation reaction (1). The effect of total dissolved solids in water matrices require further attention since it may deviate behavior from ideal conditions in ultrapure water.

6.3. Treatment of natural water samples

Senogles et al. conducted the first evaluation of photocatalytic treatment performance in natural water samples collected from North Pine Dam raw water (South East Queensland, Australia). This natural resource has typical concentrations of $< 20\ \mu g\ L^{-1}$ of CYN, with spikes of concentration reaching levels of $70\ \mu g\ L^{-1}$ due to algal blooms (Senogles et al., 2001). Natural and synthetic water samples were treated using TiO_2-P25 doses of 0.1 g L^{-1} under UV light (irradiation dose 5000 $\mu W\ s\ cm^{-2}$). Reported half-lives indicate faster abatement of CYN in real water samples ($t_{1/2} = 4.4$. min) than in ultrapure water samples ($t_{1/2} = 16.5$ min). These results were associated to the synergistic role of inorganic species in (e.g., chlorine active species generated from chloride) solution as described above, which suggest high competitivity of photocatalysis as water treatment technology to minimize the impact of cyanotoxins in raw water sources (Senogles et al., 2001).

Conversely, deleterious effects were observed on the treatment of 1.0 μM CYN spiked in real water samples collected from East Fort Lake and Toledo Water Plant (Ohio, USA). While TiO_2 treatment under UV irradiation in synthetic water reported kinetic rate constants of CYN abatement of 33.0×10^{-2} min^{-1}, the kinetic rate dramatically decreased down to 1.9×10^{-2} min^{-1} (East Fort Lake – 5.1 mg L^{-1} of TOC) and 4.59×10^{-2} min^{-1} (Toledo Water Plant – 3.2 mg L^{-1} of TOC). The reduction of performance of over 10-fold was ascribed to the scavenging effects of NOM and other water matrix components (Zhang et al., 2014a).

Dionysiou's group reported a complete study on the performance of visible-active photocatalyst in real water samples. Natural waters were collected from Lake Erie (Ohio, USA) and St. John's river (Florida, USA), which have reported increasing episodes of cyanobacterial blooms over the last decade. Fig. 12 depicts the normalized abatement of MC-LR by photocatalysis under visible light using a nitrogen and fluorine doped TiO_2 (NF-TiO_2) in different water matrix (Pelaez et al., 2011). Dotted lines illustrate removal trends of lab-made solutions in ultrapure water (i.e., no matrix effects) that show a clear dependence of pH on performance, as discussed in previous sections. Complete abatement of MC-LR was attained after 3h of treatment at pH 3.0, while a discrete removal of 15.2 % was observed at pH 8.0. This is of high relevance given the natural pH conditions of the water samples of pH 7.0 – 8.5 (see water characteristics in Fig. 12). Null degradation was reported for the visible photocatalytic treatment in real water matrices. The low performance can be explained by surface interaction and competitive phenomena involving solutes in natural waters such as the high content of NOM ranging between 2.5- 9.5 mg L^{-1} of TOC (Pelaez et al., 2011). Conversely, Fig. 12 shows that photocatalytic treatment under solar irradiation attains high degree of MC-LR degradation due to the contribution of the UV component. Treatment of Lake Erie samples and St. John's river attained 95.3 % and 86.9 % removal, respectively. Slight differences can be justified by the higher scavenger character of St. John's river water matrix that contained a higher load of NOM and alkalinity (see Table 7) which diminished the degradation ate of MC-LR.

Table 7
Physicochemical properties of water from Lake Erie and St. John's river (Pelaez et al., 2011).

	Lake Erie	St. John's river
pH	8.25	7.40
Total alkalinity (mg $CaCO_3$ L^{-1})	89.6	117.8
Total hardness (mg L^{-1})	94	110
Turbidity (NTU)	0.12	0.23
Conductivity (mS)	572	873
UV_{254}	0.04	0.17
TOC (mg L^{-1})	2.55	9.49

Even though the promising premises of sustainable character of visible photocatalysts, these cannot achieve cyanotoxins removal in natural water samples. This is a critical conclusion that should redefine research efforts towards development of engineering strategies that maximize light delivery and exploitation of UV irradiation for cyanotoxins remediation.

7. Significance of photocatalytic reactor design for technology translation

Photocatalysis was proven to be an effective technology for cyanotoxins abatement even in natural water sources. Research in small batch reactors of 5 mL – 20 mL (see Tables 1–3) was essential to develop (i) fundamental understanding of photocatalysis capabilities, (ii) degradative pathways elucidation, and (iii) breakthroughs on materials development. However, research focus at this low technology readiness level may be missing the big picture problem required to address cyanotoxins global challenges (see Fig. 1).

Translation of photocatalytic technologies should consider treatment of large volumes of water. In this frame, strategies to tackle the environmental problem of cyanotoxins should distinguish between two points of action that would condition engineering decisions for reactor design and photocatalyst material selection: (i) treatment of lakes, or (ii) detoxification of water sources for drinking purposes at point-of-entry/point-of-use.

The value proposition for the treatment of lakes with high concentration of cyanotoxins envisions the use of solar light active photocatalysts, which will reduce operational expenses associated to lamp sources (Jo and Tayade, 2014; Natarajan et al., 2011; Ye et al., 2018). Even though the resulting reduction on electrical energy per order (EE/O) requirements is a high promise, the deployment of the treatment is still a major engineering challenge. The treatment of large volumes of semi-stagnant water in lakes by photocatalytic treatment of lakes is an unreachable horizon given the actual state of the art (Loeb et al., 2019). It is obvious that sprinkling lakes with photocatalyst nanoparticles at doses of grams per liter cannot be considered feasible. Environmental risks and concerns arose from fate and transport of nanoparticles as well as from their sedimentation (Andy et al., 2008; Petosa et al., 2010). Beyond catalyst sedimentation, photocatalyst performance can be seriously undermined by limited light transport through lake water bodies. Safe implementation of nanotechnology for environmental applications may require controlled systems to tackle these engineering challenges (Friehs et al., 2016; Haynes et al., 2017; Wagner et al., 2011). Passive treatment systems that use supported

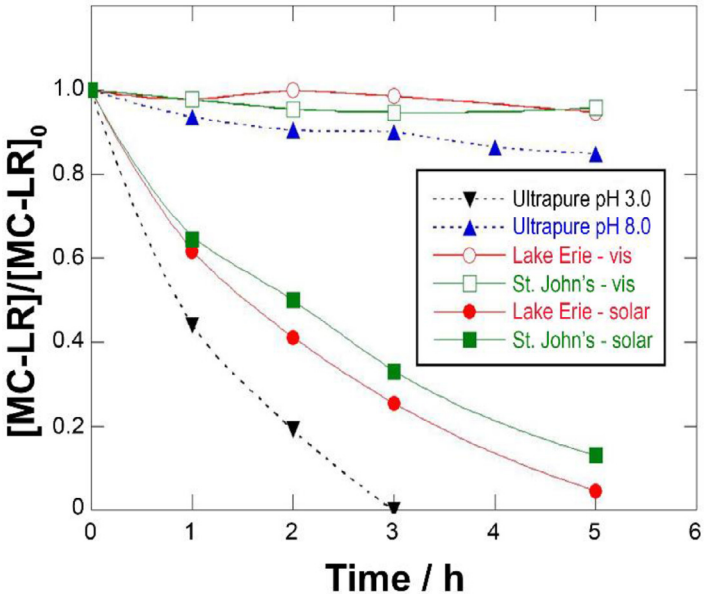

Fig. 12. Photocatalytic degradation of 500 μg L^{-1} MC-LR in ultrapure water and natural water matrix from Lake Erie and St. John's river at the pH given in the table using visible (irradiance 7.8×10^{-5} W cm^{-2}) or solar light irradiation (irradiance 9.5×10^{-5} W cm^{-2}) on doped NF-TiO_2. The side table summarizes natural water characteristics. Adapted with permission from reference (Pelaez et al., 2011).

catalyst have recently appeared as a promising strategy for the case scenario of lakes and reservoirs. Floating nanocomposite photocatalysts can be deployed and easily recovered/reuse after environmental intervention. These processes, which have been barely explored for cyanotoxins, may be an opportunity for the implementation of photo-driven cyanotoxins remediation technologies.

A different case scenario can be observed when detoxification of water sources is desired to ensure access to drinking water. Photocatalytic detoxification can be implemented to treat collected water in continuous operation mode. Solar-driven treatment can benefit of the use of photoreactors that ensure efficient solar radiation collection and/or concentration. Solar photocatalytic reactors aim to maximize the usage of solar irradiation. Direct sun irradiation on conventional flat photoreactors results in severe losses of delivered light. In this frame, alternative reactors maximize light delivery by concentration in tubular reactors. This is the case of compound parabolic collectors (CPCs) that have a light concentration factor close to one (i.e., maximum efficiency). Concentration is attained by defining reflector geometry to redirect indirect light by reflection into the tubular reactor (see Fig. 13) (Spasiano et al., 2015). Engineering design tailoring optimization of light delivery allows: (i) diminishing reactor footprint when compared to commercial flat reactors, and (ii) operation during overcast days due to concentration of indirect sunlight.

Solar-driven photocatalysis presents benefits as decentralized treatments that can operate off grid in developing areas. However, the reactor set-ups described above have a great physical-foot print. Moreover, the slower kinetic abatement observed for solar light photocatalysis when benchmarked against UV-photocatalysis raises some operational questions. Depending on techno-economic considerations, it must be more competitive to consider systems that remove cyanotoxins in compact reactors with lower residence times, despite of requiring UV-light sources. Reactors that use photocatalysts in slurry require post-treatments that separate suspended heterogeneous catalysts after treatment. For example, commercially available photo-cat systems of Purifics® depicted in Fig. 13 implements a patented continuous TiO_2 separation process that allows recapture and reintroduction of catalyst into the inlet stream in a closed loop.

Fluidized-bed reactors are continuous flow systems in which a fluid (i.e., the water being treated) is circulated at enough velocity to maintain particulate solids in continuous suspension. The solid particles remain in constant agitation and swirl around through the fluidized-bed avoiding their agglomeration, under the so-called fluidized state. Particles in fluidized state behave as they were fluids, which improves kinetics of heterogeneous catalytic processes such as photocatalysis. Fluidized bed slurries keep the photocatalysts particles within the expanded bed of the reactor for their continuous use (Fang et al., 2019; Lee et al., 2004; Rincón and La Motta, 2019; Shet and Vidya, 2016). In other words, catalyst recovery is not required since fluidized particles do not leave the fluidized bed reactor during operation. These reactors present wide opportunity of application at short residence times and can be easily modified for simultaneous UV disinfection by defining fluidized-bed height (see Fig. 13).

The use of films or deposited photocatalysts is an interesting approach that will prevent issues associated to the recovery of nanoparticles. Even though the required treatment times may be longer than those for slurry systems, several works have demonstrated the competitiveness of photocatalytic films on the removal of cyanotoxins (Antoniou et al., 2009; Han et al., 2011). Slower kinetics can be explained by the decrease on available surface area and the noticeable control of the degradation kinetics by mass transfer towards/from the photocatalyst surface (Espíndola et al., 2019; Han et al., 2011). However, the development of these static systems provides opportunities for alternative reactor designs. Alternatives to slurry operation have been explored using catalytic converters as packed bed reactors. The major issue of packed bed reactors is associated to photon transport and the possible shadowing effect of surrounding substrates in packed bed or monolith reactors, which may diminish the irradiated surface. Pinho et al. demonstrated that transparent monoliths can outperform conventional supports (e.g.., glass spheres, silica, polyvinylchloride supports, etc). The high performance of these honeycomb three-dimensional transparent arrays it attributable to the large specific photoactive surface area that can be efficiently irradiated (Pinho et al., 2015b). This can be explained by the reduced shadowing effect, as can be deduced from transmittance characteris-

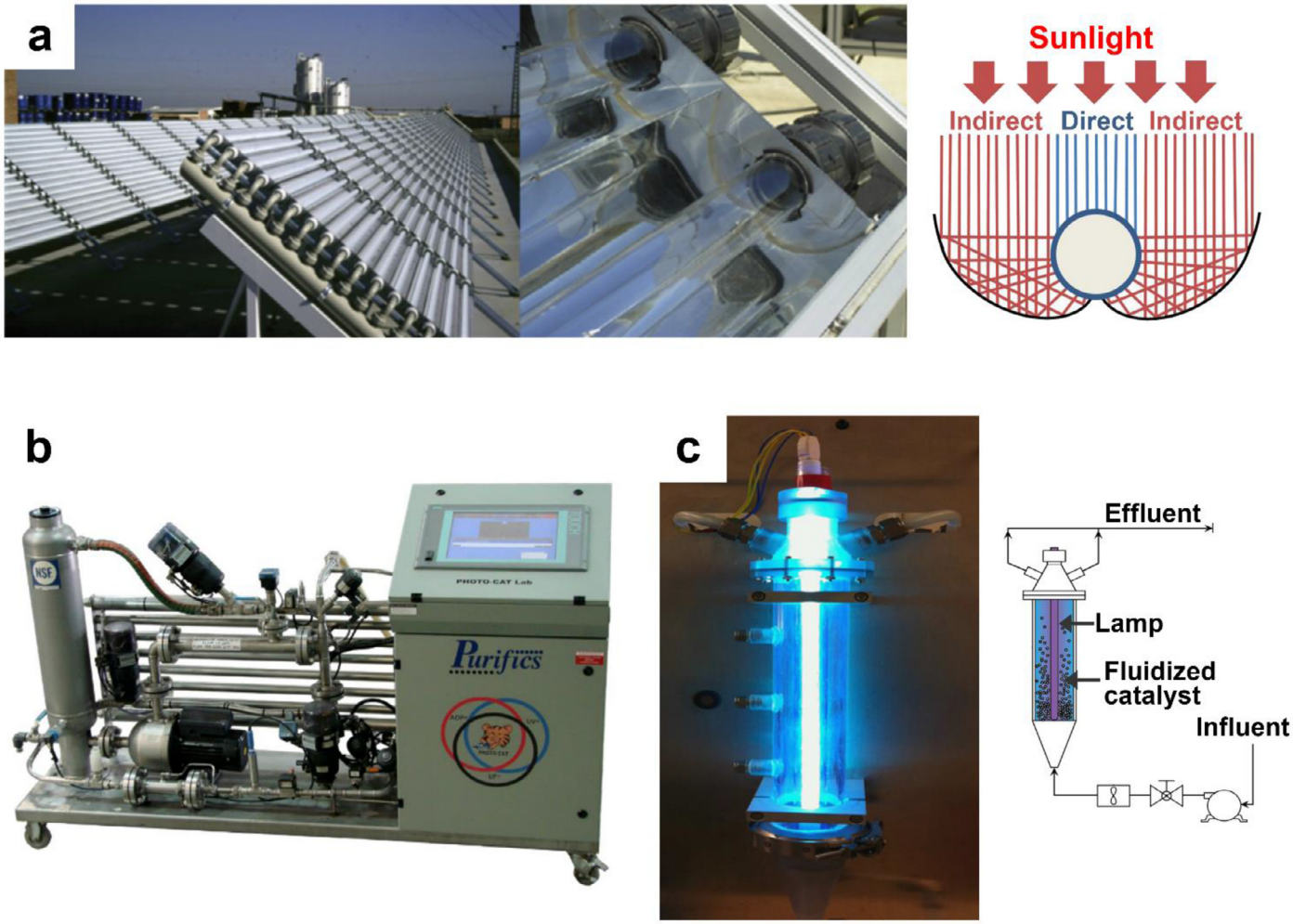

Fig. 13. (a) Compound parabolic collector photoreactor and light concentration in CPC. Adapted with permission from reference (Spasiano et al., 2015). (b) Commercial Photo-cat® reactor from Purifics. (c) Fluidized-bed. photocatalytic reactor.
Adapted with permission from reference (Reilly et al., 2017).

tics of supports illustrated in Fig. 14. These engineering approaches define possible pathways for supported photocatalysts reactor design that ensure light transport and mass transfer. Another issue observed in deposited photocatalysts systems is the loss of photocatalytic performance due to the charge carriers recombination. However, the use of heterogeneous supported systems provides a unique framework that may enable photoelectrocatalytic treatments (Garcia-Segura and Brillas, 2017). The application of a small bias potential can enhance the separation between the charge carriers due to the existence of an external electrical field, which avoids or at least slows down the recombination reaction rate (Cerrón-Calle et al., 2019). It has been observed that photoelectrocatalytic systems can have enhanced performance of film semiconductors when degrading cyanotoxins (Liao et al., 2013; Zhao et al., 2019).

Previous systems use energy intensive lamps (i.e. mercury lamps). Advances in UV-light emitting diodes (LEDs) have increased light output, energy efficiency, durability, and cost competitiveness (Chen et al., 2017). Integration of LEDs can drastically reduce physical footprint of photocatalytic reactors and their electrical energy requirements. Few attempts to implement LEDs have faced light delivery as a major engineering challenge (Hou and Ku, 2013; Natarajan et al., 2011; O'Neal Tugaoen et al., 2018a). Light transport can be improved with photocatalyst-coated optical fibers that homogeneously distribute light along the coating as illustrated in Fig. 15. Pure optical fibers transport light occurs via internal reflection with negligible refraction losses. When fibers are coated with photocatalysts of refractive index (n_2) higher than the characteristic value of the optical fiber (n_1), refraction events can deliver light to photoexcite the photocatalyst (i.e. TiO_2). Since light is delivered through the fiber at the internal interface of the catalyst light losses by absorption of solutes and scattering by solids in suspension are avoided, which increases efficient use of photons.

Despite of all the interesting approaches discussed in this section, photocatalytic treatment of cyanotoxins in water samples at reactor scale has been barely studied. Benchmarking and techno-economic analyses have not yet been conducted, therefore engineering decision factors have not yet been defined. Scaling-up and reactor testing can be highlighted as an essential element of the research roadmap to bridge promising lab scale advances with the need of proofs of concept at higher technology readiness level. This can be a niche opportunity for photocatalytic systems translation to markets.

8. Conclusions and key insights on challenges and perspectives

Worldwide, cyanotoxins are recognized as hazardous emerging pollutants in water due to their widespread distribution and occurrence. Even so, due to the limited analytical capabilities, the environmental challenge posed by cyanotoxins may be more diffi-

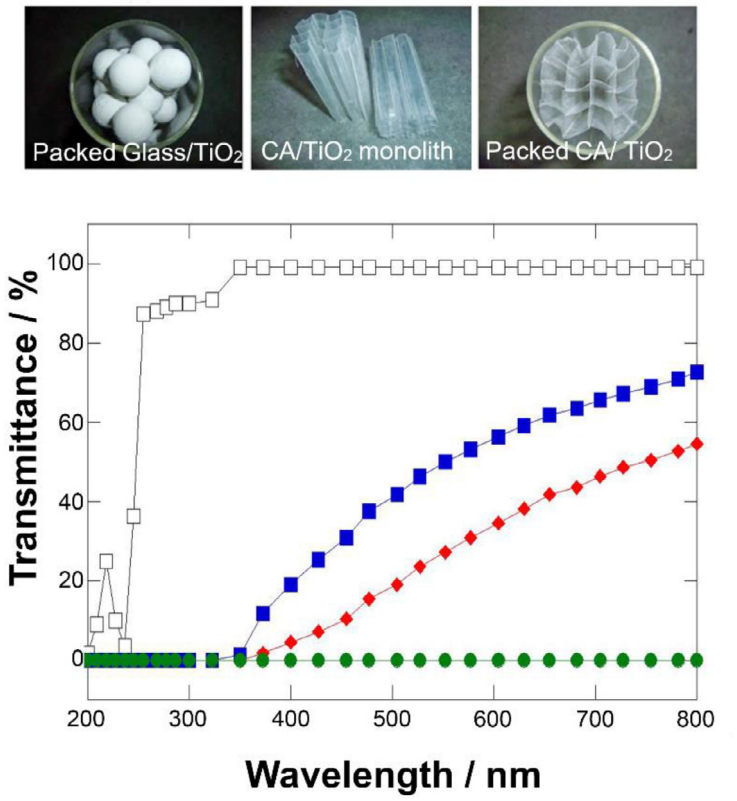

Fig. 14. Normalized absorbance spectra measured through different materials used in the packed photocatalytic reactors: (●) TiO_2 coated glass spheres, (□) uncoated cellulose acetate transparent honeycomb structured monolith (CA), (■) absorbance measured after light passed through first sheet of CA/TiO_2, (◆) lower absorbance measured after light passed through second sheet of CA/TiO_2.
Adapted with permission from reference (Pinho et al., 2015b).

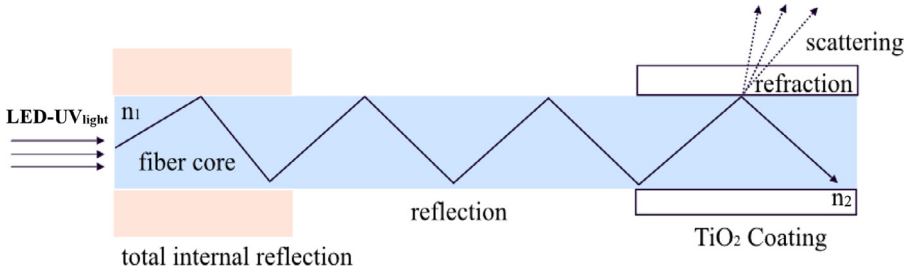

Fig. 15. Light delivery mechanism through photocatalyst coated optical fibers. Integration into compact reactors can ensure efficient light transport and enhanced photocatalytic activity. Indices of refraction are denoted: n_1 for the quartz optical fiber and n_2 for the TiO_2 coating.
Adapted with permission from reference.

cult than it seems. Worse still, conventional water treatment technologies have proven ineffective in removing all cyanotoxins simultaneously. As a solution, photocatalysis has emerged as promising alternative that has shown exceptional effectiveness in removing intra- and extracellular cyanotoxins. In addition, fundamental studies have elucidated some intricate degradation pathways of cyanotoxins (i.e., MC-LR and CYN) and demonstrated the complete abatement of parent compounds as well as their toxicity.

Reliance on the use of semiconductor photocatalysts with wide band gaps (*i.e.*, TiO_2 with E_g ~3.0 eV) require UV-irradiation sources. Because conventional UV-light lamps (*e.g.*, mercury lamps and xenon lamps) are energy intensive, researchers have sought to develop doping strategies that can enable photocatalytic response under visible light and solar irradiation. However, the ongoing development of LED technology could change the paradigm by offering a more cost-effective competitive source of light. In the same direction, relevant advances have indicated that the research roadmap should shift focus from developing materials to implementing technology at higher levels of readiness.

Although doping and using nano-composite photocatalysts are interesting approaches to that end, neither strategy has advanced the implementation of photocatalytic treatment as expected. Instead, efficient light transport and the improvement of light sources have had the most relevant impact in the field. As a result, the innovation of material is envisioned to derive from principles of biomimicry as a means to enhance selectivity and light transport. Developing materials that emulate natural structures of photosynthetic organisms (e.g., plants and bacteria) could revolutionize the efficient use of delivered photons.

Initial hype about photocatalytic treatment was based on outstanding performance under unrealistic lab settings that allowed treating small volumes of water with highly energy intensive lamps. Major challenges were identified in real water matrices, in

which degradation kinetics had decelerated due to the presence of scavengers and competing species. Gauging the effectiveness of photocatalysts thus needs to occur to more-realistic environments and consider the influence of natural organic matter and inorganic species. Further research to improve, even optimize, the photocatalyst performance in complex environments and in large volumes as well as mimicking natural water in real-world environments is also urgently needed. Understanding the effects of water matrices can aid in strategizing novel materials or at least identifying niche applications of photocatalytic processes.

Beyond that, the greatest barrier to translating technology is the lack of any reactor design that can completely exploit photocatalysis in the treatment of large volumes of water (e.g., lakes and reservoirs) polluted with cyanotoxins. Optimized treatment conditions for small volumes in batch reactors are mostly unrealistic and inapplicable when considering the true scale of the environmental challenge. Thus, it identifies the development of engineering designed reactors and treatment strategies to be truly competitive alternatives. In that sense, reactor design and techno-economic evaluation are truly major hurdles in translating the results of research into practice. Research efforts should be directly toward configuring benchmark reactors and comparing passive treatment systems with active ones to fully exploit promising photocatalytic treatments for cyanotoxins remediation.

Finally, the development of new low-cost doped, wavelength targeted catalysts are significant advances that could make photocatalytic oxidation more competitive and cost effective. This is a feature that can be fully exploited with LED lights as cheap and energy efficient light sources.

Declaration of Competing Interest

Authors declare no conflict of interest.

Acknowledgments

This work was partly funded through the Nano-Enabled Water Treatment Technologies Nanosystems Engineering Research Center by the National Science Foundation (EEC-1449500). A.S. would like to acknowledge funding from the EMPAPOSTDOCS-II program. The EMPAPOSTDOCS-II program has received funding from the European Union's Horizon 2020 research and innovation program under the Marie Sklodowska-Curie grant agreement number 754364.

References

Fujishima, A., Honda, K., 1972. Electrochemical photolysis of water at a semiconductor electrode one and two-dimensional structure of alpha-helix and beta-sheet forms of poly (L-Alanine) shown by specific heat measurements at low temperatures (1 . 5-20 K). Nature 238, 37–38. doi:10.1038/239137a0.

Al-Sammak, M.A., Hoagland, K.D., Cassada, D., Snow, D.D., 2014. Co-occurrence of the cyanotoxins BMAA, DABA and anatoxin-a in Nebraska reservoirs, fish, and aquatic plants. Toxins (Basel) 6, 488–508. doi:10.3390/toxins6020488.

Andersen, J., Han, C., O'Shea, K., Dionysiou, D.D., 2014. Revealing the degradation intermediates and pathways of visible light-induced NF-TiO_2 photocatalysis of microcystin-LR. Appl. Catal. B Environ. 154–155, 259–266. doi:10.1016/j.apcatb.2014.02.025.

Anderson, D., 2015. HABs in a changing world: a perspective on harmful algal blooms, their impacts, and research and management in a dynamic era of climactic and environmental change. In: Harmful algae 2012 Proc. 15th Int. Conf. Harmful Algae Oct. 29 - Novemb. 2, 2012, CECO, 2012, Chang. Gyeongnam, Korea, pp. 3–17 Int. Conf. Harmful Algae (15th 2012 Chang. Gyeongnam, Kore...

Andy, R.I.D.H., Yon, D.E.Y.L., Ahendra, S.H.M., Aughlin, M.I.J.M.C.L., Ead, J.A.R.L., 2008. Critical review and effects. Environ. Toxicol. Chem. 27, 1825–1851. doi:10.1897/08-090.1.

Antoniou, M.G., Boraei, I., Solakidou, M., Deligiannakis, Y., Abhishek, M., Lawton, L.A., Edwards, C., 2018. Enhancing photocatalytic degradation of the cyanotoxin microcystin-LR with the addition of sulfate-radical generating oxidants. J. Hazard. Mater. 360, 461–470. doi:10.1016/j.jhazmat.2018.07.111.

Antoniou, M.G., de la Cruz, A.A., Dionysiou, D.D., 2010. Degradation of microcystin-LR using sulfate radicals generated through photolysis, thermolysis and e- transfer mechanisms. Appl. Catal. B Environ. 96, 290–298. doi:10.1016/j.apcatb.2010.02.013.

Antoniou, M.G., Nicolaou, P.A., Shoemaker, J.A., de la Cruz, A.A., Dionysiou, D.D., 2009. Impact of the morphological properties of thin TiO_2 photocatalytic films on the detoxification of water contaminated with the cyanotoxin, microcystin-LR. Appl. Catal. B Environ. 91, 165–173. doi:10.1016/j.apcatb.2009.05.020.

Antoniou, M.G., Shoemaker, J.A., de la Cruz, A.A., Dionysiou, D.D., 2008a. LC/MS/MS structure elucidation of reaction intermediates formed during the TiO_2 photocatalysis of microcystin-LR. Toxicon 51, 1103–1118. doi:10.1016/j.toxicon.2008.01.018.

Antoniou, M.G., Shoemaker, J.A., De La Cruz, A.A., Dionysiou, D.D., 2008b. Unveiling new degradation intermediates/pathways from the photocatalytic degradation of microcystin-LR. Environ. Sci. Technol. 42, 8877–8883. doi:10.1021/es801637z.

Antoniou, M.G., Zhao, Cen, O'Shea, K.E., Zhang, G., Dionysiou, D.D., Zhao, C., Han, C., Nadagouda, M.N., Choi, H., Fotiou, T., Triantis, T.M., Hiskia, A., 2016. Photocatalytic degradation of organic contaminants in water: Process optimization and degradation pathways. RSC Energy and Environment Series. doi:10.1039/9781782627104-00001.

Asahi, R., Morikawa, T., Ohwaki, T., Aoki, K., Taga, Y., 2001. Visible-light photocatalysis in nitrogen-doped titanium oxides. Science 293 (80-.), 269–271. doi:10.1126/science.1061051.

AWWA, 2016. Cyanotoxins in US drinking water: occurrence, case studies and state approaches to regulation 1–56.

Batista, L.M.B., dos Santos, A.J., da Silva, D.R., Alves, A.P., de, M., Garcia-Segura, S., Martínez-Huitle, C.A., 2017. Solar photocatalytic application of NbO_2OH as alternative photocatalyst for water treatment. Sci. Total Environ. 596–597, 79–86. doi:10.1016/j.scitotenv.2017.04.019.

Bernard, C., Ballot, A., Thomazeau, S., Maloufi, S., Furey, A., Mankiewicz-Boczek, J., Pawlik-Skowrońska, B., Capelli, C., Salmaso, N., 2017. Appendix 2: cyanobacteria associated with the production of cyanotoxins. Handb. Cyanobacterial Monit. Cyanotoxin Anal. 501–525. doi:10.1002/9781119068761.app2.

Beydoun, D., Tse, H., Amal, R., Low, G., McEvoy, S., 2002. Effect of copper(II) on the photocatalytic degradation of sucrose. J. Mol. Catal. A Chem. 177, 265–272. doi:10.1016/S1381-1169(01)00272-2.

Bhatkhande, D.S., Pangarkar, V.G., Beenackers, A.A.C.M., 2002. Photocatalytic degradation for environmental applications - a review. J. Chem. Technol. Biotechnol. 77, 102–116. doi:10.1002/jctb.532.

Bhatnagar, A., Sillanpää, M., 2017. Removal of natural organic matter (NOM) and its constituents from water by adsorption – a review. Chemosphere 166, 497–510. doi:10.1016/j.chemosphere.2016.09.098.

Bláha, L., Babica, P., Maršálek, B., 2009. Toxins produced in cyanobacterial water blooms - toxicity and risks. Interdiscip. Toxicol. 2, 36–41. doi:10.2478/v10102-009-0006-2.

Bláhová, L., Babica, P., Maršálková, E., Maršálek, B., Bláha, L., 2007. Concentrations and seasonal trends of extracellular microcystins in freshwaters of the Czech Republic - results of the national monitoring program. Clean - Soil, Air, Water 35, 348–354. doi:10.1002/clen.200700010.

Bolton, J.R., Bircher, K.G., Tumas, W., Tolman, C.A., 2001. Figures-of-merit for the technical development and application of advanced oxidation technologies for both electric- and solar-driven systems. Pure Appl. Chem. 73, 627–637. doi:10.1351/pac200173040627.

Boopathi, T., Ki, J.S., 2014. Impact of environmental factors on the regulation of cyanotoxin production. Toxins (Basel) 6, 1951–1978. doi:10.3390/toxins6071951.

Borgnino, L., 2013. Experimental determination of the colloidal stability of Fe(III)-montmorillonite: effects of organic matter, ionic strength and pH conditions. Colloids Surfaces A Physicochem. Eng. Asp. 423, 178–187. doi:10.1016/j.colsurfa.2013.01.065.

Brown, R.F.G., Carr, C., Taylor, M.E., 1997. Effect of particle surface potential and ionic strength on pigment distribution. Prog. Org. Coat. 30, 195–206. doi:10.1016/S0300-9440(96)00687-X.

Buratti, F.M., Manganelli, M., Vichi, S., Stefanelli, M., Scardala, S., Testai, E., Funari, E., 2017. Cyanotoxins: producing organisms, occurrence, toxicity, mechanism of action and human health toxicological risk evaluation. Arch. Toxicol. 91, 1049–1130. doi:10.1007/s00204-016-1913-6.

Carmichael, W.W., 1992. Cyanobacteria secondary metabolites—the cyanotoxins.. J. Appl. Bacteriol. 72, 445–459. doi:10.1111/j.1365-2672.1992.tb01858.x.

Carmichael, W.W., Boyer, G.L., 2016. Health impacts from cyanobacteria harmful algae blooms: implications for the North American Great Lakes. Harmful Algae 54, 194–212. doi:10.1016/j.hal.2016.02.002.

Cater, S.R., Stefan, M.I., Bolton, J.R., Safarzadeh-Amiri, A., 2000. UV/H_2O_2 treatment of methyl tert-butyl ether in contaminated waters. Environ. Sci. Technol. 34, 659–662. doi:10.1021/es9905750.

Cerrón-Calle, G.A., Aranda-Aguirre, A.J., Luyo, C., Garcia-Segura, S., Alarcón, H., 2019. Photoelectrocatalytic decolorization of azo dyes with nano-composite oxide layers of ZnO nanorods decorated with Ag nanoparticles. Chemosphere 219, 296–304. doi:10.1016/j.chemosphere.2018.12.003.

Chatzitakis, A., Berberidou, C., Paspaltsis, I., Kyriakou, G., Sklaviadis, T., Poulios, I., 2008. Photocatalytic degradation and drug activity reduction of Chloramphenicol. Water Res 42, 386–394. doi:10.1016/j.watres.2007.07.030.

Chen, J., Loeb, S., Kim, J.H., 2017. LED revolution: Fundamentals and prospects for UV disinfection applications. Environ. Sci. Water Res. Technol. 3, 188–202. doi:10.1039/c6ew00241b.

Chen, L., Zhao, C., Dionysiou, D.D., O'Shea, K.E., 2015. TiO2 photocatalytic degradation and detoxification of cylindrospermopsin. J. Photochem. Photobiol. A Chem. 307–308, 115–122. doi:10.1016/j.jphotochem.2015.03.013.

Chen, P., Zhu, L., Fang, S., Wang, C., Shan, G., 2012. Photocatalytic degradation efficiency and mechanism of microcystin-RR by mesoporous Bi_2WO_6 under near ultraviolet light. Environ. Sci. Technol. 46, 2345–2351. doi:10.1021/es2036338.

Chen, X., Chuai, X., Yang, L., Zhao, H., 2012. Climatic warming and overgrazing induced the high concentration of organic matter in Lake Hulun, a large shallow eutrophic steppe lake in northern China. Sci. Total Environ. 431, 332–338. doi:10.1016/j.scitotenv.2012.05.052.

Chen, X., Mao, S.S., 2007. Titanium dioxide nanomaterials: synthesis, properties, modifications and applications. Chem. Rev. 107, 2891–2959. doi:10.1021/cr0500535.

Chia, M.A., Kramer, B.J., Jankowiak, J.G., Bittencourt-Oliveira, M.D.C., Gobler, C.J., 2019. The individual and combined effects of the cyanotoxins, anatoxin-a and microcystin-LR, on the growth, toxin production, and nitrogen fixation of prokaryotic and eukaryotic algae. Toxins (Basel) 11. doi:10.3390/toxins11010043.

Chong, M.N., Jin, B., Chow, C.W.K., Saint, C., 2010. Recent developments in photocatalytic water treatment technology: a review. Water Res 44, 2997–3027. doi:10.1016/j.watres.2010.02.039.

Chong, R., Cheng, X., Chang, Z., Li, D., Zhang, L., 2015. Effects of common metal cations on Ag3PO4-photocatalytic water decontamination. J. Environ. Chem. Eng. 3, 1215–1222. doi:10.1016/j.jece.2015.04.015.

Chorus, I., 2001. Introduction: cyanotoxins — research for environmental safety and human health. In: Chorus, I. (Ed.), Cyanotoxins: Occurrence, Causes, Consequences. Springer Berlin Heidelberg, Berlin, Heidelberg, pp. 1–4. doi:10.1007/978-3-642-59514-1_1.

Christoffersen, K., Kaas, H., 2000. Toxic cyanobacteria in water. A guide to their public health consequences, monitoring, and management, limnology and oceanography. 10.4319/lo.2000.45.5.1212

Christophoridis, C., Zervou, S.K., Manolidi, K., Katsiapi, M., Moustaka-Gouni, M., Kaloudis, T., Triantis, T.M., Hiskia, A., 2018. Occurrence and diversity of cyanotoxins in Greek lakes. Sci. Rep. 8, 1–22. doi:10.1038/s41598-018-35428-x.

Chuang, Y.H., Chen, S., Chinn, C.J., Mitch, W.A., 2017. Comparing the UV/monochloramine and UV/free chlorine advanced oxidation processes (AOPs) to the UV/hydrogen peroxide AOP under scenarios relevant to potable reuse. Environ. Sci. Technol. 51, 13859–13868. doi:10.1021/acs.est.7b03570.

Cirés, S., Wörmer, L., Ballot, A., Agha, R., Wiedner, C., Velázquez, D., Casero, M.C., Quesada, A., 2014. Phylogeography of cylindrospermopsin and paralytic shellfish toxin-producing Nostocales cyanobacteria from Mediterranean Europe (Spain). Appl. Environ. Microbiol. 80, 1359–1370. doi:10.1128/AEM.03002-13.

Codd, G., Bell, S., Kaya, K., Ward, C., Beattie, K., Metcalf, J., 1999. Cyanobacterial toxins, exposure routes and human health. Eur. J. Phycol. 34, 405–415. doi:10.1080/09670269910001736462.

Cornish, B.J.P.A., Lawton, L.A., Robertson, P.K.J., 2000. Hydrogen peroxide enhanced photocatalytic oxidation of microcystin-LR using titanium dioxide. Appl. Catal. B Environ. 25, 59–67. doi:10.1016/S0926-3373(99)00121-6.

Dávila-Jiménez, M.M., Elizalde-González, M.P., Guerrero-Morales, M.A., Mattusch, J., 2018. Preparation, characterization, and application of TiO_2/Carbon composite: Adsorption, desorption and photocatalysis of Gd-DOTA. Process Saf. Environ. Prot. 120, 195–205. doi:10.1016/j.psep.2018.09.012.

De Lange, H.J., 2000. The attenuation of ultraviolet and visible radiation in Dutch inland waters. Aquat. Ecol. 34, 215–226. doi:10.1023/A:1009943211779.

De Maagd, P.G.J., Hendriks, A.J., Seinen, W., Sijm, D.T.H.M., 1999. pH-dependent hydrophobicity of the cyanobacteria toxin microcystin-LR. Water Res. 33, 677–680. doi:10.1016/S0043-1354(98)00258-9.

Dittmann, E., Fewer, D.P., Neilan, B.A., 2013. Cyanobacterial toxins: biosynthetic routes and evolutionary roots. FEMS Microbiol. Rev. 37, 23–43. doi:10.1111/j.1574-6976.2012.12000.x.

Du, X., Liu, H., Yuan, L., Wang, Y., Ma, Y., Wang, R., Chen, X., Losiewicz, M.D., Guo, H., Zhang, H., 2019. The diversity of cyanobacterial toxins on structural characterization, distribution and identification: a systematic review. Toxins (Basel) 11, 1–34. doi:10.3390/toxins11090530.

Duran, J.E., Taghipour, F., Mohseni, M., 2010. Irradiance modeling in annular photoreactors using the finite-volume method. J. Photochem. Photobiol. A Chem. 215, 81–89. doi:10.1016/j.jphotochem.2010.07.027.

Duta, A., Andronic, L., Enesca, A., 2018. The influence of low irradiance and electrolytes on the mineralization efficiency of organic pollutants using the Visactive photocatalytic tandem $CuInS_2/TiO_2/SnO_2$. Catal. Today 300, 18–27. doi:10.1016/j.cattod.2017.03.018.

Dziga, D., Kokociński, M., Barylski, J., Nowicki, G., Maksylewicz, A., Antosiak, A., Banaś, A.K., Strzałka, W., 2019. Correlation between specific groups of heterotrophic bacteria and microcystin biodegradation in freshwater bodies of central Europe. FEMS Microbiol. Ecol. 95, 1–11. doi:10.1093/femsec/fiz162.

Edition, T., First, I.T.H.E., 2008. Guidelines for drinking-water quality 1.

El-Sheikh, S.M., Khedr, T.M., Zhang, G., Vogiazi, V., Ismail, A.A., O'Shea, K., Dionysiou, D.D., 2017. Tailored synthesis of anatase–brookite heterojunction photocatalysts for degradation of cylindrospermopsin under UV–Vis light. Chem. Eng. J. 310, 428–436. doi:10.1016/j.cej.2016.05.007.

El-Sheikh, S.M., Zhang, G., El-Hosainy, H.M., Ismail, A.A., O'Shea, K.E., Falaras, P., Kontos, A.G., Dionysiou, D.D., 2014. High performance sulfur, nitrogen and carbon doped mesoporous anatase-brookite TiO_2 photocatalyst for the removal of microcystin-LR under visible light irradiation. J. Hazard. Mater. 280, 723–733. doi:10.1016/j.jhazmat.2014.08.038.

Environmental Protection Agency, 2014. Cyanobacteria and cyanotoxins: information for drinking water systems 1–11.

Espíndola, J.C., Cristóvão, R.O., Mendes, A., Boaventura, R.A.R., Vilar, V.J.P., 2019. Photocatalytic membrane reactor performance towards oxytetracycline removal from synthetic and real matrices: suspended vs immobilized TiO_2-P25. Chem. Eng. J. 378, 122114. doi:10.1016/j.cej.2019.122114.

Etacheri, V., Di Valentin, C., Schneider, J., Bahnemann, D., Pillai, S.C., 2015. Visible-light activation of TiO_2 photocatalysts: advances in theory and experiments. J. Photochem. Photobiol. C Photochem. Rev. 25, 1–29. doi:10.1016/j.jphotochemrev.2015.08.003.

Fan, G., Hong, L., Luo, J., You, Y., Zhang, J., Hua, P., Du, B., Zhan, J., Ning, R., Bao, M., 2020. Photocatalytic inactivation of harmful algae and degradation of cyanotoxins microcystin-LR using GO-based Z-scheme nanocatalysts under visible light. Chem. Eng. J. 392, 123767. doi:10.1016/j.cej.2019.123767.

Fang, Z., Hu, Y., Cheng, J., Chen, Y., 2019. Continuous removal of trace bisphenol A from water by high efficacy TiO_2 nanotube pillared graphene-based macrostructures in a photocatalytically fluidized bed. Chem. Eng. J. 372, 581–589. doi:10.1016/j.cej.2019.04.129.

Farrer, D., Counter, M., Hillwig, R., Cude, C., 2015. Health-based cyanotoxin guideline values allow for cyanotoxin-based monitoring and efficient public health response to cyanobacterial blooms. Toxins (Basel) 7, 457–477. doi:10.3390/toxins7020457.

Feitz, A.J., Waite, T.D., Jones, G.J., Boyden, B.H., Orr, P.T., 1999. Photocatalytic degradation of the blue green algal toxin microcystin-LR in a natural organic-aqueous matrix. Environ. Sci. Technol. 33, 243–249. doi:10.1021/es970952d.

Ferrão-Filho, A.D.S., Kozlowsky-Suzuki, B., 2011. Cyanotoxins: bioaccumulation and effects on aquatic animals. Mar. Drugs 9, 2729–2772. doi:10.3390/md9122729.

Flores, N.M., Miller, T.R., Stockwell, J.D., 2018. A global analysis of the relationship between concentrations of microcystins in water and fish. Front. Mar. Sci. 5, 1–14. doi:10.3389/fmars.2018.00030.

Fotiou, T., Triantis, T., Kaloudis, T., Hiskia, A., 2015. Photocatalytic degradation of cylindrospermopsin under UV-A, solar and visible light using TiO_2. Mineralization and intermediate products.. Chemosphere 119, S89–S94. doi:10.1016/j.chemosphere.2014.04.045.

Fotiou, T., Triantis, T.M., Kaloudis, T., O'Shea, K.E., Dionysiou, D.D., Hiskia, A., 2016. Assessment of the roles of reactive oxygen species in the UV and visible light photocatalytic degradation of cyanotoxins and water taste and odor compounds using C-TiO_2. Water Res. 90, 52–61. doi:10.1016/j.watres.2015.12.006.

Fraga, L.E., Anderson, M.A., Beatriz, M.L.P.M.A., Paschoal, F.M.M., Romão, L.P., Zanoni, M.V.B., 2009. Evaluation of the photoelectrocatalytic method for oxidizing chloride and simultaneous removal of microcystin toxins in surface waters. Electrochim. Acta 54, 2069–2076. 10.1016/j.electacta.2008.08.060

Friehs, E., AlSalka, Y., Jonczyk, R., Lavrentieva, A., Jochums, A., Walter, J.G., Stahl, F., Scheper, T., Bahnemann, D., 2016. Toxicity, phototoxicity and biocidal activity of nanoparticles employed in photocatalysis. J. Photochem. Photobiol. C Photochem. Rev. 29, 1–28. doi:10.1016/j.jphotochemrev.2016.09.001.

Funari, E., Manganelli, M., Buratti, F.M., Testai, E., 2017. Cyanobacteria blooms in water: Italian guidelines to assess and manage the risk associated to bathing and recreational activities. Sci. Total Environ. 598, 867–880. doi:10.1016/j.scitotenv.2017.03.232.

Garcia-Segura, S., Brillas, E., 2017. Applied photoelectrocatalysis on the degradation of organic pollutants in wastewaters. J. Photochem. Photobiol. C Photochem. Rev. 31, 1–35. doi:10.1016/j.jphotochemrev.2017.01.005.

Garcia-Segura, S., Tugaoen, H.O.N., Hristovski, K., Westerhoff, P., 2018. Photon flux influence on photoelectrochemical water treatment. Electrochem. Commun. 87, 63–65. doi:10.1016/j.elecom.2017.12.026.

Gaya, U.I., Abdullah, A.H., 2008. Heterogeneous photocatalytic degradation of organic contaminants over titanium dioxide: a review of fundamentals, progress and problems. J. Photochem. Photobiol. C Photochem. Rev. 9, 1–12. doi:10.1016/j.jphotochemrev.2007.12.003.

Gkelis, S., Zaoutsos, N., 2014. Cyanotoxin occurrence and potentially toxin producing cyanobacteria in freshwaters of Greece: a multi-disciplinary approach. Toxicon 78, 1–9. doi:10.1016/j.toxicon.2013.11.010.

Graham, D., Kisch, H., Lawton, L.A., Robertson, P.K.J., 2010. The degradation of microcystin-LR using doped visible light absorbing photocatalysts. Chemosphere 78, 1182–1185. doi:10.1016/j.chemosphere.2009.12.003.

Greer, B., Maul, R., Campbell, K., Elliott, C.T., 2017. Detection of freshwater cyanotoxins and measurement of masked microcystins in tilapia from Southeast Asian aquaculture farms. Anal. Bioanal. Chem. 409, 4057–4069. doi:10.1007/s00216-017-0352-4.

Gustafsson, M.G.L., Patterson, G.H., Lippincott-Schwartz, J., Davidson, M.W., 2013. Education in microscopy and digital imaging. Zeiss 1–18.

Han, C., Andersen, J., Likodimos, V., Falaras, P., Linkugel, J., Dionysiou, D.D., 2014. The effect of solvent in the sol-gel synthesis of visible light-activated, sulfur-doped TiO_2 nanostructured porous films for water treatment. Catal. Today 224, 132–139. doi:10.1016/j.cattod.2013.11.052.

Han, C., Machala, L., Medrik, I., Prucek, R., Kralchevska, R.P., Dionysiou, D.D., 2017. Degradation of the cyanotoxin microcystin-LR using iron-based photocatalysts under visible light illumination. Environ. Sci. Pollut. Res. 24, 19435–19443. doi:10.1007/s11356-017-9566-4.

Han, C., Pelaez, M., Likodimos, V., Kontos, A.G., Falaras, P., O'Shea, K., Dionysiou, D.D., 2011. Innovative visible light-activated sulfur doped TiO_2 films for water treatment. Appl. Catal. B Environ. 107, 77–87. doi:10.1016/j.apcatb.2011.06.039.

Haque, M.M., Muneer, M., 2007. Photodegradation of norfloxacin in aqueous suspensions of titanium dioxide. J. Hazard. Mater. 145, 51–57. doi:10.1016/j.jhazmat.2006.10.086.

Hasegawa, K., Neta, P., 1978. Rate constants and mechanisms of reaction of Cl_2- radicals. J. Phys. Chem. 82, 854–857. doi:10.1021/j100497a003.

Hayat, K., Gondal, M.A., Khaled, M.M., Ahmed, S., Shemsi, A.M., 2011. Nano ZnO synthesis by modified sol gel method and its application in heterogeneous photocatalytic removal of phenol from water. Appl. Catal. A Gen. 393, 122–129. doi:10.1016/j.apcata.2010.11.032.

Haynes, V.N., Ward, J.E., Russell, B.J., Agrios, A.G., 2017. Photocatalytic effects of titanium dioxide nanoparticles on aquatic organisms—current knowledge and sug-

gestions for future research. Aquat. Toxicol. 185, 138–148. doi:10.1016/j.aquatox.2017.02.012.
Henderson, M.A., 2011. A surface science perspective on TiO_2 photocatalysis. Surf. Sci. Rep. 66, 185–297. doi:10.1016/j.surfrep.2011.01.001.
Hoff-Risseti, C., Dörr, F.A., Schaker, P.D.C., Pinto, E., Werner, V.R., Fiore, M.F., 2013. Cylindrospermopsin and saxitoxin synthetase genes in cylindrospermopsis raciborskii strains from Brazilian freshwater. PLoS One 8, 35–39. doi:10.1371/journal.pone.0074238.
Hoffmann, M.R., Martin, S.T., Choi, W., Bahnemann, D.W., 1995. Environmental applications of semiconductor photocatalysis. Chem. Rev. 95, 69–96. doi:10.1021/cr00033a004.
Hoigné, J., Faust, B.C., Haag, W.R., Scully, F.E., Zepp, R.G., 1989. And sinks of photochemically produced.
Hou, W.M., Ku, Y., 2013. Photocatalytic decomposition of gaseous isopropanol in a tubular optical fiber reactor under periodic UV-LED illumination. J. Mol. Catal. A Chem. 374–375, 7–11. doi:10.1016/j.molcata.2013.03.016.
Hu, J.D., Zevi, Y., Kou, X.M., Xiao, J., Wang, X.J., Jin, Y., 2010. Effect of dissolved organic matter on the stability of magnetite nanoparticles under different pH and ionic strength conditions. Sci. Total Environ. 408, 3477–3489. doi:10.1016/j.scitotenv.2010.03.033.
Hu, Xi, Hu, Xinjiang, Tang, C., Wen, S., Wu, X., Long, J., Yang, X., Wang, H., Zhou, L., 2017. Mechanisms underlying degradation pathways of microcystin-LR with doped TiO_2 photocatalysis. Chem. Eng. J 330, 355–371. doi:10.1016/j.cej.2017.07.161.
Hudnell, H.K., 2010. The state of U.S. freshwater harmful algal blooms assessments, policy and legislation. Toxicon 55, 1024–1034. doi:10.1016/j.toxicon.2009.07.021.
Ibelings, B.W., Backer, L.C., Kardinaal, W.E.A., Chorus, I., 2014. Current approaches to cyanotoxin risk assessment and risk management around the globe. Harmful Algae 40, 63–74. doi:10.1016/j.hal.2014.10.002.
Jacoby, J.M., Kann, J., 2007. The occurrence and response to toxic cyanobacteria in the Pacific Northwest. North America. Lake Reserv. Manag. 23, 123–143. doi:10.1080/07438140709353916.
Jafari, N., Ebrahimpour, K., Abdolahnejad, A., Karimi, M., Ebrahimi, A., 2020. Efficient degradation of microcystin-LR by $BiVO_4/TiO_2$ photocatalytic nanocomposite under visible light. J. Environ. Heal. Sci. Eng. 17, 1171–1183. doi:10.1007/s40201-019-00432-4.
Jayson, G.G., Parsons, B.J., Swallow, A.J., 1973. Some simple, highly reactive, inorganic chlorine derivatives in aqueous solution. J. Chem. Soc. Faraday Trans. 1 Phys. Chem. Condens. Phases 69, 1597–1607. doi:10.1039/F19736901597.
Jefferson, B., Jarvis, P., Bhagianathan, G.K., Smith, H., Autin, O., Goslan, E.H., MacAdam, J., Carra, I., 2016. Effect of elevated UV dose and alkalinity on metaldehyde removal and THM formation with UV/TiO_2 and UV/H_2O_2. Chem. Eng. J. 288, 359–367. doi:10.1016/j.cej.2015.11.071.
Jo, W.K., Tayade, R.J., 2014. New generation energy-efficient light source for photocatalysis: LEDs for environmental applications. Ind. Eng. Chem. Res. 53, 2073–2084. doi:10.1021/ie404176g.
Kaushik, R., Balasubramanian, R., 2013. Methods and approaches used for detection of cyanotoxins in environmental samples: a review. Crit. Rev. Environ. Sci. Technol. 43, 1349–1383.
Khadgi, N., Upreti, A.R., 2019. Photocatalytic degradation of Microcystin-LR by visible light active and magnetic, $ZnFe_2O_4$-Ag/rGO nanocomposite and toxicity assessment of the intermediates. Chemosphere 221, 441–451. doi:10.1016/j.chemosphere.2019.01.046.
Kim, S., Jahandar, M., Jeong, J.H., Lim, D.C., 2019. Recent progress in solar cell technology for low-light indoor applications. Curr. Altern. Energy 3, 3–17. doi:10.2174/1570180816666190112141857.
Kisch, H., 2010. On the problem of comparing rates or apparent quantum yields in heterogeneous photocatalysis. Angew. Chemie - Int. Ed. 49, 9588–9589. doi:10.1002/anie.201002653.
Kochuveedu, S.T., Jang, Y.H., Kim, D.H., 2013. A study on the mechanism for the interaction of light with noble metal-metal oxide semiconductor nanostructures for various photophysical applications. Chem. Soc. Rev. 42, 8467–8493. doi:10.1039/c3cs60043b.
Kositzi, M., Poulios, I., Samara, K., Tsatsaroni, E., Darakas, E., 2007. Photocatalytic oxidation of Cibacron Yellow LS-R. J. Hazard. Mater. 146, 680–685. doi:10.1016/j.jhazmat.2007.04.071.
Krienitz, L., Dadheech, P.K., Fastner, J., Kotut, K., 2013. The rise of potentially toxin producing cyanobacteria in Lake Naivasha, Great African Rift Valley. Kenya. Harmful Algae 27, 42–51. doi:10.1016/j.hal.2013.04.005.
Kubickova, B., Babica, P., Hilscherová, K., Šindlerová, L., 2019. Effects of cyanobacterial toxins on the human gastrointestinal tract and the mucosal innate immune system. Environ. Sci. Eur. 31. doi:10.1186/s12302-019-0212-2.
Kudlek, E., Dudziak, M., Bohdziewicz, J., 2016. Influence of inorganic ions and organic substances on the degradation of pharmaceutical compound in water matrix. Water 8. doi:10.3390/w8110532.
Kurmayer, R., Schober, E., Tonk, L., Visser, P.M., Christiansen, G., 2011. Spatial divergence in the proportions of genes encoding toxic peptide synthesis among populations of the cyanobacterium Planktothrixin European lakes. FEMS Microbiol. Lett. 317, 127–137. doi:10.1111/j.1574-6968.2011.02222.x.
Lanzarini-Lopes, M., Cruz, B., Garcia-Segura, S., Alum, A., Abbaszadegan, M., Westerhoff, P., 2019. Nanoparticle and transparent polymer coatings enable UV-C side-emission optical fibers for inactivation of escherichia coli in water. Environ. Sci. Technol. 53, 10880–10887. doi:10.1021/acs.est.9b01958.
Lawton, L.A., Robertson, P.K.J., Cornish, B.J.P.A., Marr, I.L., Jaspars, M., 2003. Processes influencing surface interaction and photocatalytic destruction of microcystins on titanium dioxide photocatalysts. J. Catal. 213, 109–113. doi:10.1016/S0021-9517(02)00049-0.
Lee, D.K., Kim, S.C., Cho, I.C., Kim, S.J., Kim, S.W., 2004. Photocatalytic oxidation of microcystin-LR in a fluidized bed reactor having TiO_2-coated activated carbon. Sep. Purif. Technol. 34, 59–66. doi:10.1016/S1383-5866(03)00175-8.
Lee, K.M., Lai, C.W., Ngai, K.S., Juan, J.C., 2016. Recent developments of zinc oxide based photocatalyst in water treatment technology: a review. Water Res 88, 428–448. doi:10.1016/j.watres.2015.09.045.
Lei, Y., Cheng, S., Luo, N., Yang, X., An, T., 2019. Rate constants and mechanisms of the reactions of $Cl^{\bullet}$ and $Cl_2^{\bullet-}$ with trace organic contaminants. Environ. Sci. Technol. doi:10.1021/acs.est.9b02462.
Liang, Y., He, X., Chen, L., Zhang, Y., 2014. Preparation and characterization of TiO_2-Graphene@Fe_3O_4 magnetic composite and its application in the removal of trace amounts of microcystin-LR. RSC Adv. 4, 56883–56891. doi:10.1039/c4ra08258c.
Liao, W., Zhang, Y., Zhang, M., Murugananthan, M., Yoshihara, S., 2013. Photoelectrocatalytic degradation of microcystin-LR using Ag/AgCl/TiO_2 nanotube arrays electrode under visible light irradiation. Chem. Eng. J. 231, 455–463. doi:10.1016/j.cej.2013.07.054.
Light, V., Using, I., n.d. By UV-A, solar and visible light irradiation using 1–16.
Likodimos, V., Han, C., Pelaez, M., Kontos, A.G., Liu, G., Zhu, D., Liao, S., De La Cruz, A.A., O'Shea, K., Dunlop, P.S.M., Byrne, J.A., Dionysiou, D.D., Falaras, P., 2013. Anion-doped TiO_2 nanocatalysts for water purification under visible light. Ind. Eng. Chem. Res. 52, 13957–13964. doi:10.1021/ie3034575.
Liu, G., Han, C., Pelaez, M., Zhu, D., Liao, S., Likodimos, V., Kontos, A.G., Falaras, P., Dionysiou, D.D., 2013. Enhanced visible light photocatalytic activity of CN-codoped TiO_2 films for the degradation of microcystin-LR. J. Mol. Catal. A Chem. 372, 58–65. doi:10.1016/j.molcata.2013.02.006.
Liu, I., Lawton, L.A., Bahnemann, D.W., Liu, L., Proft, B., Robertson, P.K.J., 2009. The photocatalytic decomposition of microcystin-LR using selected titanium dioxide materials. Chemosphere 76, 549–553. doi:10.1016/j.chemosphere.2009.02.067.
Liu, I., Lawton, L.A., Bahnemann, D.W., Robertson, P.K.J., 2005. The photocatalytic destruction of the cyanotoxin, nodularin using TiO_2. Appl. Catal. B Environ. 60, 245–252. doi:10.1016/j.apcatb.2005.03.006.
Liu, Y., He, X., Duan, X., Fu, Y., Fatta-Kassinos, D., Dionysiou, D.D., 2016. Significant role of UV and carbonate radical on the degradation of oxytetracycline in UV-AOPs: kinetics and mechanism. Water Res. 95, 195–204. doi:10.1016/j.watres.2016.03.011.
Liu, Y., Chen, W., Li, D., Huang, Z., Shen, Y., Liu, Yongding, 2011. Cyanobacteria-/cyanotoxin-contaminations and eutrophication status before Wuxi Drinking Water Crisis in Lake Taihu. China. J. Environ. Sci 23, 575–581. doi:10.1016/S1001-0742(10)60450-0.
Livraghi, S., Pelaez, M., Biedrzycki, J., Corazzari, I., Giamello, E., Dionysiou, D.D., 2013. Influence of the chemical synthesis on the physicochemical properties of N-TiO_2 nanoparticles. Catal. Today 209, 54–59. doi:10.1016/j.cattod.2012.12.020.
Loeb, S.K., Alvarez, P.J.J., Brame, J.A., Cates, E.L., Choi, W., Crittenden, J., Dionysiou, D.D., Li, Q., Li-Puma, G., Quan, X., Sedlak, D.L., David Waite, T., Westerhoff, P., Kim, J.H., 2019. The technology horizon for photocatalytic water treatment: sunrise or sunset? Environ. Sci. Technol. 53, 2937–2947. doi:10.1021/acs.est.8b05041.
Loftin, K.A., Graham, J.L., Hilborn, E.D., Lehmann, S.C., Meyer, M.T., Dietze, J.E., Griffith, C.B., 2016. Cyanotoxins in inland lakes of the United States: occurrence and potential recreational health risks in the EPA National Lakes Assessment 2007. Harmful Algae 56, 77–90. doi:10.1016/j.hal.2016.04.001.
Lopes, V.R., Vasconcelos, V.M., 2011. Planktonic and benthic cyanobacteria of European brackish waters: a perspective on estuaries and brackish seas. Eur. J. Phycol. 46, 292–304. doi:10.1080/09670262.2011.602429.
Lu, M.C., Chang, Y.F., Chen, I.M., Huang, Y.Y., 2005. Effect of chloride ions on the oxidation of aniline by Fenton's reagent. J. Environ. Manag. 75, 177–182. doi:10.1016/j.jenvman.2004.12.003.
Lv, K., Zuo, H., Sun, J., Deng, K., Liu, S., Li, X., Wang, D., 2009. (Bi, C and N) codoped TiO2 nanoparticles. J. Hazard. Mater. 161, 396–401. doi:10.1016/j.jhazmat.2008.03.111.
Lv, N., Li, Y., Huang, Z., Li, T., Ye, S., Dionysiou, D.D., Song, X., 2019. Synthesis of GO/TiO_2/Bi_2WO_6 nanocomposites with enhanced visible light photocatalytic degradation of ethylene. Appl. Catal. B Environ. 246, 303–311. doi:10.1016/j.apcatb.2019.01.068.
Mantzouki, E., Campbell, J., Loon, E.Van, Visser, P., Konstantinou, I., Antoniou, M., Giuliani, G., Machado-Vieira, D., Oliveira, A.G.De, Maronić, D.Š., Stević, F., Pfeiffer, T.Ž., Vucelić, I.B., Žutinić, P., Udovič, M.G., Plenković-Moraj, A., Tsiarta, N., Bláha, L., Geriš, R., Fránková, M., Christoffersen, K.S., Warming, T.P., Feldmann, T., Laas, A., Panksep, K., Tuvikene, L., Kangro, K., Häggqvist, K., Salmi, P., Arvola, L., Fastner, J., Straile, D., Rothhaupt, K.O., Fonvielle, J., Grossart, H.P., Avagianos, C., Kaloudis, T., Triantis, T., Zervou, S.K., Hiskia, A., Gkelis, S., Panou, M., McCarthy, V., Perello, V.C., Obertegger, U., Boscaini, A., Flaim, G., Salmaso, N., Cerasino, L., Koreivienė, J., Karosienė, J., Kasperovičienė, J., Savadova, K., Vitonytė, I., Haande, S., Skjelbred, B., Grabowska, M., Karpowicz, M., Chmura, D., Nawrocka, L., Kobos, J., Mazur-Marzec, H., Alcaraz-Párraga, P., Wilk-Woźniak, E., Krztoń, W., Walusiak, E., Gagala, I., Mankiewicz-Boczek, J., Toporowska, M., Pawlik-Skowronska, B., Niedźwieck, M., Pęczuła, W., Napiórkowska-Krzebietke, A., Dunalska, J., Sieńska, J., Szymański, D., Kruk, M., Budzyńska, A., Goldyn, R., Kozak, A., Rosińska, J., Szeląg-Wasielewska, E., Domek, P., Jakubowska-Krepska, N., Kwasizur, K., Messyasz, B., Pełechata, A., Pełechaty, M., Kokocinski, M., Madrecka, B., Kostrzewska-Szlakowska, I., Frąk, M., Bańkowska-Sobczak, A., Wasilewicz, M., Ochocka, A., Pasztalenie, A., Jasser, I., Antão-Geraldes, A.M., Leira, M., Hernández, A., Vasconcelos, V., Morais, J., Vale, M., Raposeiro, P.M., Gonçalves, V., Aleksovski, B., Krstić, S.,

Nemova, H., Drastichova, I., Chomova, L., Remec-Rekar, S., Elerse, T., Delgado-Martín, J., García, D., Cereijo, J.L., Gomà, J., Trapote, M.C., Vegas-Vilarrúbia, T., Obrador, B., García-Murcia, A., Real, M., Romans, E., Noguero-Ribes, J., Duque, D.P., Fernández-Morán, E., Úbeda, B., Gálvez, J.Á., Marcé, R., Catalán, N., Pérez-Martínez, C., Ramos-Rodríguez, E., Cillero-Castro, C., Moreno-Ostos, E., Blanco, J.M., Rodríguez, V., Montes-Pérez, J.J., Palomino, R.L., Rodríguez-Pérez, E., Carballeira, R., Camacho, A., Picazo, A., Rochera, C., Santamans, A.C., Ferriol, C., Romo, S., Soria, J.M., Hansson, L.A., Urrutia-Cordero, P., Özen, A., Bravo, A.G., Buck, M., Colom-Montero, W., Mustonen, K., Pierson, D., Yang, Y., Verspagen, J.M.H., De Senerpont Domis, L.N., Seelen, L., Teurlincx, S., Verstijnen, Y., Lürling, M., Maliaka, V., Faassen, E.J., Latour, D., Carey, C.C., Paerl, H.W., Torokne, A., Karan, T., Demir, N., Beklioğlu, M., Filiz, N., Levi, E.E., Iskin, U., Bezirci, G., Tavşanoğlu, Ü.N., Çelik, K., Özhan, K., Karakaya, N., Koçer, M.A.T., Yilmaz, M., Maraşlıoğlu, F., Fakioglu, Ö., Soylu, E.N., Yağcı, M.A., Çınar, Ş., Çapkın, K., Yağcı, A., Cesur, M., Bilgin, F., Bulut, C., Uysal, R., Köker, L., Akçaalan, R., Albay, M., Alp, M.T., Özkan, K., Sevindik, T.O., Tunca, H., Önem, B., Richardson, J., Edwards, C., Bergkemper, V., O'leary, S., Beirne, E., Cromie, H., Ibelings, B.W., 2018. A European Multi Lake Survey dataset of environmental variables, phytoplankton pigments and cyanotoxins. Sci. Data 5, 1–13. doi:10.1038/sdata.2018.226.

Marks, R., Doudrick, K., 2019. Photocatalytic reduction of chlorite in water using bismuth vanadate ($BiVO_4$): effect of irradiance conditions and presence of oxalate on the reactivity and by-product selectivity. Environ. Sci. Water Res. Technol. 5, 2015–2026. doi:10.1039/c9ew00636b.

Matilainen, A., Gjessing, E.T., Lahtinen, T., Hed, L., Bhatnagar, A., Sillanpää, M., 2011. An overview of the methods used in the characterisation of natural organic matter (NOM) in relation to drinking water treatment. Chemosphere 83, 1431–1442. doi:10.1016/j.chemosphere.2011.01.018.

Matilainen, A., Vepsäläinen, M., Sillanpää, M., 2010. Natural organic matter removal by coagulation during drinking water treatment: a review. Adv. Colloid Interface Sci. 159, 189–197. doi:10.1016/j.cis.2010.06.007.

Mauter, M.S., Zucker, I., Perreault, F., Werber, J.R., Kim, J.H., Elimelech, M., 2018. The role of nanotechnology in tackling global water challenges. Nat. Sustain. 1, 166–175. doi:10.1038/s41893-018-0046-8.

Melegari, S.P., Perreault, F., Moukha, S., Popovic, R., Creppy, E.E., Matias, W.G., 2012. Induction to oxidative stress by saxitoxin investigated through lipid peroxidation in Neuro 2A cells and Chlamydomonas reinhardtii alga. Chemosphere 89. doi:10.1016/j.chemosphere.2012.04.009.

Merel, S., Walker, D., Chicana, R., Snyder, S., Baurès, E., Thomas, O., 2013a. State of knowledge and concerns on cyanobacterial blooms and cyanotoxins. Environ. Int. 59, 303–327. doi:10.1016/j.envint.2013.06.013.

Meriluoto, J., Blaha, L., Bojadzija, G., Bormans, M., Brient, L., Codd, G.A., Drobac, D., Faassen, E.J., Fastner, J., Hiskia, A., Ibelings, B.W., Kaloudis, T., Kokocinski, M., Kurmayer, R., Pantelić, D., Quesada, A., Salmaso, N., Tokodi, N., Triantis, T.M., Visser, P.M., Svirčev, Z., 2017. Toxic cyanobacteria and cyanotoxins in European waters - recent progress achieved through the CYANOCOST action and challenges for further research. Adv. Oceanogr. Limnol. 8, 161–178. doi:10.4081/aiol.2017.6429.

Metsämuuronen, S., Sillanpää, M., Bhatnagar, A., Mänttäri, M., 2014. Natural organic matter removal from drinking water by membrane technology. Sep. Purif. Rev. 43, 1–61. doi:10.1080/15422119.2012.712080.

Mostafa, E., Reinsberg, P., Garcia-Segura, S., Baltruschat, H., 2018. Chlorine species evolution during electrochlorination on boron-doped diamond anodes: In-situ electrogeneration of Cl_2, Cl_2O and ClO_2. Electrochim. Acta 281, 831–840. doi:10.1016/j.electacta.2018.05.099.

Mrowetz, M., Selli, E., 2006. Photocatalytic degradation of formic and benzoic acids and hydrogen peroxide evolution in TiO_2 and ZnO water suspensions. J. Photochem. Photobiol. A Chem. 180, 15–22. doi:10.1016/j.jphotochem.2005.09.009.

Nakatani, N., Kozaki, D., Mori, M., Hasebe, K., Nakagoshi, N., Tanaka, K., 2011. Ion-exclusion/cation-exchange chromatography with dual detection of the conductivity and spectrophotometry for the simultaneous determination of common inorganic anionic species and cations in river and wastewater. Anal. Sci. 27, 499–504. doi:10.2116/analsci.27.499.

Natarajan, K., Natarajan, T.S., Bajaj, H.C., Tayade, R.J., 2011. Photocatalytic reactor based on UV-LED/TiO_2 coated quartz tube for degradation of dyes. Chem. Eng. J. 178, 40–49. doi:10.1016/j.cej.2011.10.007.

Neilan, B.A., Pearson, L.A., Muenchhoff, J., Moffitt, M.C., Dittmann, E., 2013. Environmental conditions that influence toxin biosynthesis in cyanobacteria. Environ. Microbiol. 15, 1239–1253. doi:10.1111/j.1462-2920.2012.02729.x.

Nikanorov, A.M., Brazhnikova, L.V., Sketches, B. Water Chemical Composition Of Rivers, Lakes And Wetlands. Types and properties of Water.

Nitoda, T., Fan, M.D., Kubo, I., 2008. Effects of cuminaldehyde on melanoma cells. Phyther. Res. 22, 809–813. doi:10.1002/ptr.2374.

Tugaoen, H.O., Garcia-Segura, S., Hristovski, K., Westerhoff, P., 2018a. Compact light-emitting diode optical fiber immobilized TiO_2 reactor for photocatalytic water treatment. Sci. Total Environ. 613–614, 1331–1338. doi:10.1016/j.scitotenv.2017.09.242.

Tugaoen, H.O., Davis, T.W., Burford, M.A., Gobler, C.J., 2012. The rise of harmful cyanobacteria blooms: The potential roles of eutrophication and climate change. Harmful Algae 14, 313–334. doi:10.1016/j.hal.2011.10.027.

Ohtani, B., 2011. *Photocatalysis A to Z—What we know and what we do not know in a scientific sense*, J. Photochem. Photobiol. C 11, 157–178. doi:10.1016/j.jphotochemrev.2011.02.001.

Oliveros, A.N., Pimentel, J.A.I., de Luna, M.D.G., Garcia-Segura, S., Abarca, R.R.M., Doong, R.A., 2021. Visible-light photocatalytic diclofenac removal by tunable vanadium pentoxide/boron-doped graphitic carbon nitride composite. Chem. Eng. J. 403. doi:10.1016/j.cej.2020.126213.

Olivo-Alanis, D., García-Reyes, R.B., Ramirez-Valencia, M., Castellanos Escamilla, E.M., García-González, A., Cerino-Córdova, F.J., Soto-Regalado, E., 2019. Effective photocatalytic mechanism on dye decolorization in different water matrices with phenolic resins as a photocatalyst under visible LED irradiation. J. Photochem. Photobiol. A Chem. 372, 296–308. doi:10.1016/j.jphotochem.2018.12.023.

Ong, C.B., Ng, L.Y., Mohammad, A.W., 2018. A review of ZnO nanoparticles as solar photocatalysts: synthesis, mechanisms and applications. Renew. Sustain. Energy Rev. 81, 536–551. doi:10.1016/j.rser.2017.08.020.

Orha, C., Pode, R., Manea, F., Lazau, C., Bandas, C., 2017. Titanium dioxide-modified activated carbon for advanced drinking water treatment. Process Saf. Environ. Prot. 108, 26–33. doi:10.1016/j.psep.2016.07.013.

Oturan, M.A., Aaron, J.J., 2014. Advanced oxidation processes in water/wastewater treatment: principles and applications. A review.. Crit. Rev. Environ. Sci. Technol. 44, 2577–2641. doi:10.1080/10643389.2013.829765.

Ovhal, S.D., Thakur, P., 2010. Kinetics of photocatalytic degradation of methylene blue in a TiO_2 slurry reactor. Res. J. Chem. Environ. 14, 9–13.

Paerl, H.W., Otten, T.G., 2013. Harmful cyanobacterial blooms: causes, consequences, and controls. Microb. Ecol. 65, 995–1010. doi:10.1007/s00248-012-0159-y.

Pantelić, D., Svirčev, Z., Simeunović, J., Vidović, M., Trajković, I., 2013. Cyanotoxins: characteristics, production and degradation routes in drinking water treatment with reference to the situation in Serbia. Chemosphere 91, 421–441. doi:10.1016/j.chemosphere.2013.01.003.

Pelaez, M., Baruwati, B., Varma, R.S., Luque, R., Dionysiou, D.D., 2013. Microcystin-LR removal from aqueous solutions using a magnetically separable N-doped TiO2 nanocomposite under visible light irradiation. Chem. Commun. 49, 10118–10120. doi:10.1039/c3cc44415e.

Pelaez, M., de la Cruz, A.A., O'Shea, K., Falaras, P., Dionysiou, D.D., 2011. Effects of water parameters on the degradation of microcystin-LR under visible light-activated TiO_2 photocatalyst. Water Res. 45, 3787–3796. doi:10.1016/j.watres.2011.04.036.

Pelaez, M., Falaras, P., Likodimos, V., Kontos, A.G., de la Cruz, A.A., O'shea, K., Dionysiou, D.D., 2010. Synthesis, structural characterization and evaluation of sol-gel-based NF-TiO_2 films with visible light-photoactivation for the removal of microcystin-LR. Appl. Catal. B Environ. 99, 378–387. doi:10.1016/j.apcatb.2010.06.017.

Pelaez, M., Nolan, N.T., Pillai, S.C., Seery, M.K., Falaras, P., Kontos, A.G., Dunlop, P.S.M., Hamilton, J.W.J., Byrne, J.A., O'Shea, K., Entezari, M.H., Dionysiou, D.D., 2012. A review on the visible light active titanium dioxide photocatalysts for environmental applications. Appl. Catal. B Environ. 125, 331–349. doi:10.1016/j.apcatb.2012.05.036.

Perreault, F., Seleme Matias, M., Pedroso Melegari, S., de Carvalho Pinto, C.R.S., Ekué Creppy, E., Popovic, R., Gerson Matias, W., 2011. Investigation of animal and algal bioassays for reliable saxitoxin ecotoxicity and cytotoxicity risk evaluation. Ecotoxicol. Environ. Saf. 74. doi:10.1016/j.ecoenv.2011.01.016.

Pestana, C.J., Edwards, C., Prabhu, R., Robertson, P.K.J., Lawton, L.A., 2015. Photocatalytic degradation of eleven microcystin variants and nodularin by TiO_2 coated glass microspheres. J. Hazard. Mater. 300, 347–353. doi:10.1016/j.jhazmat.2015.07.016.

Petosa, A.R., Jaisi, D.P., Quevedo, I.R., Elimelech, M., Tufenkji, N., 2010. Aggregation and deposition of engineered nanomaterials in aquatic environments: role of physicochemical interactions. Environ. Sci. Technol. 44, 6532–6549. doi:10.1021/es100598h.

Pinho, L.X., 2014. Photocatalytic degradation of cyanobacteria and cyanotoxins using suspended and immobilized TiO_2 168.

Pinho, L.X., Azevedo, J., Brito, A., Santos, A., Tamagnini, P., Vilar, V.J.P., Vasconcelos, V.M., Boaventura, R.A.R., 2015a. Effect of TiO_2 photocatalysis on the destruction of Microcystis aeruginosa cells and degradation of cyanotoxins microcystin-LR and cylindrospermopsin. Chem. Eng. J. 268, 144–152. doi:10.1016/j.cej.2014.12.111.

Pinho, L.X., Azevedo, J., Miranda, S.M., Ângelo, J., Mendes, A., Vilar, V.J.P., Vasconcelos, V., Boaventura, R.A.R., 2015b. Oxidation of microcystin-LR and cylindrospermopsin by heterogeneous photocatalysis using a tubular photoreactor packed with different TiO2 coated supports. Chem. Eng. J. 266, 100–111. doi:10.1016/j.cej.2014.12.023.

Pirhashemi, M., Habibi-Yangjeh, A., Rahim Pouran, S., 2018. Review on the criteria anticipated for the fabrication of highly efficient ZnO-based visible-light-driven photocatalysts. J. Ind. Eng. Chem. 62, 1–25. doi:10.1016/j.jiec.2018.01.012.

Qian, X., Zhao, Y., Alsaid, Y., Wang, X., Hua, M., Galy, T., Gopalakrishna, H., Yang, Y., Cui, J., Liu, N., Marszewski, M., Pilon, L., Jiang, H., He, X., 2019a. Artificial phototropism for omnidirectional tracking and harvesting of light. Nat. Nanotechnol. 14, 1048–1055. doi:10.1038/s41565-019-0562-3.

Qian, X., Zhao, Y., Alsaid, Y., Wang, X., Hua, M., Galy, T., Gopalakrishna, H., Yang, Y., Cui, J., Liu, N., Marszewski, M., Pilon, L., Jiang, H., He, X., 2019b. Artificial phototropism for omnidirectional tracking and harvesting of light. Nat. Nanotechnol. 14, 1048–1055. doi:10.1038/s41565-019-0562-3.

Rastogi, R.P., Sinha, R.P., Incharoensakdi, A., 2014. The cyanotoxin-microcystins: current overview.. Rev. Environ. Sci. Biotechnol. 13, 215–249. doi:10.1007/s11157-014-9334-6.

Reilly, K., Fang, B., Taghipour, F., Wilkinson, D.P., 2017. Enhanced photocatalytic hydrogen production in a UV-irradiated fluidized bed reactor. J. Catal. 353, 63–73. doi:10.1016/j.jcat.2017.07.003.

Rincón, G.J., La Motta, E.J., 2019. A fluidized-bed reactor for the photocatalytic mineralization of phenol on TiO_2-coated silica gel. Heliyon 5. doi:10.1016/j.heliyon.2019.e01966.

Robertson, P.K.J., Lawton, L.A., Cornish, B.J.P.A., Jaspars, M., 1998. photocatalysis 6030, 1–5.
Robertson, P.K.J., Robertson, J.M.C., Bahnemann, D.W., 2012. Removal of microorganisms and their chemical metabolites from water using semiconductor photocatalysis. J. Hazard. Mater. 211–212, 161–171. doi:10.1016/j.jhazmat.2011.11.058.
Ruiz, M., Galanti, L., Ruibal, A.L., Rodriguez, M.I., Wunderlin, D.A., Amé, M.V., 2013. First report of microcystins and anatoxin-a co-occurrence in San Roque reservoir (Córdoba, Argentina).. Water. Air. Soil Pollut. 224. doi:10.1007/s11270-013-1593-2.
Sampaio, M.J., Pastrana-Martinez, L.M., Silva, A.M.T., Buijnsters, J.G., Han, C., Silva, C.G., Carabineiro, S.A.C., Dionysiou, D.D., Fariaa, J.L., 2015a. Nanodiamond TiO_2 composites for photocatalytic degradation of microcystin-LA in aqueous solutions under simulated solar light. RSC Adv. 5, 58363–58370. doi:10.1039/c5ra08812g.
Sampaio, M.J., Silva, C.G., Silva, A.M.T., Pastrana-Martínez, L.M., Han, C., Morales-Torres, S., Figueiredo, J.L., Dionysiou, D.D., Faria, J.L., 2015b. Carbon-based TiO_2 materials for the degradation of Microcystin-LA. Appl. Catal. B Environ. 170–171, 74–82. doi:10.1016/j.apcatb.2015.01.013.
Sanchez, C., Arribart, H., Guille, M.M.G., 2005. Biomimetism and bioinspiration as tools for the design of innovative materials and systems. Nat. Mater. 4, 277–288. doi:10.1038/nmat1339.
Schneider, M., Bláha, L., 2020. Advanced oxidation processes for the removal of cyanobacterial toxins from drinking water. Environ. Sci. Eur. 32. doi:10.1186/s12302-020-00371-0.
Schwegmann, H., Ruppert, J., Frimmel, F.H., 2013. Influence of the pH-value on the photocatalytic disinfection of bacteria with TiO_2 - explanation by DLVO and XDLVO theory. Water Res. 47, 1503–1511. doi:10.1016/j.watres.2012.11.030.
Sellner, K.G., Doucette, G.J., Kirkpatrick, G.J., 2003. Harmful algal blooms: causes, impacts and detection. J. Ind. Microbiol. Biotechnol. 30, 383–406. doi:10.1007/s10295-003-0074-9.
Senogles, P.J., Scott, J.A., Shaw, G., Stratton, H., 2001. Photocatalytic degradation of the cyanotoxin cylindrospermopsin, using titanium dioxide and UV irradiation. Water Res. 35, 1245–1255. doi:10.1016/S0043-1354(00)00372-9.
Serpone, N., 2006. Is the band gap of pristine TiO_2 narrowed by anion- and cation-doping of titanium dioxide in second-generation photocatalysts? J. Phys. Chem. B 110, 24287–24293. doi:10.1021/jp065659r.
Serrà, A., Artal, R., García-Amorós, J., Sepúlveda, B., Gómez, E., Nogués, J., Philippe, L., 2020a. Hybrid Ni@ZnO@ZnS-microalgae for circular economy: a smart route to the efficient integration of solar photocatalytic water decontamination and bioethanol production. Adv. Sci. 7, 1–9. doi:10.1002/advs.201902447.
Serrà, A., Gómez, E., Philippe, L., 2019a. Bioinspired ZnO-based solar photocatalysts for the efficient decontamination of persistent organic pollutants and hexavalent chromium in wastewater. Catalysts 9, 1–16. doi:10.3390/catal9120974.
Serrà, A., Philippe, L., 2020. Simple and scalable fabrication of hairy ZnO@ZnS core@shell Cu cables for continuous sunlight-driven photocatalytic water remediation. Chem. Eng. J. 401. doi:10.1016/j.cej.2020.126164.
Serrà, A., Pip, P., Gómez, E., Philippe, L., 2020b. Efficient magnetic hybrid ZnO-based photocatalysts for visible-light-driven removal of toxic cyanobacteria blooms and cyanotoxins. Appl. Catal. B Environ. 268, 118745. doi:10.1016/j.apcatb.2020.118745.
Serrà, A., Zhang, Y., Sepúlveda, B., Gómez, E., Nogués, J., Michler, J., Philippe, L., 2020c. Highly reduced ecotoxicity of ZnO-based micro/nanostructures on aquatic biota: Influence of architecture, chemical composition, fixation, and photocatalytic efficiency. Water Res. 169. doi:10.1016/j.watres.2019.115210.
Serrà, A., Zhang, Y., Sepúlveda, B., Gómez, E., Nogués, J., Michler, J., Philippe, L., 2019b. Highly active ZnO-based biomimetic fern-like microleaves for photocatalytic water decontamination using sunlight. Appl. Catal. B Environ. 248, 129–146. doi:10.1016/j.apcatb.2019.02.017.
Sharma, V.K., Triantis, T.M., Antoniou, M.G., He, X., Pelaez, M., Han, C., Song, W., O'Shea, K.E., De La Cruz, A.A., Kaloudis, T., Hiskia, A., Dionysiou, D.D., 2012. Destruction of microcystins by conventional and advanced oxidation processes: A review. Sep. Purif. Technol. 91, 3–17. doi:10.1016/j.seppur.2012.02.018.
Shet, A., Vidya, S.K., 2016. Solar light mediated photocatalytic degradation of phenol using Ag core - TiO_2 shell (Ag@TiO2) nanoparticles in batch and fluidized bed reactor. Sol. Energy 127, 67–78. doi:10.1016/j.solener.2015.12.049.
Shi, H.X., Qu, J.H., Wang, A.M., Ge, J.T., 2005. Degradation of microcystins in aqueous solution with in situ electrogenerated active chlorine. Chemosphere 60, 326–333. doi:10.1016/j.chemosphere.2004.11.070.
Sillanpää, M., Matilainen, A., Lahtinen, T., 2015. Characterization of NOM. Nat. Org. Matter Water Charact. Treat. Methods 17–53. doi:10.1016/B978-0-12-801503-2.00002-1.
Sontakke, S., Modak, J., Madras, G., 2011. Effect of inorganic ions, H_2O_2 and pH on the photocatalytic inactivation of Escherichia coli with silver impregnated combustion synthesized TiO_2 catalyst. Appl. Catal. B Environ. 106, 453–459. doi:10.1016/j.apcatb.2011.06.003.
Spasiano, D., Marotta, R., Malato, S., Fernandez-Ibañez, P., Di Somma, I., 2015. Solar photocatalysis: Materials, reactors, some commercial, and pre-industrialized applications. A comprehensive approach. Appl. Catal. B Environ. 170–171, 90–123. doi:10.1016/j.apcatb.2014.12.050.
Sun, J., Bu, L., Deng, L., Shi, Z., Zhou, S., 2018. Removal of Microcystis aeruginosa by UV/chlorine process: inactivation mechanism and microcystins degradation. Chem. Eng. J. 349, 408–415. doi:10.1016/j.cej.2018.05.116.
Thiel, P.A., Madey, T.E., 1987. The interaction of water with solid surfaces: fundamental aspects. Surf. Sci. Rep. 7, 211–385. doi:10.1016/0167-5729(87)90001-X.
Triantis, T.M., Fotiou, T., Kaloudis, T., Kontos, A.G., Falaras, P., Dionysiou, D.D., Pelaez, M., Hiskia, A., 2012. Photocatalytic degradation and mineralization of microcystin-LR under UV-A, solar and visible light using nanostructured nitrogen doped TiO 2. J. Hazard. Mater. 211–212, 196–202. doi:10.1016/j.jhazmat.2011.11.042.
Tugaoen, H.O.N., Garcia-Segura, S., Hristovski, K., Westerhoff, P., 2017. Challenges in photocatalytic reduction of nitrate as a water treatment technology. Sci. Total Environ. 599–600, 1524–1551. doi:10.1016/j.scitotenv.2017.04.238.
Umebayashi, T., Yamaki, T., Itoh, H., Asai, K., 2002. Band gap narrowing of titanium dioxide by sulfur doping. Appl. Phys. Lett. 81, 454–456. doi:10.1063/1.1493647.
Valadés-Pelayo, P.J., Guayaquil Sosa, F., Serrano, B., de Lasa, H., 2015. Photocatalytic reactor under different external irradiance conditions: validation of a fully predictive radiation absorption model. Chem. Eng. Sci. 126, 42–54. doi:10.1016/j.ces.2014.12.003.
Vieira, J.M.D.S., Azevedo, M.T.D.P., De Oliveira Azevedo, S.M.F., Honda, R.Y., Corrêa, B., 2005. Toxic cyanobacteria and microcystin concentrations in a public water supply reservoir in the Brazilian Amazonia region. Toxicon 45, 901–909. doi:10.1016/j.toxicon.2005.02.008.
Villaluz, F.J.A., de Luna, M.D.G., Colades, J.I., Garcia-Segura, S., Lu, M.C., 2019. Removal of 4-chlorophenol by visible-light photocatalysis using ammonium iron(II) sulfate-doped nano-titania. Process Saf. Environ. Prot. 125, 121–128. doi:10.1016/j.psep.2019.03.001.
Vogiazi, V., De La Cruz, A., Mishra, S., Shanov, V., Heineman, W.R., Dionysiou, D.D., 2019. A comprehensive review: development of electrochemical biosensors for detection of cyanotoxins in freshwater. ACS Sens. 4, 1151–1173. doi:10.1021/acssensors.9b00376.
Wagner, S., Bloh, J., Kasper, C., Bahnemann, D., 2011. Toxicological issues of nanoparticles employed in photocatalysis. Green 1, 171–188. doi:10.1515/GREEN.2011.013.
Wang, H., Zhang, L., Chen, Z., Hu, J., Li, S., Wang, Z., Liu, J., Wang, X., 2014. Semiconductor heterojunction photocatalysts: design, construction, and photocatalytic performances. Chem. Soc. Rev. 43, 5234–5244. doi:10.1039/c4cs00126e.
Wang, S., Liu, K., Yao, X., Jiang, L., 2015. Bioinspired surfaces with superwettability: New insight on theory, design, and applications. Chem. Rev. 115, 8230–8293. doi:10.1021/cr400083y.
Wang, X., Utsumi, M., Yang, Y., Li, D., Zhao, Y., Zhang, Z., Feng, C., Sugiura, N., Cheng, J.J., 2015. Degradation of microcystin-LR by highly efficient $AgBr/Ag_3PO_4/TiO_2$ heterojunction photocatalyst under simulated solar light irradiation. Appl. Surf. Sci. 325, 1–12. doi:10.1016/j.apsusc.2014.10.078.
Wang, Y., Wang, Q., Zhan, X., Wang, F., Safdar, M., He, J., 2013. Visible light driven type II heterostructures and their enhanced photocatalysis properties: a review. Nanoscale 5, 8326–8339. doi:10.1039/c3nr01577g.
Watts, M.J., Linden, K.G., 2007. Chlorine photolysis and subsequent OH radical production during UV treatment of chlorinated water. Water Res. 41, 2871–2878. doi:10.1016/j.watres.2007.03.032.
Watts, M.J., Rosenfeldt, E.J., Linden, K.G., 2007. Comparative OH radical oxidation using UV-Cl_2 and UV-H_2O_2 processes. J. Water Supply Res. Technol. - AQUA 56, 469–477. doi:10.2166/aqua.2007.028.
Wei, W., Dai, Y., Huang, B., 2009. First-principles characterization of Bi-based photocatalysts: $Bi_{12}TiO_{20}$, $Bi_2Ti_2O_7$, and $Bi_4Ti_3O_{12}$. J. Phys. Chem. C 113, 5658–5663. doi:10.1021/jp810344e.
Welker, M., Steinberg, C., 1999. Indirect photolysis of cyanotoxins: one possible mechanism for their low persistence. Water Res. 33, 1159–1164. doi:10.1016/S0043-1354(98)00318-2.
Wert, E.C., Korak, J.A., Trenholm, R.A., Rosario-Ortiz, F.L., 2014. Effect of oxidant exposure on the release of intracellular microcystin, MIB, and geosmin from three cyanobacteria species. Water Res. 52, 251–259. doi:10.1016/j.watres.2013.11.001.
WHO, 2013. WHO | Guidelines for safe recreational water environments.
WHO, 2011. Management of Cyanobacteria in drinking water supplies : Information for regulators and water suppliers. Geneva, Switz. 6206, 1–12. 10.1117/12.673072
WHO, 2006. Guidelines for safe recreational water. Environments 2, 3505–3518.
Wilhelm, S.W., Farnsley, S.E., LeCleir, G.R., Layton, A.C., Satchwell, M.F., DeBruyn, J.M., Boyer, G.L., Zhu, G., Paerl, H.W., 2011. The relationships between nutrients, cyanobacterial toxins and the microbial community in Taihu (Lake Tai). China. Harmful Algae 10, 207–215. doi:10.1016/j.hal.2010.10.001.
Wiltsie, D., Schnetzer, A., Green, J., Borgh, M.Vander, Fensin, E., 2018. Algal blooms and cyanotoxins in Jordan Lake. North Carolina. Toxins (Basel) 10. doi:10.3390/toxins10020092.
Wu, Y., Lu, G., Li, S., 2009. The doping effect of Bi on TiO_2 for photocatalytic hydrogen generation and photodecolorization of rhodamine B. J. Phys. Chem. C 113, 9950–9955. doi:10.1021/jp9009433.
Xiong, Z., Lei, Z., Li, Y., Dong, L., Zhao, Y., Zhang, J., 2018. A review on modification of facet-engineered TiO_2 for photocatalytic CO_2 reduction. J. Photochem. Photobiol. C Photochem. Rev. 36, 24–47. doi:10.1016/j.jphotochemrev.2018.07.002.
Yamamura, H., Okimoto, K., Kimura, K., Watanabe, Y., 2014. Hydrophilic fraction of natural organic matter causing irreversible fouling of microfiltration and ultrafiltration membranes. Water Res. 54, 123–136. doi:10.1016/j.watres.2014.01.024.
Yang, B., Park, H.D., Hong, S.W., Lee, S.H., Park, J.A., Choi, J.W., 2020. Photocatalytic degradation of microcystin-LR and anatoxin-a with presence of natural organic matter using UV-light emitting diodes/TiO_2 process. J. Water Process Eng. 34, 101163. doi:10.1016/j.jwpe.2020.101163.
Yang, J., Chen, D.X., Deng, A.P., Huang, Y.P., Chen, C.C., 2011. Visible-light-driven photocatalytic degradation of microcystin-LR by Bi-doped TiO_2. Res. Chem. Intermed. 37, 47–60. doi:10.1007/s11164-010-0224-4.
Ye, Y., Feng, Y., Bruning, H., Yntema, D., Rijnaarts, H.H.M., 2018. Photocatalytic degradation of metoprolol by TiO2 nanotube arrays and UV-LED: Effects of catalyst properties, operational parameters, commonly present water constituents, and

photo-induced reactive species. Appl. Catal. B Environ. 220, 171–181. doi:10.1016/j.apcatb.2017.08.040.
Yu, J.C., Yu, J., Ho, W., Jiang, Z., Zhang, L., 2002. Effects of F- doping on the photocatalytic activity and microstructures of nanocrystalline TiO_2 powders. Chem. Mater. 14, 3808–3816. doi:10.1021/cm020027c.
Zan, G., Wu, Q., 2016. Biomimetic and Bioinspired Synthesis of Nanomaterials/Nanostructures. Adv. Mater. 28, 2099–2147. doi:10.1002/adma.201503215.
Zareei, M., Yoozbashizadeh, H., Madaah Hosseini, H.R., 2019. Investigating the effects of pH, surfactant and ionic strength on the stability of alumina/water nanofluids using DLVO theory. J. Therm. Anal. Calorim. 135, 1185–1196. doi:10.1007/s10973-018-7620-1.
Zhang, G., Nadagouda, M.N., O'Shea, K., El-Sheikh, S.M., Ismail, A.A., Likodimos, V., Falaras, P., Dionysiou, D.D., 2014a. Degradation of cylindrospermopsin by using polymorphic titanium dioxide under UV-Vis irradiation. Catal. Today 224, 49–55. doi:10.1016/j.cattod.2013.10.072.
Zhang, G., Zhang, Y.C., Nadagouda, M., Han, C., O'Shea, K., El-Sheikh, S.M., Ismail, A.A., Dionysiou, D.D., 2014b. Visible light-sensitized S, N and C co-doped polymorphic TiO_2 for photocatalytic destruction of microcystin-LR. Appl. Catal. B Environ. 144, 614–621. doi:10.1016/j.apcatb.2013.07.058.
Zhang, S., Zhang, G., Yu, S., Chen, X., Zhang, X., 2009. Efficient photocatalytic removal of contaminant by $Bi_3Nb_xTa_{1-x}O_7$ nanoparticles under visible light irradiation. J. Phys. Chem. C 113, 20029–20035. doi:10.1021/jp907831y.
Zhang, X., He, J., Xiao, S., Yang, X., 2019a. Elimination kinetics and detoxification mechanisms of microcystin-LR during UV/Chlorine process. Chemosphere 214, 702–709. doi:10.1016/j.chemosphere.2018.09.162.
Zhang, X., He, J., Xiao, S., Yang, X., 2019b. Elimination kinetics and detoxification mechanisms of microcystin-LR during UV/Chlorine process. Chemosphere 214, 702–709. doi:10.1016/j.chemosphere.2018.09.162.
Zhang, Y., Chen, Y., Westerhoff, P., Crittenden, J., 2009. Impact of natural organic matter and divalent cations on the stability of aqueous nanoparticles. Water Res. 43, 4249–4257. doi:10.1016/j.watres.2009.06.005.
Zhao, C., Li, D., Liu, Y., Feng, C., Zhang, Z., Sugiura, N., Yang, Y., 2015. Photocatalytic removal of microcystin-LR by advanced WO_3-based nanoparticles under simulated solar light. Sci. World J. doi:10.1155/2015/720706, 2015.
Zhao, C., Pelaez, M., Dionysiou, D.D., Pillai, S.C., Byrne, J.A., O'Shea, K.E., 2014. UV and visible light activated TiO_2 photocatalysis of 6-hydroxymethyl uracil, a model compound for the potent cyanotoxin cylindrospermopsin. Catal. Today 224, 70–76. doi:10.1016/j.cattod.2013.09.042.
Zhao, G., Dai, C., Gu, C., You, Q., Sun, Y., 2019. Expandable graphite particles as a novel in-depth steam channeling control agent in heavy oil reservoirs. Chem. Eng. J. 368, 668–677. doi:10.1016/j.cej.2019.03.028.
Zhou, H., Fan, T., Li, X., Zhang, D., Guo, Q., Ogawa, H., 2009. Biomimetic photocatalyst system derived from the natural prototype in leaves for efficient visible-light-driven catalysis. J. Mater. Chem. 19, 2695–2703. doi:10.1039/b818395c.